

Maintenance and Distribution of Mammalian Mitochondrial Nucleoids

Inaugural-Dissertation

zur

Erlangung des Doktorgrades
der Mathematisch-Naturwissenschaftlichen Fakultät
der Universität zu Köln

vorgelegt von

EDUARDO SILVA RAMOS

aus Guadalajara, Mexico

2018

Berichterstatter: **Prof. Dr. Nils-Göran Larsson**

Prof. Dr. Elena Rugarli

Prof. Dr. Jan Riemer

Tag der mündlichen Prüfung: **15.10.2018**

TABLE OF CONTENTS

ABSTRACT	I
ZUSAMMENFASSUNG	II
1.0 INTRODUCTION	1
1.1 Mitochondrial origin	1
1.2 Mitochondrial structure and functions	1
1.3 Oxidative phosphorylation system	3
1.4 Mitochondrial DNA composition.....	5
1.5 Mitochondrial DNA transcription	7
1.6 Mitochondrial DNA replication	8
1.7 Mitochondrial DNA point mutations	11
1.8 Mitochondrial DNA deletions.....	12
1.9 Mitochondrial DNA depletion	13
1.10 Mitochondrial DNA distribution	14
1.11 Mitochondrial network dynamics	16
1.12 Mitochondrial fission.....	18
1.13 Mitochondrial fusion	20
1.14 Research aims	22
2.0 RESULTS	23
2.1 Generation and verification of mitofusin1-2 knockout mice	23
2.2 Loss of <i>Mfn1</i> and <i>Mfn2</i> in heart tissue was verified	24
2.3 Physiological characterization of heart <i>dMfn</i> KO animals.....	25
2.4 <i>dMfn</i> KO animals exhibit mitochondrial respiratory dysfunction.....	27
2.5 <i>dMfn</i> KO heart mitochondria have mevalonate pathway defects.....	31
2.6 No change in mtDNA integrity upon loss of fusion	34
2.7 Loss of OMM fusion results in mtDNA depletion	34
2.8 Loss of OMM fusion leads to nucleoid clustering.....	36
2.9 Loss of OMM fusion does not affect mtDNA compaction	42
2.10 Loss of OMM fusion does not affect mt-transcription activity	43
2.11 Loss of mitochondrial fusion affects replisome composition	50
2.12 mt-fusion is required to sustain high rates of mtDNA replication	53
2.13 OMM fusion is necessary for postnatal mtDNA replication.....	55
3.0 DISCUSSION	59
4.0 REFERENCES	66
5.0 MATERIAL AND METHODS	77
5.1 GENERATION AND MAINTENANCE OF MICE	77
5.1.1 Generation of mutant mice	77
5.1.2 Mouse husbandry.....	77
5.1.3 Mouse genotyping	77

5.2 CELL MODLES AND MAINTENANCE	79
5.2.1 Cell lines.....	79
5.2.2 Cell culture.....	79
5.3 BIOENERGETIC METHODS	80
5.3.1 Isolation of heart mitochondria for bioenergetics	80
5.3.2 High resolution respirometry: Mitochondria.....	81
5.3.3 High resolution respirometry: Whole cells	82
5.3.4 Mitochondrial ATP production	82
5.3.5 Respiratory chain enzymatic activity	83
5.4 PROTEIN BIOCHEMISTRY METHODS	84
5.4.1 Isolation of heart mitochondria	84
5.4.2 Isolation of MEF mitochondria	84
5.4.3 DC protein assay	85
5.4.4 Western blot.....	86
5.4.5 Blue Native PAGE	88
5.4.6 Glycerol gradient fractionation and immunoblotting	88
5.5 MOLECULAR BIOLOGY METHODS	91
5.5.1 Northern blot	91
5.5.2 Phenol chloroform extraction	95
5.5.3 Southern blot.....	95
5.5.4 D-loop Southern blot	96
5.5.5 mtDNA topology analysis	96
5.5.6 Quantitative PCR	97
5.5.7 Mutation load analysis	100
5.5.8 DNA sequencing	100
5.6 IN ORGANELLO ASSAYS	101
5.6.1 <i>de novo</i> mtDNA transcription.....	101
5.6.2 <i>de novo</i> mtDNA replication	103
5.7 CELLULAR ASSAYS	104
5.7.1 Growth curves.....	104
5.7.2 mtDNA depletion and repopulation	104
5.8 MASS SPECTROMETRY	105
5.8.1 UPLC-MS/MS: Coenzyme Q analysis.....	105
5.8.2 UPLC-MS/MS: Cellular dNTP analysis	106
5.8.3 LC-MS/MS: Proteomic analysis	108
5.9 MICROSCOPY.....	112
5.9.1 Immunocytochemistry	112
5.9.2 Fluorescence <i>in situ</i> Hybridization.....	113
5.9.3 Bromouridine labeling.....	114
5.9.4 Confocal microscopy	114
5.9.5 Confocal microscopy image analysis	114
5.9.6 Cytochemistry for STED microscopy.....	115
5.9.7 STED microscopy	115
5.9.8 STED microscopy image analysis.....	115
5.9.9 Transmission electron microscopy.....	116
5.9.10 Image processing	116

5.10 QUANTIFICATION AND STATISTICAL ANALYSIS	116
6.0 ABBREVIATIONS	117
7.0 ERKLÄRUNG	122
8.0 ACKNOWLEDGEMENTS	123
9.0 CURRICULUM VITAE	124

ABSTRACT

Mitochondria derive from the capture of an ancestral α -proteobacteria within an archaeal cell about 2 billion years ago. Since then mitochondria have retained a small proportion of genes within their multi-copy genome mitochondrial DNA (mtDNA) that encode proteins essential to the oxidative phosphorylation system. They have also evolved into a major metabolic hub in eukaryotic cells. Many biosynthetic pathways require mitochondria such as the synthesis of iron-sulfur clusters, heme, lipids and coenzyme Q. However, mitochondria are best known for their efficient ATP production through aerobic metabolism.

The mitochondrial network is a dynamic structure. Through coordinated actions of membrane fusion and fission, mitochondria are able to remodel their shapes and sizes, but also their distribution within the cell. Mitochondrial dynamics is an essential process that impacts mammalian physiology in many different ways. One of the clearest examples is the relationship between mitochondrial fusion and mtDNA maintenance. In animal studies, the absence of mitochondrial fusion proteins resulted in severe reduction in mtDNA copy number. Moreover, loss of mitochondrial fusion proteins, mitofusins, was also associated with an increase in mtDNA point mutations and deletions. However, the molecular basis of these findings is poorly understood.

The research presented in this thesis aims to address the underlying link between mitochondrial fusion and mtDNA maintenance. We report that inactivation of mitofusin 1 and 2 leads to mtDNA depletion and nucleoid clustering in mouse embryonic fibroblasts and heart tissue. With super-resolution microscopy and fluorescent *in situ* hybridization, we show that clustered nucleoids have normal diameters and are transcribed. We report that the loss of mtDNA accounts for the reduction in transcription and bioenergetic defects. Moreover, we demonstrate that the profound mtDNA depletion is not explained by genome instability, but instead it is caused by altered stoichiometry of protein components of the mtDNA replisome. Lastly, we show that outer membrane fusion is necessary to sustain rapid mtDNA replication in MEFs recovering from mtDNA depletion and in the mouse heart during postnatal development. We thus report an unexpected link between OMM fusion and replication and distribution of mtDNA in mammalian cells.

ZUSAMMENFASSUNG

Mitochondrien entstanden vor etwa 2 Milliarden Jahren aus der endosymbiotischen Aufnahme eines α -Proteobakteriums in ein Archaeon. Die Evolution führte zu einer starken Reduktion von genetischer Information im mitochondrialen Erbgut. Dieses mitochondriale Multi-Kopien-Genom, die sogenannte mtDNA, kodiert ausschließlich für RNAs und Proteine, welche essentiell für die oxidative Phosphorylierung sind. Ferner haben sich Mitochondrien während der Evolution zu einem wichtigen metabolischen Zentrum in eukaryotischen Zellen entwickelt. So sind Mitochondrien unter anderem an der Biosynthese von Eisen-Schwefel-Clustern, Häm-, Lipid- und Coenzym-Q Molekülen beteiligt. Mitochondrien sind jedoch am bekanntesten für ihre Effizienz bei der ATP-Produktion durch den aeroben Stoffwechsel.

In Zellen formen Mitochondrien ein dynamisches Netzwerk, welches durch die koordinierte Fusion und –Spaltung von Membranen die mitochondriale Form, Größe und Verteilung innerhalb der Zelle beeinflusst. Diese mannigfaltigen Prozesse werden unter dem Begriff der mitochondrialen Dynamik zusammengefasst und haben entscheidenden Einfluss die Physiologie der Zelle. Diesbezüglich konnten experimentelle Tierstudien zeigen, dass das Fehlen von mitochondrialen Fusionsproteinen die Gesamtmenge an mtDNA und die Anzahl von mtDNA-Molekülen reduziert. Darüber hinaus berichtet eine Studie, dass der Verlust von Mitofusinen mit einer Steigerung von mtDNA-Punktmutationen und -Deletionen einhergeht. Die molekulare Grundlage dieser Beobachtungen ist jedoch kaum verstanden.

Das Ziel dieser Dissertation ist es, die exakten molekularen Mechanismen zwischen mitochondrialer Fusion und mtDNA-Integrität zu untersuchen. Wir zeigen, dass die Inaktivierung von Mitofusin 1 und 2 in embryonalen Mausfibroblasten (MEF) und in konditionalen Maus-Knock-outs zu einer Reduktion und Clusterbildung der mtDNA führt. Mit Hilfe von Super-Resolution-Mikroskopie und Fluoreszenz-*in-situ*-Hybridisierung können wir nachweisen, dass geclusterte Nukleotide interessanterweise eine normale Morphologie haben und transkribiert werden. Ferner können wir durch biochemische Experimente demonstrieren, dass die mtDNA Reduktion die Gesamttranskription verringert und so zu bioenergetischen

Defekten beiträgt. Außerdem, zeigen unsere Experimente, dass die starke mtDNA Reduktion nicht durch Genom-Instabilität ausgelöst wird, sondern durch eine gestörte Stöchiometrie der Proteinkomponenten der mtDNA Replikationsmaschinerie. Des Weiteren können wir experimentell beweisen, dass die Fusion der äußeren mitochondrialen Membran notwendig ist, um eine schnelle mtDNA-Replikation in MEFs zu gewährleisten. Letzteres erklärt somit auch die wichtige Bedeutung der mitochondrialen Fusion für die postnatale Entwicklung des Mausherzens. Zusammenfassend berichten wir über eine unerwartete Verbindung zwischen der Fusion der äußeren mitochondrialen Membran und der mtDNA Replikation und Verteilung in Säugetierzellen.

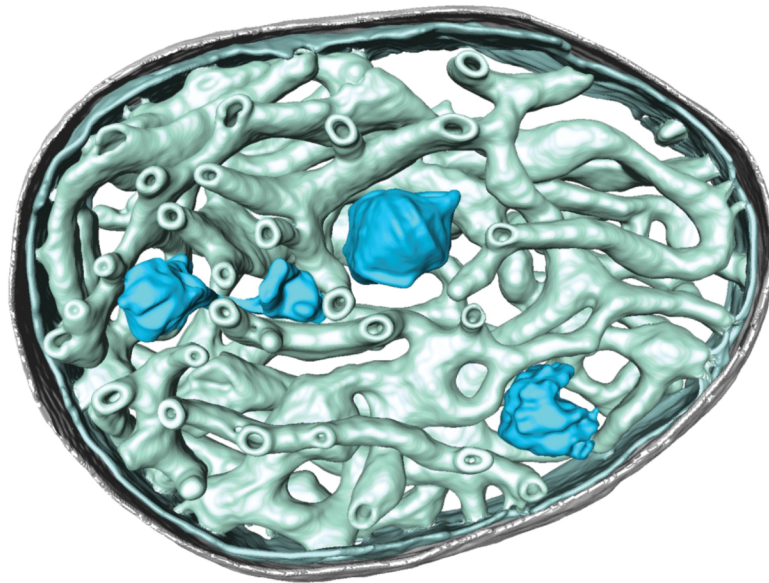
1.0 INTRODUCTION

1.1 Mitochondrial origin

Present day mammalian mitochondria have bacterial ancestry (Gray et al., 1999). The endosymbiosis theory postulates that mitochondria evolved from the capture of an ancestral α -proteobacterium within an archaeal cell. This acquisition occurred about 2 billion years ago and since then an evolving symbiotic relationship between the archaeal cell and ancestral bacterium has given rise to the mitochondria found today in mammals (Kurland and Andersson, 2000). Endosymbiosis likely lead to mutual benefits to both host and captive with regards to the exchange of lipids, iron, and aerobic respiration, and lead to the development of new biology and the evolution of eukaryotes (McBride, 2018). This relationship was further solidified by the early, maybe rapid, loss or integration of parts of the ancestral mitochondrial genetic material into the host DNA (Keeling and Palmer, 2008; Gray, 2015).

1.2 Mitochondrial structure and functions

Mitochondria have a distinct architecture that facilitates the wide variety of cellular functions (Neupert, 2012). A mitochondrion contains two lipid membranes, which compartmentalizes the mitochondrion into four subcompartments. The outer mitochondrial membrane (OMM) acts as a barrier to the cytosol and delineates the aqueous intermembrane space (IMS) where specialized redox reactions take place (Herrmann and Köhl, 2007; Hu et al., 2008). The second lipid membrane, the inner mitochondria membrane (IMM), forms a boundary with the IMS allowing for the generation of a membrane potential important for respiratory chain activity and import/export of ions between compartments (Zorova et al., 2018). Additionally, IMM invaginations form cristae that not only increase the surface area of IMM but are important structures housing the respiratory chain (Gilkerson et al., 2003). Lastly, the innermost compartment is the mitochondrial matrix where numerous metabolic pathways converge (Spinelli and Haigis, 2018) and where the mitochondrial genome resides (Figure 1.1, Kukat et al., 2015).




 Gustafsson CM, et al. 2016.
Annu. Rev. Biochem. 85:133–60

Figure 1.1 Mitochondrial architecture and nucleoids

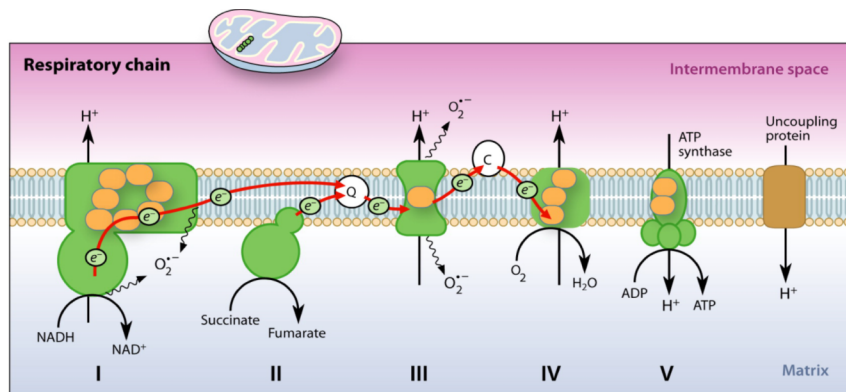
This image is a segmented surface representation of a tomographic slice through the mitochondrion of a bovine heart generated by cryo-electron tomography. The OMM shown in gray, the cristae form by the IMM are shown in green, and the mitochondrial nucleoids are shown in blue. Annual review of biochemistry by ANNUAL REVIEWS. Reproduced with permission of ANNUAL REVIEWS in the format Thesis/Dissertation via Copyright Clearance Center. Permission for use with license ID: 4410720644506 .

The contribution of mitochondria to cell metabolism is multifaceted. Mitochondria are best known for their role in ATP production by using pyruvate and fatty acids as fuel sources (Nicholls and Ferguson, 2013a). They can also initiate gluconeogenesis by carboxylation pyruvate into oxaloacetate followed by export to the cytosol where it can be converted into glucose (Berg et al., 2002). Many other biosynthetic pathways require mitochondria, such as the synthesis of iron-sulfur clusters, heme, phospholipids, cholesterol, fatty acids, coenzyme Q, amino acids, and nucleotides (Spinelli and Haigis, 2018). These diverse biosynthetic pathways are intimately connected, sharing the TCA or amino acid intermediates as well as anabolic and catabolic reactions (Spinelli and Haigis, 2018). Lastly, mitochondria also facilitate broader cellular functions like thermoregulation and apoptosis (Cannon and Nedergaard, 2008; Wang and Youle, 2009).

1.3 Oxidative phosphorylation system

Mitochondria are energy powerhouses that supply the cell with ATP. The oxidative phosphorylation system (OXPHOS) is at the core of ATP production. The proteins involved in OXPHOS have dual genetic origins (Gustafsson et al., 2016). The majority of the OXPHOS subunits (76 proteins) are nuclear-encoded, translated in the cytosol and imported into mitochondria, while 13 additional components are encoded by the multi-copy mitochondrial genome (Larsson, 2010). There is no definitive explanation for this dual genetic origin; however, three theories have been proposed. One theory refers to differences in the decoding system for mitochondrial and nuclear DNA. In contrast to the universal genetic code, mitochondria uses four different nucleotide triplets and different modified bases at the wobble position (Suzuki et al., 2011). A second theory postulates that mitochondrially encoded proteins are too hydrophobic to be transported through the cytosol and imported into mitochondria (Björkholm et al., 2015). This hypothesis is in line with the fact that mitochondrial proteins are rapidly inserted into the IMM upon their translation (Mai et al., 2017). The third theory proposes that having additional genetic source in mitochondria would grant mitochondria the advantage to locally modulate assembly and quantity of respiratory chain complexes by redox regulation of gene expression (Maier et al., 2013; Allen, 2015).

The oxidative phosphorylation system is composed of five complexes with specialized functions embedded in the IMM (Figure 1.2), these include: the NADH:ubiquinone reductase (Complex I, COI), the succinate dehydrogenase (COII), the quinol-cytochrome c reductase (COIII), the cytochrome c oxidase (COIV), and the F_0F_1 -ATP synthase (COV) (Signes and Fernandez-Vizarra, 2018).




 Larsson N-G. 2010.
Annu. Rev. Biochem. 79:683–706

Figure 1.2 The mammalian oxidative phosphorylation system

The oxidative phosphorylation system consists of five enzyme complexes embedded in the IMM. Respiratory subunits encoded by mtDNA (orange) are important components of COI, III, and IV. Production of ATP begins when COI and COII receive electrons (e^-) from intermediary metabolism. Electrons are channeled to coenzyme Q (Q) that then acts a mobile electron carrier to deliver electrons to COIII. Electrons are then shuttled to cytochrome c (C), which delivers the electrons to COIV. At this stage, COIV orchestrates the oxidation of cytochrome c followed by the reduction of oxygen into water. At complexes I, III, and IV electron transfer is coupled to the translocation of protons (H^+) from the mitochondrial matrix to the intermembrane space. The resulting proton gradient is utilized by complex V to drive the synthesis of ATP. Protons may also be translocated in the matrix by activated uncoupling proteins, which result in the uncoupling of electron transfer and ATP synthesis. The reactive oxygen species, superoxide (O_2^-) may form when electrons exits the respiratory chain at COI and COII. Annual review of biochemistry by ANNUAL REVIEWS. Reproduced with permission of ANNUAL REVIEWS in the format Thesis/Dissertation via Copyright Clearance Center. Permission for use with license ID: 4413160293838.

The production of ATP begins with the formation of the reducing electron carriers NADH and $FADH_2$ through catabolism of pyruvate or fatty acids in the TCA cycle or beta-oxidation (Spinelli and Haigis, 2018). These carriers then deliver electrons to COI and COII (by using NADH and $FADH_2$, respectively), which are channeled within the complexes to their respective CoQ binding site. CoQ enters the binding site, undergoes two one-electron reductions steps, and then acts a mobile electron carrier to deliver electrons to COIII (Wang and Hekimi, 2016). Through the Q-cycle mechanism, COIII accepts the electrons from CoQ which are then used to reduce the electron carrier cytochrome c (cyt c) (Trumpower, 1990). At this stage, COIV orchestrates the oxidation cyt c followed by the reduction of oxygen into water (Wikström et al., 2018). This series of reactions taking place between COI through COIV is referred to as the electron transport chain (ETC). An additional feature of ETC is the coupling of electron transfer to the translocation of protons at COI, COII, and COIV. An increasing concentration of protons in the IMS

generates a proton motive force (Nicholls and Ferguson, 2013b). The prevailing model of how COV synthesizes ATP is through a binding-change mechanism (Boyer, 1975). In this model, COV uses the proton motive force to translocate one proton at a time from the IMS into the matrix. Proton translocation causes mechanical rotation of the COV-F_o subunit followed by conformation changes in the COV-F₁ subunits (Boyer, 1993; Abrahams et al., 1994; Wang and Oster, 1998; Cherepanov et al., 1999). The COV-F₁ conformational changes (open, tight, and loose) are coupled to proton translocation, and allow for ADP+Pi binding, ATP synthesis, and ATP release (Štrajbl et al., 2003). Hence, the production of ATP depends on the coupling of redox reactions and proton translocation to accomplish oxidative phosphorylation (Mitchell, 1961).

1.4 Mitochondrial DNA composition

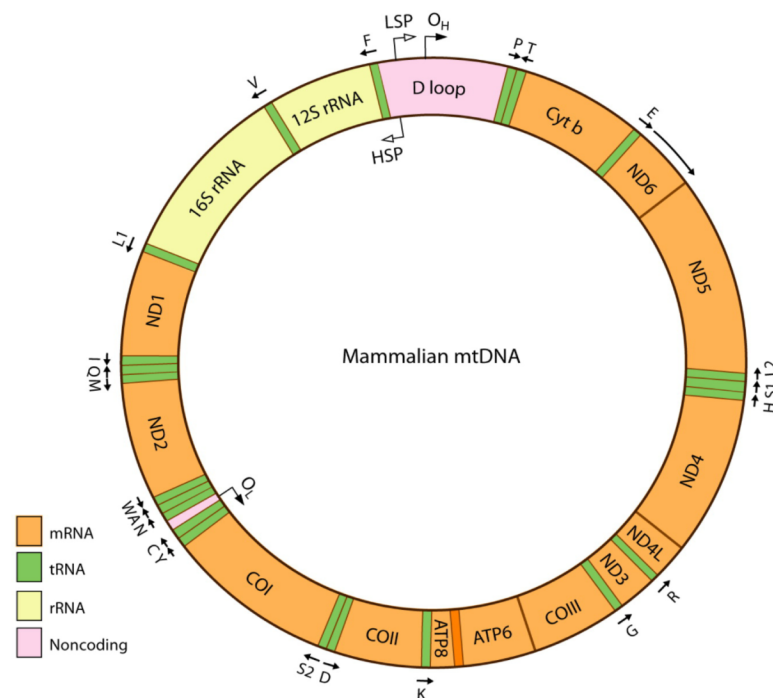
A small proportion of genes were retained during the reductive evolutionary course of the present-day mammalian mtDNA (Falkenberg et al., 2007). Mammalian mtDNA, like its bacterial ancestors, is protein-coated and packaged (Fisher et al., 1992). The main protein in mammals that can achieve packaging of mtDNA is the mammalian transcription factor activator A (TFAM) (Kaufman et al., 2007). Approximately 1000 TFAM molecules bind randomly to mtDNA and the combination of cooperative and cross-strand binding results in complete compaction of mtDNA to form a nucleoid (Kukat et al., 2015). A mammalian nucleoid has a diameter of about 100 nm and has an ellipsoidal shape (Figure 1.1) (Brown et al., 2011; Kukat et al., 2011).

Mouse mtDNA is a circular double-stranded molecule roughly 16.3 kilobases in length (Bibb et al., 1981). The two DNA strands are denoted as heavy-strand (H-strand, higher guanine content) and light-strand (L-strand) based on their separation in alkaline cesium chloride density gradients (Berk and Clayton, 1974).

The mitochondrial genome has coding and non-coding regions (Figure 1.3). The majority of mtDNA is coding. In mammalian mtDNA there are 37 genes; most found on the H-strand (coding for 12 proteins, 14 tRNAs, and 2 rRNAs), making the L-strand the minor coding strand (coding for 1 protein and 8 tRNAs) (Bibb et al.,

1981). The main non-coding region of mtDNA is small and contains several regulatory elements for mtDNA transcription and replication.

Secondary structures can also form in mtDNA. As a consequence of terminated mtDNA replication at the control region, a 500-620-nucleotide fragment (7S DNA) remains bound to the L-strand while the H-strand is displaced; thus, leading to the formation of a displacement loop (D-loop) (Robberson and Clayton, 1972; Berk and Clayton, 1974; Bogenhagen and Clayton, 1978). Moreover, RNA:DNA hybrids (R-loops) can form close to the control region during transcription of mtDNA (Wanrooij et al., 2012; Akman et al., 2016).




 Larsson N-G. 2010.
Annu. Rev. Biochem. 79:683–706

Figure 1.3 Mammalian mitochondrial DNA composition

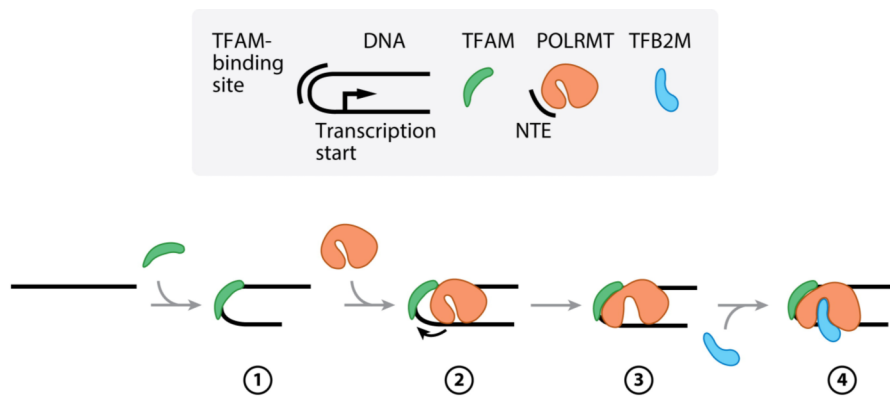
Mammalian mtDNA is a circular double-stranded molecule. The two strands are referred to as the heavy-strand and light-strand. The mitochondrial genome has coding and non-coding regions. The largest non-coding region (pink) is also referred to as the displacement loop (D loop). The D loop region contains the regulatory elements for replication of the leading strand (O_H) and promoter sites for transcription (HSP and LSP). A smaller non-coding region found within a tRNA cluster holds the origin of replication for the lagging strand (O_L). The majority of mtDNA is coding for mRNAs (orange), tRNAs (green), and rRNAs (yellow). tRNAs with an arrow pointing towards the left are transcribed from the HSP promoter and arrows pointing towards the right are transcribed from the LSP promoter. Annual review of biochemistry by ANNUAL REVIEWS. Reproduced with permission of ANNUAL REVIEWS in the format Thesis/Dissertation via Copyright Clearance Center. Permission for use with license ID: 4413160293838.

1.5 Mitochondrial DNA transcription

Expression of the mitochondrial genome is essential for the assembly and activity of the respiratory chain (Larsson et al., 1998; Kühl et al., 2016). Transcription of mtDNA is achieved by the mitochondrial RNA polymerase (POLRMT) (Kühl et al., 2014). POLRMT is a single-unit polymerase that is distantly related to the bacteriophage T7 RNA polymerase (Ringel et al., 2011). However, unlike the T7 RNA polymerase, POLRMT is incapable of initiating or performing elongation of transcription alone. POLRMT requires the following auxiliary proteins: TFAM, the mitochondrial transcription factor B2 (TFB₂M), and the mitochondrial transcription elongation factor (TEFM) (Gustafsson et al., 2016).

The regulatory elements for mitochondrial transcription are located in the non-coding region (NCR) of mtDNA. These elements are the L-strand promoter (LSP) and H-strand promoter (HSP) and from here mitochondrial transcription is initiated (Falkenberg et al., 2007). The current model of initiation states that DNA-bound TFAM recruits POLRMT via its N-terminus to the promoter, leading to a structural change in POLRMT (Figure 1.4). The structural change in POLRMT allows for binding of TFB₂M to POLRMT forming a fully assembled initiation complex and leads to promoter melting (Hillen et al., 2017; Posse and Gustafsson, 2017; Ramachandran et al., 2017). After initiation POLRMT enters the elongation phase, whereby TEFM binding to POLRMT promotes transcription processivity (Posse et al., 2015). MTERF1 was previously proposed to act as a termination factor for sense rRNA gene transcription, but knockout mouse models have shown that its function instead is to terminate antisense transcription (Martin et al., 2005; Terzioglu et al., 2013).

The product of mitochondrial transcription is a single primary near genome-length transcript containing no introns (Gustafsson et al., 2016). This long transcript is cleaved to release 2 rRNAs, 22 tRNAs, and 11 mRNAs (Anderson et al., 1981; Ojala et al., 1981). Two of the mRNAs are bicistronic and encode two proteins each (ATP8 & ATP6; ND₄L & ND₄). The nascent transcripts are stabilized by the LRPPRC-SLIRP protein complex and translated by the mitochondrial ribosome (Ruzzenente et al., 2012; Lagouge et al., 2015). Translated proteins are then inserted into the IMM and assembled into respiratory complexes (Szyrach et al., 2003).



AR Gustafsson CM, et al. 2016.
 Annu. Rev. Biochem. 85:133–60

Figure 1.4 mtDNA transcription initiation

Model of mitochondrial DNA transcription initiation. Transcription initiation requires the following proteins: TFAM, POLRMT, and TFB2M. 1) TFAM binds to mtDNA just upstream of the transcription promoter and bends the DNA. 2) POLRMT via its N-terminal extension is recruited by TFAM and interacts with DNA in a sequence-specific manner. 3) The interaction between TFAM and DNA leads to a conformational change in POLRMT. 4) TFB2M is then able to bind to POLRMT to form a fully assembled initiation complex. Abbreviations: NTE, N-terminal extension; POLRMT, mitochondrial DNA-directed RNA polymerase; TFAM, mitochondrial transcription factor A; TFB2M, mitochondrial transcription factor B2. Annual review of biochemistry by ANNUAL REVIEWS. Reproduced with permission of ANNUAL REVIEWS in the format Thesis/Dissertation via Copyright Clearance Center. Permission for use with license ID: 4413560306680.

1.6 Mitochondrial DNA replication

Maintaining or increasing mtDNA levels in early development and in post-mitotic tissues requires replication of mtDNA. While most studies find replication of mtDNA independent of nuclear DNA replication, there are contrasting reports whether or not its coordinated with cell division (Bogenhagen and Clayton, 1977; Chatre and Ricchetti, 2013). Continuous replication of mtDNA ensures that sufficient numbers of copies are present to meet the energetic demands of the cell. In contrast, dysfunctional mtDNA replication results in mtDNA depletion and can also cause deletion of mitochondrial genomic regions or accumulation of point mutations (Viscomi and Zeviani, 2017).

The core mtDNA replication machinery (the replisome, Figure 1.5) is composed of: mitochondrial RNA polymerase (POLRMT), the mitochondrial DNA helicase twinkle (TWINK), the mitochondrial DNA polymerase γ (POL γ), and the single-stranded DNA binding protein 1 (SSBP $_1$) (Gustafsson et al., 2016). Loss of POLRMT, POL γ , and TWINK are embryonic lethal in mice (Hance et al., 2005; Milenkovic et al., 2013; Kühl et al., 2016). Other proteins are also involved in this process, such as the mitochondrial genome maintenance exonuclease 1 (MGME1) that processes the 5' mtDNA ends generated during replication, and the ribonuclease H1 (RNASEH1) that removes the RNA primer used to initiate mtDNA replication (Cerritelli et al., 2003; Uhler et al., 2016).

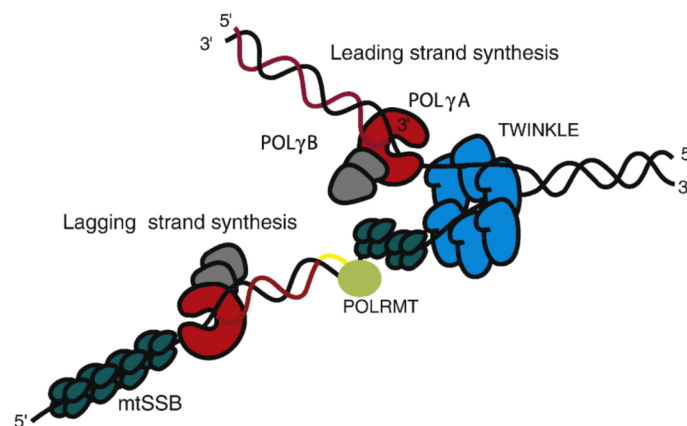


Figure 1.5 The mtDNA replisome

Replication of mtDNA requires the coordinated actions of the replisome proteins: POLRMT, TWINKLE, POL γ , mtSSB (also known as SSBP $_1$). During synthesis of mtDNA, the hexameric TWINKLE (blue) helicase unwinds dsDNA on the lagging strand. On the leading strand, the heterodimeric POL γ (red and gray) synthesizes DNA in a 5' to 3' direction. Meanwhile, the single-stranded lagging strand is coated by multiple mtSSB tetramers (green) until POLRMT (light green) generates the RNA primer at O_L required for DNA synthesis of the lagging strand. Abbreviations: POL γ , DNA polymerase gamma; mtSSB, mitochondrial single-stranded DNA binding protein 1; POLRMT, mitochondrial RNA polymerase. Reprinted from *Biochimica et Biophysica Acta (BBA) - Bioenergetics*, Vol: 1797, Sjoerd Wanrooij and Maria Falkenberg, *The human mitochondrial replication fork in health and disease*, pages 1378-1388, published Aug 1, 2010, with permission from Elsevier; license number: 4413591207459.

Poly is the sole mitochondrial DNA polymerase that can synthesize mtDNA. Other DNA polymerases present are suggested to be present in mitochondria, e.g. PrimPol, Pol β , Pol θ , Pol ζ , but they cannot substitute for loss of Poly (Hance et al., 2005; Humble et al., 2013). The mammalian Poly is present as a heterotrimeric complex consisting of one A-subunit and two B-subunits (Carrodeguas et al., 2002). PolyA is the catalytic subunit with 3' to 5' exonuclease activity and proofreading capabilities (Trifunovic et al., 2004; Macao et al., 2015). The PolyB dimer serves to enhance the catalytic activity of PolyA while also promoting processivity (Carrodeguas et al., 2002; Farge et al., 2007).

The DNA helicase TWNK is present as a hexamer (Fernández-Millán et al., 2015). Studies suggest TWNK may be anchored to the IMM and may even serve as a platform for mtDNA replication (Rajala et al., 2014; Gerhold et al., 2015a). The main function of TWNK is to unwind dsDNA at the replication fork because POLRMT is unable to interact with dsDNA (Spelbrink et al., 2001; Wanrooij and Falkenberg, 2010).

The mitochondrial SSBP₁ is present as multiple tetramer on single-stranded mtDNA (Yang et al., 1997). The main role of SSBP₁ is to stabilize the long stretches of single-stranded mtDNA and to prevent the formation of secondary structures (Tiranti et al., 1993). SSBP₁ can influence mtDNA replication in two ways, by stimulating the helicase activity of TWNK and by increasing the processivity of PolyA (Farr et al., 1999; Korhonen et al., 2003a).

The prevailing model for mtDNA replication is the strand displacement model whereby initiation of mtDNA replication begins within the non-coding region (Brown et al., 2005). The regulatory elements for mitochondrial DNA replication are found on different regions in the mitochondrial genome. The NCR holds the origin of H-strand (O_H), while origin of L-strand (O_L) can be found in the middle of the W-A-N-C-Y tRNA cluster. Initiation requires an RNA primer synthesized by POLRMT at the LSP. PolyA utilizes the 3' end of this primer to initiate replication at the O_H. About 95 % of the initiation events are terminated prematurely and it is unclear what regulates this termination event (Doda et al., 1981). The TWNK helicase is loaded on the lagging strand of DNA to unwind the DNA duplex and the lagging strand, which will be replicated later, is coated with SSBP₁ (Korhonen et al., 2003b).

After the replisome passes the O_L , a stem-loop structure is created on the nascent H-strand and POLRMT uses this stem-loop to initiate synthesis of a 25-nucleotide primer. PolyA utilizes the RNA primer and proceeds with synthesis of the L-strand (Figure 1.5). The replication cycle ends with two complete molecules of double-stranded mtDNA (Falkenberg, 2018).

As mentioned, the replisome factors influence each other's activity. For example, SSBP1 is important for TWNK helicase activity and both PolyB and SSBP1 enhance PolyA processivity (Farr et al., 1999; Korhonen et al., 2003a; Farge et al., 2007). In an *in vitro* system, no DNA synthesis can take place in the absence of TWNK, regardless of the presence of Poly and SSBP1 (Farge et al., 2008). Moreover, low levels of Poly were shown to lead to uncoupling of the L-strand synthesis (Roos et al., 2013). In mice, conditional knockouts of TWNK leads to a reduction in mtDNA copy number by 80 % (Milenkovic et al., 2013; Ignatenko et al., 2018). In contrast, overexpression of TWNK in mice can increase mtDNA levels (Tynismaa et al., 2004). Yet, overexpression of PolyB in cell lines does not change mtDNA levels and in *Drosophila* overexpression caused mtDNA depletion (Lefai et al., 2000; Spelbrink et al., 2000). Altogether, it is evident that proper stoichiometry of the replisome factors is important for maintenance of mtDNA.

1.7 Mitochondrial DNA point mutations

The mitochondrial genome can contain point mutations. Mutations can be generated *de novo* or can be maternally inherited. A mouse model expressing a proofreading defective version of PolyA (mtDNA mutator mouse) showed that *de novo* mutations are generated during errors in mtDNA replication and high levels of mutations can cause premature aging (Trifunovic et al., 2004). It was proposed that oxidative damage could also generate mutations. Recent studies in mice having deficiencies in mtDNA repair and increased oxidative stress revealed no change in the mtDNA point mutation load (Kauppila et al., 2018). Notably, aged wildtype mice display no increase in mutations compared to younger mice (Ameur et al., 2011).

Mitochondria are maternally inherited, as is their genetic material. Two mechanisms are in place during early embryogenesis that helps preserve wildtype copies. First, a strong purifying selection against mutations within protein-coding

genes occurs in the germ line (Stewart et al., 2008). Second, the large number of mtDNA molecules in the oocyte is derived from a small number of maternal mtDNAs. The unclear mechanism whereby only a subset of the pool of mtDNAs in the mother is transferred to the offspring is referred to as the mtDNA bottleneck (Cao et al., 2007). Pathogenic mutations of mtDNA that do get past the germ-line purifying selection may undergo clonal expansion in somatic cells and can lead to disease. Within a population of mtDNA, there can be wildtype copies of mtDNA and copies carrying mutations, a condition known as heteroplasmy. In fact, low levels of mtDNA heteroplasmy is observed in healthy individuals at different ages (Li et al., 2010; Payne et al., 2013). Increasing levels of heteroplasmy can cause clinical symptoms if the fraction of mutated mtDNA exceeds the threshold for causing respiratory chain dysfunction. In the mouse brain, 20 % of nerve cells with deficient respiratory chain function is sufficient to cause clinical symptoms of late-onset neurodegeneration, whereas >60 % of deficient cells leads to severe neurodegeneration and premature death of the animal (Dufour et al., 2008).

1.8 Mitochondrial DNA deletions

Single large deletions of mtDNA can range from 5-7 to kilobases in length (Holt et al., 1988; Schon et al., 1989). The formation of deleted molecules is believed to arise from slippage during mtDNA replication. The earliest observations of mtDNA deletions were made in patients with myopathies and progressive external ophthalmoplegia (PEO) (Holt et al., 1988; Ozawa et al., 1988; Zeviani et al., 1989; Moraes et al., 1989; Shoubridge et al., 1990; Suomalainen et al., 1992). Low levels of mtDNA deletions were also reported from postmortem heart and brain tissue of adult humans, suggesting deletions could play a role in ageing (Cortopassi and Arnheim, 1990). However, a recent study with mice lacking *Mgme1* showed no signs of premature aging or respiratory chain dysfunction despite having higher levels of linear deleted mtDNA molecules than the mtDNA mutator mouse, a model with pathological symptoms similar to age-related diseases (Trifunovic et al., 2004; Matic et al., 2018). This finding indicates that point mutations rather than deletions drive the observed pathology in mtDNA mutator mice.

1.9 Mitochondrial DNA depletion

A balance between mtDNA synthesis and degradation maintains a stable copy number of mtDNA. Mitochondrial DNA depletion syndromes are characterized by a reduction in mtDNA levels, roughly down to 30 % of normal levels, which affect mitochondrial function in liver, skeletal muscle, and nerve cells (Rötig and Poulton, 2009). In animal models, mutation or absence of proteins involved in mtDNA replication, dNTP synthesis, and mitochondrial fusion can cause mtDNA depletion (Chen et al., 2010; Hance et al., 2005; Zhou et al., 2008). Patients with mtDNA depletion syndromes can have mutations in genes that are involved in mtDNA maintenance, such as *Poly*, *TWNK*, *RNASEH1*, and *MGME1* (Viscomi and Zeviani, 2017). Furthermore, mitochondria rely on cytosolic dNTPs and the salvage pathway for a constant supply of dNTPs required for mtDNA synthesis. Mutations in two major deoxyribonucleoside kinases of the mitochondrial salvage pathway, i.e. thymidine kinase (*Tk2*) and deoxyguanosine kinase (*Dguok*), lead to mtDNA depletion (Mandel et al., 2001; Saada et al., 2001). Another cause for mtDNA depletion is the inability of mutant mitochondria to fuse their membranes. Patients with optic atrophy protein 1 (*Opa1*) mutations have decreased mtDNA copy number (Spiegel et al., 2016). Moreover, *mitofusin1-2* and *Opa1* tissue-specific knockout animals also display severely reduced levels of mtDNA (Chen et al., 2010; Papanicolaou et al., 2012; Tezze et al., 2017). How mitochondrial fusion is linked to mtDNA maintenance remains an open question.

1.10 Mitochondrial DNA distribution

The discovery of mtDNA was reported in 1963 and relied on electron microscopy analysis of mitochondria from chick embryos (Nass and Nass, 1963). Since then we have learned that the mitochondrial genome can be found in hundreds to thousands of copies per cell and that mtDNA is distributed throughout the mitochondrial network (Sato and Kuroiwa, 1991; Kukat et al., 2011). In fibroblasts, nucleoids are distributed evenly within a mitochondrion and small differences in nucleoid-to-nucleoid distances are observed between perinuclear and periphery nucleoids (Figure 1.6). Very little is known about the mechanism behind mtDNA distribution as well as the identity of all key proteins.

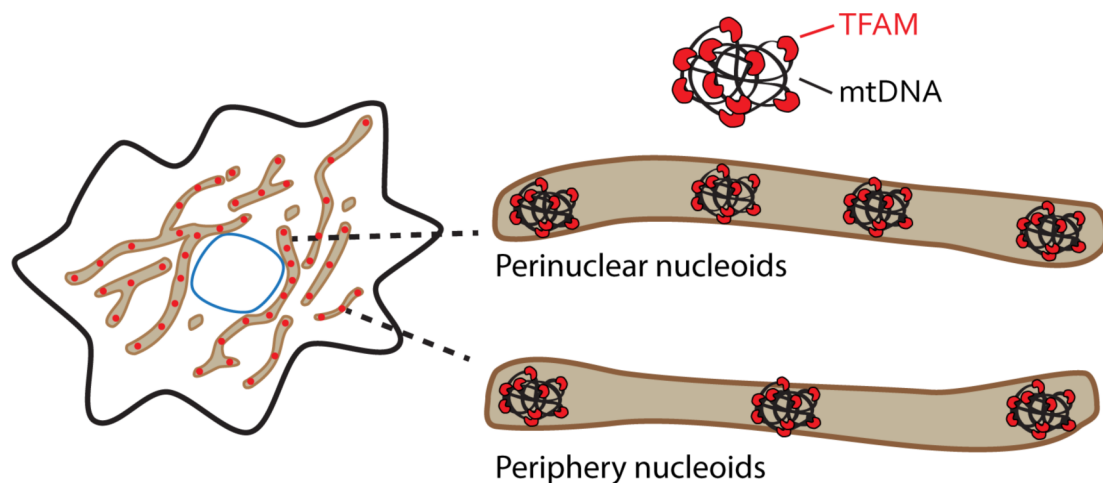


Figure 1.6 Mitochondrial DNA distribution

The mitochondrial genome is coated and compacted by approximately a thousand TFAM proteins to form a nucleoid. The multi-copy mitochondrial genome is distributed throughout the mitochondrial network of a cell. Most elongated mitochondria contain many nucleoids, whereas small mitochondria may have fewer or maybe devoid of nucleoids. Within a mitochondrion, nucleoids are found evenly distributed. Small differences in nucleoid-to-nucleoid distances are present between perinuclear and periphery nucleoids. Perinuclear nucleoids tend to have a smaller nucleoid-to-nucleoid distance, whereas periphery nucleoids tend to be more spaced apart.

A recent study of this process, suggests that newly synthesized mtDNA molecules are segregated at mitochondria-ER contact sites (Lewis et al., 2016). This model argues that the OMM may serve as organizational platform for mtDNA distribution. Indeed, the GTPase dynamin-related protein 1 (DRP1), which divides mitochondria by constricting the OMM, was necessary to prevent mtDNA clustering (Ban-Ishihara et al., 2013). Inside mitochondria, several mtDNA-associated proteins were also described to take part in mtDNA segregation. For example, the mitochondrial topoisomerase 3 α (TOP3 α) which decatenates newly synthesized mtDNA molecules (Nicholls et al., 2018). Other proteins like the leucine zipper and EF-hand containing transmembrane protein 1 (LETM1), the ATPase family AAA domain containing 3A protein (ATAD3A), and the RNASEH1 protein have been also associated with mtDNA clustering but the mode of action remains unknown (Desai et al., 2017; Durigon et al., 2018; Akman et al., 2016).

Interestingly, mtDNA distribution may also rely on cholesterol homeostasis. Human fibroblasts treated with either an inhibitor of cholesterol synthesis (pravastatin) or an intracellular cholesterol transport inhibitor (U18666A) for one week showed increased mtDNA clustering (Desai et al., 2017). This suggests that mtDNA may depend on cholesterol for its segregation. A cholesterol-DNA interaction is supported by a study finding mtDNA co-sediments with cholesterol (Gerhold et al., 2015b). Additionally, nutrient availability may also play a role in mtDNA distribution. In control fibroblasts, withdrawal of pyruvate for 48 hours was sufficient to induce mtDNA clustering (Durigon et al., 2018). Moreover, supplementing cells with ketone bodies instead of glucose and pyruvate also induced mtDNA clustering (Durigon et al., 2018). Further studies are needed to examine if nutrient availability and cholesterol synthesis are linked. It would also be important understand how various proteins implicated in mtDNA distribution are united in a common mechanism.

1.11 Mitochondrial dynamics

The mitochondrial network is a dynamic structure. Through coordinated actions of membrane fusion and fission, mitochondria are able to remodel their shapes and sizes and also their distribution within the cell (Figure 1.7). The precise definition of mitochondrial fission is the division of one mitochondrion into two daughter mitochondria; the opposite action, the union of two mitochondria into one, is representative of a mitochondrial fusion event (Tilokani et al., 2018). The mammalian proteins that govern mitochondria morphology are dynamin-related GTPase: mitochondrial constriction is carried out by the dynamin-related/-like protein 1 (DRP1) and dynamin 2 (DNM2); OMM fusion is directed by mitofusin 1 and 2 (MFN1, MFN2) and IMM fusion is mediated by OPA1 (Smirnova et al., 1998; Lee et al., 2016; Chen et al., 2003; Griparic et al., 2004).

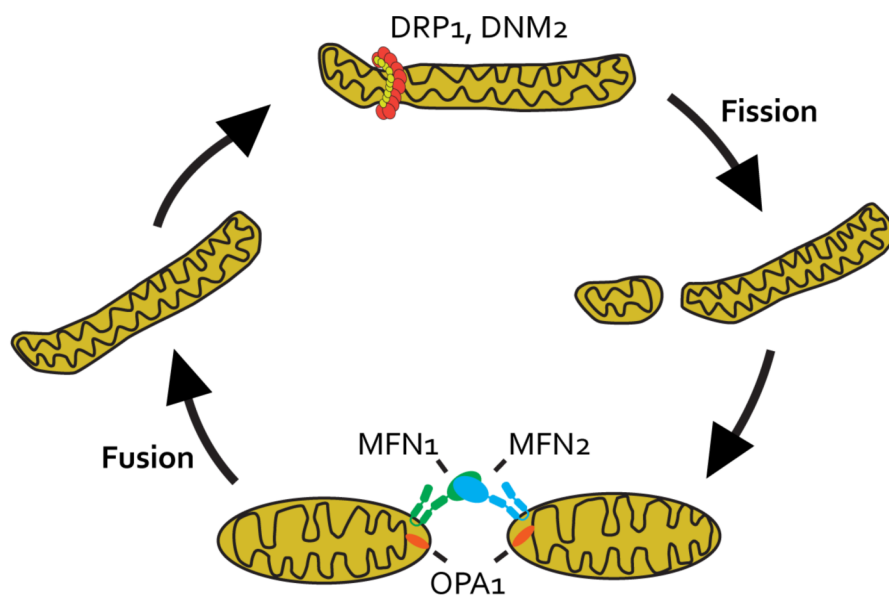


Figure 1.7 Mitochondrial fusion and fission

Mitochondria morphology is dynamic. Through coordinated actions of membrane fusion and fission, mitochondria are able to remodel their shapes and sizes. Division of one mitochondrion into two daughter mitochondria is carried out by dynamin-related/-like protein 1 (DRP1, red) and dynamin 2 (DNM2, yellow). The union of two mitochondria into one is directed by mitofusin 1 (MFN1, green) and mitofusin 2 (MFN2, blue) for OMM fusion and the optic atrophy protein 1 (OPA1, orange) for IMM fusion.

In cultured cells, a balance between mitochondrial fusion and fission maintains a dispersed tubular network (Figure 1.8, Yu and Pekkurnaz, 2018). When the fission activity is not properly controlled, the tubular structure disintegrates into many fragmented mitochondria. The formation of hyperfused mitochondria can occur when the fusion activity is unopposed. In neurons, mitochondria can be observed as being fused in the soma and as individual units in the axons (Misgeld and Schwarz, 2017). In muscle tissue mitochondria are typically organized between the myofibrils as individual spheres. A recent study of skeletal muscle has shown that mitochondria can be remodeled to meet the metabolic state of the fiber through mitochondrial fusion (Mishra et al., 2015). Overall, morphological transitions of mitochondria play a key role in mitochondrial content mixing of protein and lipids, recycling of mitochondria, apoptosis, metabolic adaptations, and immunity.

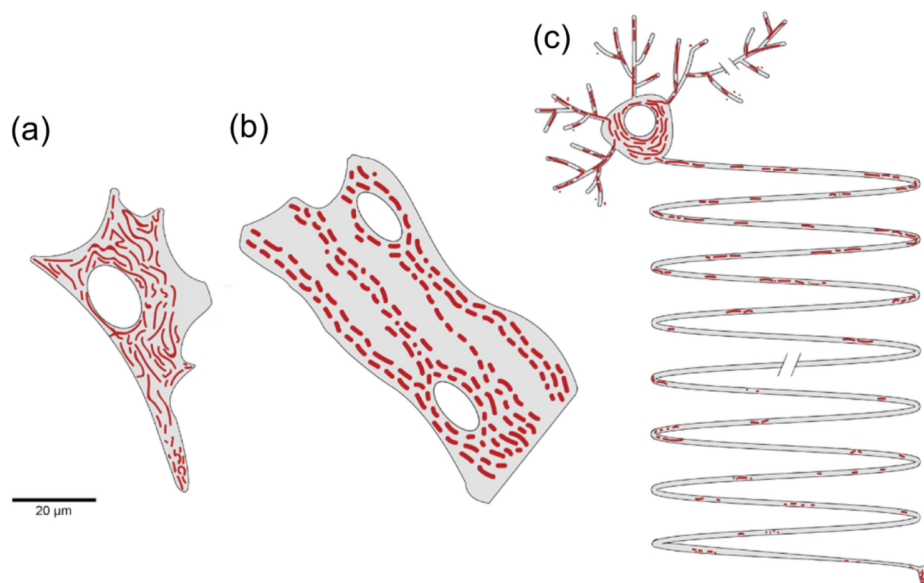


Figure 1.8 The mitochondrial network is tailored to the cellular energetic need

Mitochondrial dynamics influences the shape and distribution of mitochondria to meet the specific bioenergetic demands of different cell types. Cultured fibroblast (a) spread their plasma membrane in all directions. In these cells, mitochondria are evenly distributed throughout all areas of the cell. The mitochondria in fibroblast can be present as elongated and branched structures or in smaller fragments. Cardiomyocytes (b) are highly organized cells. In this cell type, mitochondria are abundant and aligned with the nucleus. Unlike fibroblast, mitochondria in cardiomyocytes are spherical in shape. Neurons (c), on the other hand, have a unique cellular architecture, comprised of a soma body, branched dendrites, and a long axon. In neurons, the majority of mitochondria are found in the soma as an interconnected network, while axonal mitochondria are smaller and fragmented. Most axonal mitochondria are stationary, but a subset of mitochondria travels in anterograde or retrograde directions. Reprinted from Journal of Molecular Biology, Seungyoon B. Yu and Gulcin Pekkurnaz, *Mechanisms orchestrating mitochondrial dynamics for energy homeostasis*, published Aug 5, 2018, with permission from Elsevier; license number: 4414331037700.

1.12 Mitochondrial fission

Much of our understanding about mammalian mitochondrial fission comes from seminal work in budding yeast (Bleazard et al., 1999). The fission GTPases, DRP1 and DNM2, are evolutionary conserved from yeast to mammals. Both of these proteins are found in the cytosol and are recruited not only to mitochondria but also peroxisomes and endocytic vesicles (Tilokani et al., 2018). The mitochondrial fission factor (MFF) and mitochondrial dynamics proteins (MiD49/51) are tail-anchored proteins that mediate recruitment of DRP1 to the OMM under basal conditions (Figure 1.9, Otera et al., 2010; Palmer et al., 2011).

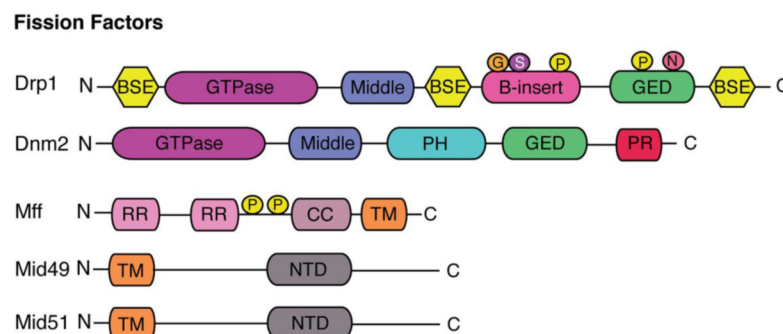


Figure 1.9 Mitochondrial fission proteins

A schematic representation of proteins domains found in Drp1, Dnm2, Mff, Mid49, and Mid51. Abbreviations: post-translational modifications are indicated by P (Phosphorylation), N (S-nitrosylation), S (SUMOylation), G (O-GlcNAcylation), A (Acetylation) or U (Ubiquitination); BSE, bundle signalling elements; CC, coil-coil; GED, GTPase effector domain; NTD, nucleotidyl transferase domains; PH, Pleckstrin homology; PR, Proline rich; RR, repeat regions; TM, transmembrane. Reprinted from *Essays in Biochemistry, Mitochondrial dynamics: overview of molecular mechanisms*, Lisa Tilokani, Shun Nagashima, Vincent Paupe, Julien Prudent, Jul 2018, 62 (3) 341-360; DOI: 10.1042/EBC20170104.

The multi-step process of mitochondrial fission is believed to begin with ER pre-constriction of mitochondria (Figure 1.10, Farmer et al., 2018), decreasing the diameter of mitochondria from 500 nm to 150 nm (Legesse-Miller et al., 2003; Friedman et al., 2011). This pre-constriction of mitochondria allows for recruitment of DRP1 by the adaptor proteins MFF or MiD49/51, followed by DRP1 oligomerization in a ring-like structure (Ingberman et al., 2005; Losón et al., 2013). Lastly, DRP1 constricts mitochondria down to about 55 nm in diameter, a suitable size for DNM2 assembly and oligomerization that finalizes scission of the mitochondrion (Lee et al., 2016).

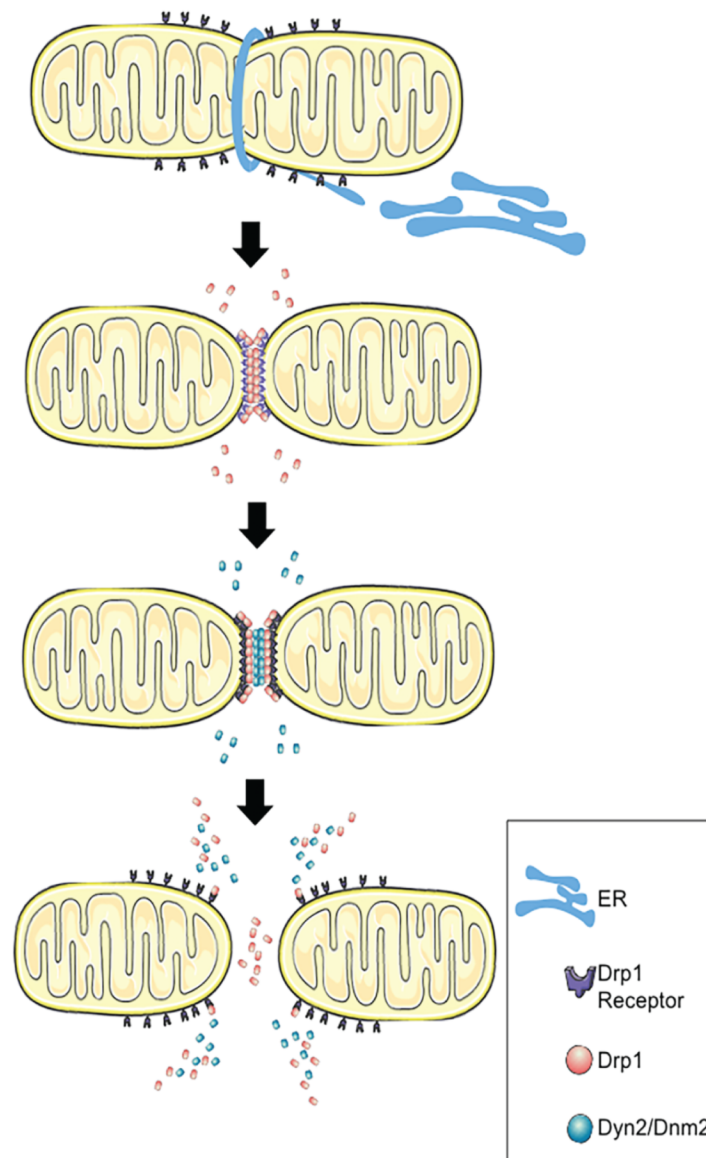


Figure 1.10 Mitochondrial fission

Mitochondrial fission is a multi-step process. The current model suggests that constriction of mitochondria begins with ER pre-constriction of mitochondria to decrease the diameter of mitochondria. This pre-constriction of mitochondria is followed by recruitment of DRP1 to the outer mitochondrial membrane via receptor proteins. DRP1 then oligomerizes into a ring-like structure and further constricts the mitochondrial division site. Lastly, it is proposed that DNM2 assembles on the constriction site, oligomerizes, and scissions the mitochondrion into two daughter mitochondria. Reprinted from Traffic publication, by Trey Farmer, Naava Naslavsky, and Steve Caplan, Tying trafficking to fusion and fission at the mighty mitochondria, published May 11, 2018, with permission from John Wiley and Sons; license number: 4414810252318.

1.13 Mitochondrial fusion

The first mitochondrial fusion protein was described in *Drosophila* and is evolutionary conserved from yeast to humans (Hales and Fuller, 1997; Hermann et al., 1998; Santel and Fuller, 2001). In mammals there are three large transmembrane GTPase proteins that mediate mitochondrial fusion: MFN1, MFN2, and OPA1. In heart tissue, the RNA expression of human MFN2 is the highest (98.9 RPKM) compared to OPA1 (17.2 RPKM) and MFN1 (9.7 RPKM). The sequence similarity between MFN1 and MFN2 is about 77 % (Figure 1.11) and they can form homotypic and heterotypic complexes with each other (Santel and Fuller, 2001; Chen et al., 2003). In addition to mitochondrial fusion, MFN2 has secondary roles in mitochondria-ER tethering and maintenance of coenzyme Q (de Brito and Scorrano, 2008; Mourier et al., 2015). OPA1 is present in two primary isoforms, the S-isoform is produced by proteolytic cleavage of the L-isoform inside mitochondria (Ishihara et al., 2006). The L-isoform was recently shown to heterotypically cooperate with cardiolipin in the IMM and this interaction was sufficient for mitochondrial fusion in proteoliposomes (Ban et al., 2017). However, for complete fusion of OMM and IMM, OPA1 functionally requires MFN1 (Cipolat et al., 2004).

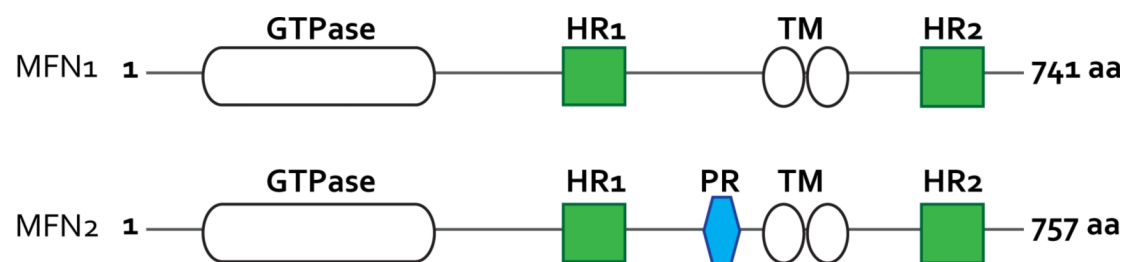


Figure 1.11 OMM fusion proteins

A schematic representation of MFN1 and MFN2 protein domains. Both proteins contain a GTPase domain, two very close transmembrane regions (TM), and two coil-coil heptad repeat domains (HR). Notably, only MFN2 contains a proline-rich domain (PR), believed to be responsible for MFN2's unique protein interactions.

Classical membrane fusion requires tethering, docking, and merging of membranes (Bonifacino and Glick, 2004). The current model of mitochondrial fusion describes the initial step as the tethering of mitofusins on opposing mitochondria (Figure 1.12). Exactly which domain in mitofusins is used for tethering is under debate, which centers on whether the C-terminal coil-coil heptad repeat 2 (HR2) domain or the GTPase domain is the main tethering unit (Koshiba et al., 2004; Cao et al., 2017). A recent study suggest that the C-terminal domain of mitofusins faces the IMS and is redox-regulated to drive fusion (Mattie et al., 2017). After tethering, cycles of GTPase hydrolysis promotes docking of membranes and initial fusion of the OMM (Brandt et al., 2016). This is followed by inner membrane anchoring by OPA1-cardiolipin. Lastly, the Williams-Beuren syndrome critical region 16 protein (WBSCR16) was recently described to act as an OPA1 nucleotide exchange factor that drives the OPA1 GTPase activity required for merger of the IMMs (Huang et al., 2017).

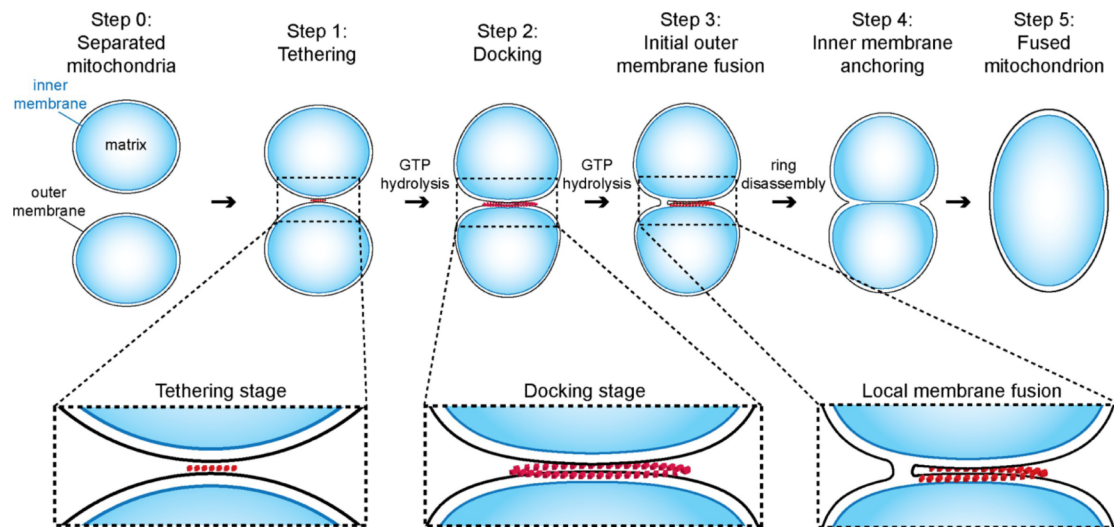


Figure 1.12 Mitochondrial fusion

Fusion of two mitochondria requires tethering and docking at the OMMs by GTPase protein complexes (mitofusin 1 and 2, red). Docking and fusion of the OMMs is driven by GTP hydrolysis. After fusion of the OMMs, protein-lipid complexes (OPA1-cardiolipin) anchor the IMMs and drive membrane fusion. Figure was originally published in the research article *A mitofusin-dependent docking ring complex triggers mitochondrial fusion in vitro*, by Tobias Brandt et al., *eLife*, 2016; DOI: 10.7554/eLife.14618. Published June 02, 2016, Figure is licensed for use under Creative Commons Attribution 4.0 International license (CC BY 4.0), <http://creativecommons.org/licenses/by/4.0/>.

1.14 Research aims

1) To determine the link between mitochondria fusion and mtDNA maintenance

The connection between mitochondrial dynamics and mtDNA maintenance is poorly understood. In the budding yeast, maintenance of mtDNA is absolutely dependent on OMM fusion, whereas the situation is less drastic in mammals (Jones and Fangman, 1992; Rapaport et al., 1998; Chen et al., 2010). The absence of mitochondrial fusion in animal models leads to a strong reduction in mtDNA copy number and has been associated with mtDNA mutagenesis and deletions (Chen et al., 2010; Papanicolaou et al., 2012). However, reduced mitochondrial fusion activity or impaired fission does not affect mtDNA maintenance (Ishihara et al., 2009; Chen et al., 2010; Del Dotto et al., 2017). To address the link between mtDNA maintenance and mitochondrial fusion proteins, molecular and biochemical characterization of mtDNA gene expression and maintenance was performed in heart double *Mfn1-2* knockout animals and mouse embryonic fibroblasts.

2) To determine whether mitochondria fusion plays a role in mtDNA distribution

Although the even distribution of mtDNA within a cell was observed over two decades ago, we still don't fully understand the mechanism. We used super-resolution microscopy of tissues from heart double *Mfn1-2* knockout animals and knockout tissue culture cells to determine how proteins involved in mitochondrial dynamics could influence mtDNA distribution.

2.0 RESULTS

2.1 Generation of *Mfn1* and *Mfn2* conditional heart double knockout mice

The C57BL/6 mouse strain was first generated in the 1920's by Clarence Little in the Jackson Laboratory and the substrain 6N later established in the National Institutes of Health (Kiselycznyk and Holmes, 2011). This mouse strain was chosen for this project as it is widely used in metabolic and mitochondrial studies (Trifunovic et al., 2004; Nikkanen et al., 2016). The genes encoding for *Mfn1* and *Mfn2* were genetically modified to carry loxP sites flanking exon 3 of the *Mfn1* and exon 5 of *Mfn2*. Mice with *Mfn1*^{loxP/loxP} or *Mfn2*^{loxP/loxP} genes were generated by Taconic Biosciences and previously described in (Lee et al., 2012).

To generate double mitofusin1-2 loxP-flanked homozygous mice (*dMfn*), *Mfn1*^{loxP/loxP} and *Mfn2*^{loxP/loxP} animals were crossed. It was previously reported that whole body mitofusin 1-2 knockout animals are embryonic lethal (Chen et al., 2010; Papanicolaou et al., 2012). Therefore, we chose to conditionally knockout (KO) both mitofusins in heart tissue, where mitochondria are abundant and mitofusins highly expressed. The muscle creatine kinase promoter (Ckmm) was chosen to control the expression of the Cre-recombinase (Cre) gene in heart and skeletal muscle. *Mfn1* and *Mfn2* conditional heart double knockout mice (*dMfn* KO) were generated by crossing *Mfn1*^{loxP/loxP}, *Mfn2*^{loxP/loxP}, *Cre*^{-/-} and *Mfn1*^{loxP/loxP}, *Mfn2*^{loxP/+}, *Cre*^{-/+} animals. Pups were born at the expected mendelian ratios (Figure 2.1A and B).

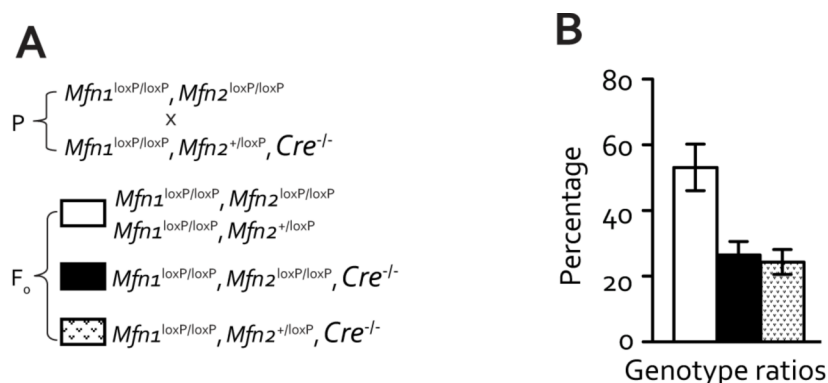


Figure 2.1 Breeding Scheme and Mendelian Ratios

(A) Breeding scheme with genotypes of parents (P) that were intercrossed to generate control and *dMfn* heart KO pups (F₀). (B) Genotype distribution of progeny born from seven intercrosses (n=52) between *Mfn1*^{loxP/loxP}, *Mfn2*^{loxP/loxP}, *Cre*^{-/-} and *Mfn1*^{loxP/loxP}, *Mfn2*^{+/loxP}, *Cre*^{-/-} animals.

2.2 Loss of *Mfn1* and *Mfn2* in heart tissue was verified

Gene deletion was verified by assessing mitofusin1 and 2 transcript levels in heart tissue. Mitofusin1 and 2 transcripts in heart tissue were dramatically reduced in *dMfn* KO animals compared to controls (Figure 2.2A). Additionally, gene deletion was verified by western blot analysis. The steady-state protein levels of mitofusin 1 were absent, while traces of mitofusin 2 were detected *dMfn* KO mitochondria (Figure 2.2B). The residual mitofusin transcripts and protein levels observed may be explained by the fact that heart tissue contains other cell types besides cardiomyocytes, such as endothelial cells and fibroblast (Pinto et al., 2016). Together these data confirmed the generation of *Mfn1* and *Mfn2* conditional heart double knockout mice.

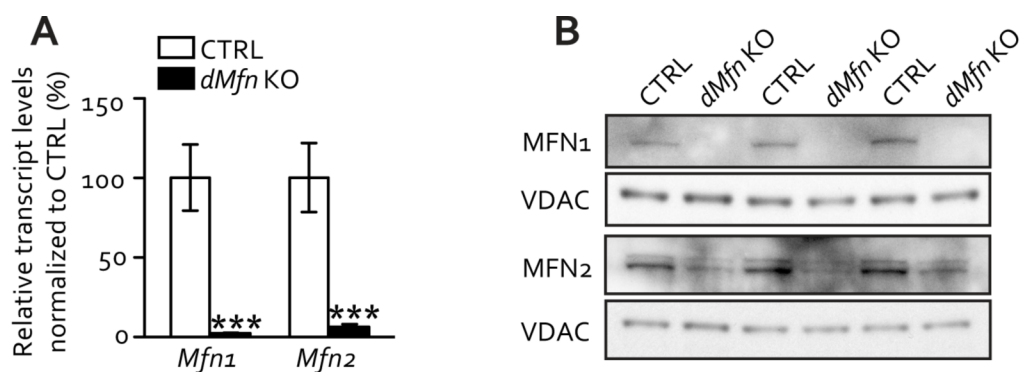


Figure 2.2 Verification of the loss *Mfn1* and *Mfn2* in heart tissue

(A) RT-PCR quantification of transcripts in heart from control (n=4) and *dMfn* KO (n=5) animals at 4 weeks of age. Normalization to beta-2-microglobulin. (B) Steady-state levels of mitofusin proteins determined by western blot analysis of heart mitochondria from control and *dMfn* KO animals at 3 weeks of age. Error bars indicate \pm SEM. Student T-test; ***, $P < 0.001$.

2.3 Physiological characterization of *dMfn* KO animals

Pups of the different genotypes were indistinguishable up to two weeks of age, when a minor decrease in body size was observed in *dMfn* KO animals. At five weeks of age, *dMfn* KO animals showed no difference in heart weight compared to control littermates (Figure 2.3A). However, the same animals had nearly 50 % less body weight (Figure 2.3B). The heart weight to body weight ratio showed that the *dMfn* KO animals had cardiomyopathy (Figure 2.3C). Most *dMfn* KO animals survived until postnatal age of 5-6 weeks and likely died from heart failure or arrhythmia. Transmission electron microscopy analysis of heart sections at 5 weeks of age revealed an increase in mitochondrial mass in *dMfn* KO animals (Figure 2.4A). Mitochondria were also disorganized, no longer displaying a classical linear arrangement between the myofibrils (Figure 2.4B). At higher magnifications, aberrant mitochondrial ultrastructure could be observed (Figure 2.4B).

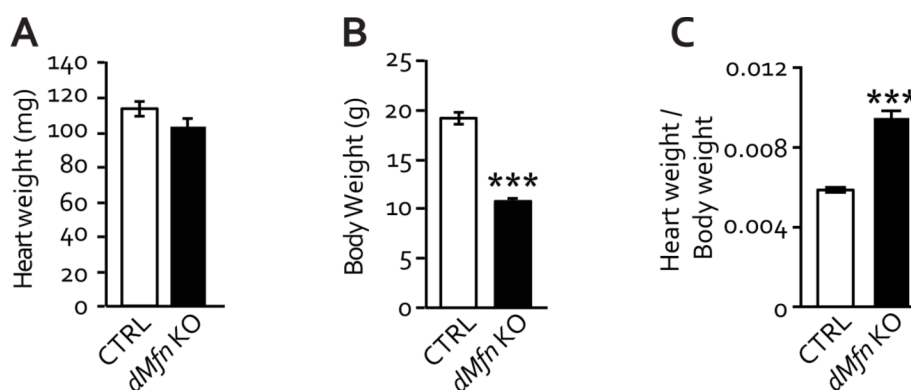


Figure 2.3 Characterization of *dMfn* KO animals

(A) Heart weight of male and females control and *dMfn* KO mice at 5-6 weeks of age. (B) Body weight of male and females control and *dMfn* KO mice at 5-6 weeks of age. (C) Heart weight to body weight ratio of male and female control and *dMfn* KO mice at 5-6 weeks of age. For (A-C), control (n=19), *dMfn* KO (n=13) mice. Error bars indicate \pm SEM. Student T-test; ***, P < 0.001.

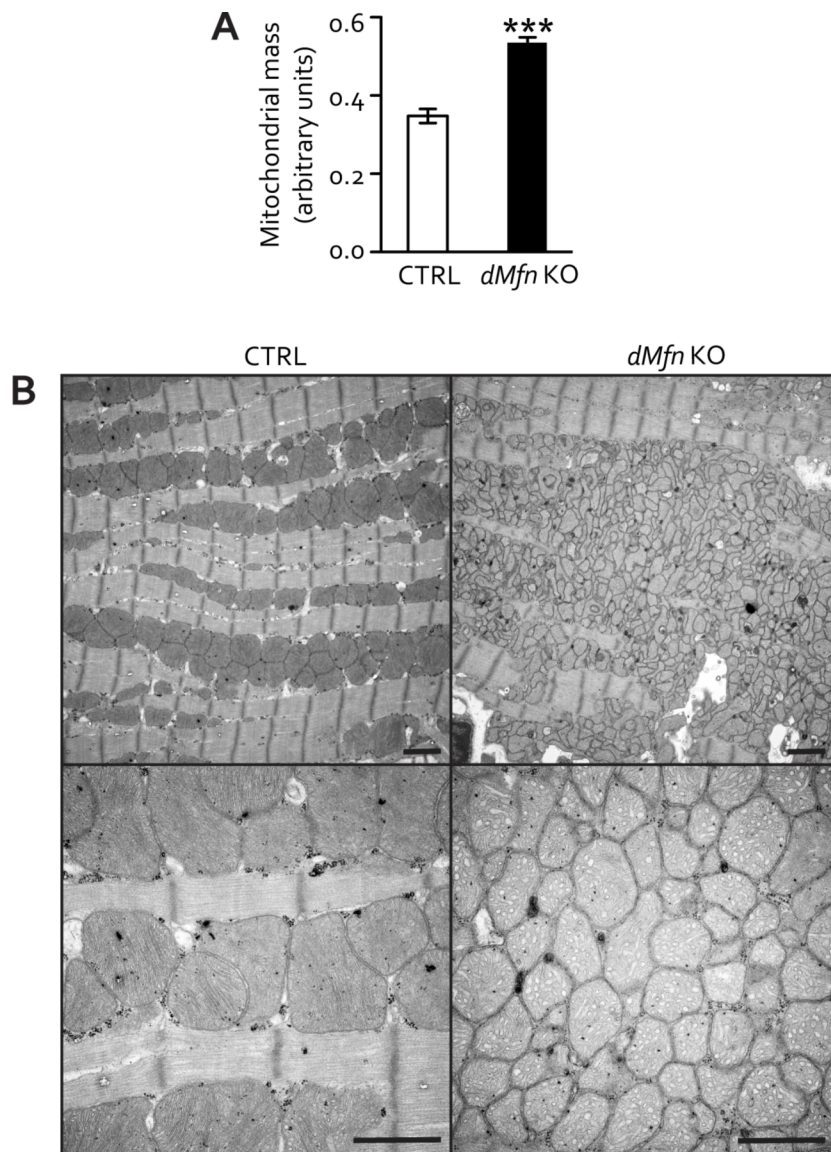


Figure 2.4 *dMfn* KO animals have an increase in mitochondrial mass

(A) Electron microscopy analysis for mitochondrial mass in heart tissue of control (n=5) and *dMfn* KO (n=3) at 5 weeks of age. (B) Representative electron microscopy images of heart tissue from control and *dMfn* KO animals at 5 weeks of age. For each genotype, 3-5 biological replicates were analyzed. Scale bars represent 2 μ m (top) and 1 μ m (bottom). Error bars indicate \pm SEM. Student T-test; ***, $P < 0.001$.

2.4 *dMfn* KO animals exhibit mitochondrial respiratory dysfunction

Mitochondrial respiration is essential for the conversion of ADP into ATP, the cellular energy currency (Figure 2.5A). Moreover, mitochondrial fusion proteins have been implicated in maintaining mitochondrial respiration (Mishra et al., 2014; Mourier et al., 2015). To examine the consequences of loss of outer mitochondrial fusion, extensive bioenergetic characterization was performed. The steady-state levels of various respiratory subunits as determined by western blot were reduced in *dMfn* KO heart mitochondria (Figure 2.5B). Proteomic analysis of isolated heart mitochondria revealed many other respiratory subunits decreased in *dMfn* KOs, the majority belonging to complex I (Figure 2.6). Proteins involved in the intra-mitochondrial CoQ synthesis pathway proteins BN-PAGE analysis of heart mitochondria solubilized in DDM showed individual OXPHOS complexes decreased in *dMfn* KO, with the exception of complex II (Figure 2.5C). Similar to other mouse models displaying mitochondrial respiratory defects (Kühl et al., 2016; Mourier et al., 2014), the ATP_{5A}-containing free F₁ part of complex V was detected in *dMfn* KO heart mitochondria (Figure 2.5C). Additional BN-PAGE analysis of heart mitochondria solubilized in digitonin revealed reduced levels of respiratory chain supercomplexes and respirasomes (I+III₂+IV₁) in *dMfn* KO animals (Figure 2.5D).

Functional assessment of the mitochondrial respiratory complexes showed impaired enzymatic activity in *dMfn* KO heart mitochondria, at the level of complex I and V (Figure 2.7A). High-resolution respirometry with substrates that will deliver electrons to complex I (pyruvate, glutamate, malate) or complex II (succinate + rotenone) demonstrated a significant loss of respiration under phosphorylating and uncoupled conditions in *dMfn* KO heart mitochondria (Figure 2.7B). The impairment of respiration limited mitochondrial ATP production in *dMfn* KO heart mitochondria (Figure 2.7C). Interestingly, in *dMfn* KO heart mitochondria the yield of ATP relative to oxygen consumption reached a similar ratio as controls (Figure 2.7D). This suggests that the OXPHOS defects were not due to uncoupling of mitochondria, because there was no change in non-phosphorylating respiration (Figure 2.7B) or per ATP produced and per oxygen consumed (Figure 2.7D). In summary, loss of mitochondrial fusion in heart tissue impairs OXPHOS capacity but does not alter the proton conductance of the IMM.

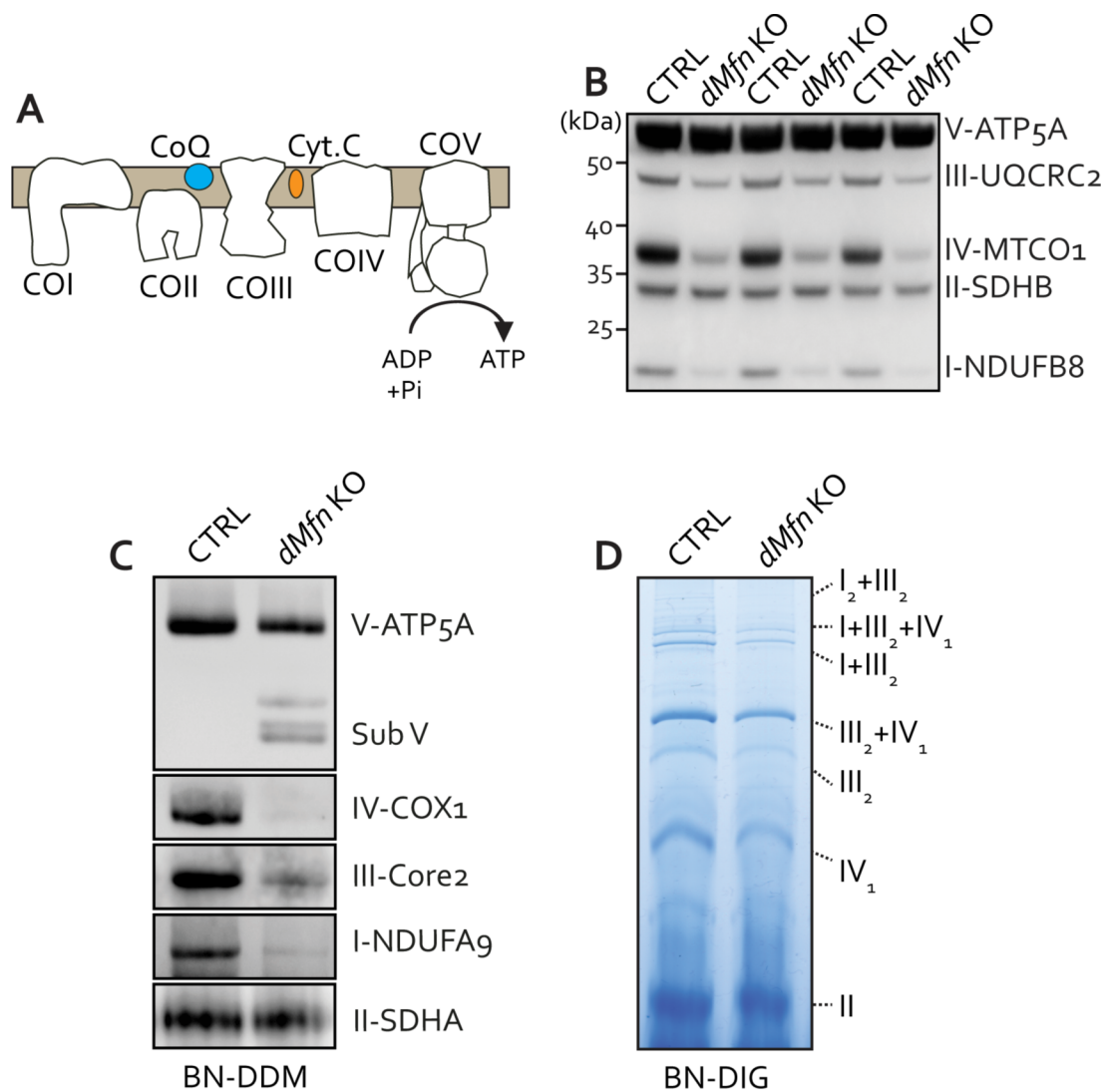


Figure 2.5 *dmfn* KO animals have reduced respiratory subunits and complexes

(A) Simplified scheme of the oxidative phosphorylation system composed of complex I (COI) through complex V (COV) as well as the soluble electron carriers coenzyme Q (CoQ) and cytochrome C (Cyt.C). Conversion of ADP into ATP by the addition of inorganic phosphate (Pi) takes place at COV. (B) Western blot on heart mitochondria showing steady-state levels of different OXPHOS subunits of control and *dmfn* KO between 6 weeks of age, $n=3$ for each genotype. (C) Representative blot of BN-PAGE analysis showing individual OXPHOS complexes of control and *dmfn* KO heart mitochondria solubilized in 1 % DDM at 5 weeks of age, $n=4$ for each genotype. ATP₅A subassemble complexes (Sub V) were observed. (D) Representative Coomassie stained BN-PAGE gel showing various supercomplexes of the respiratory chain in control and *dmfn* KO heart mitochondria solubilized in 1 % digitonin at 4-5 weeks of age, $n=3$ for each genotype.

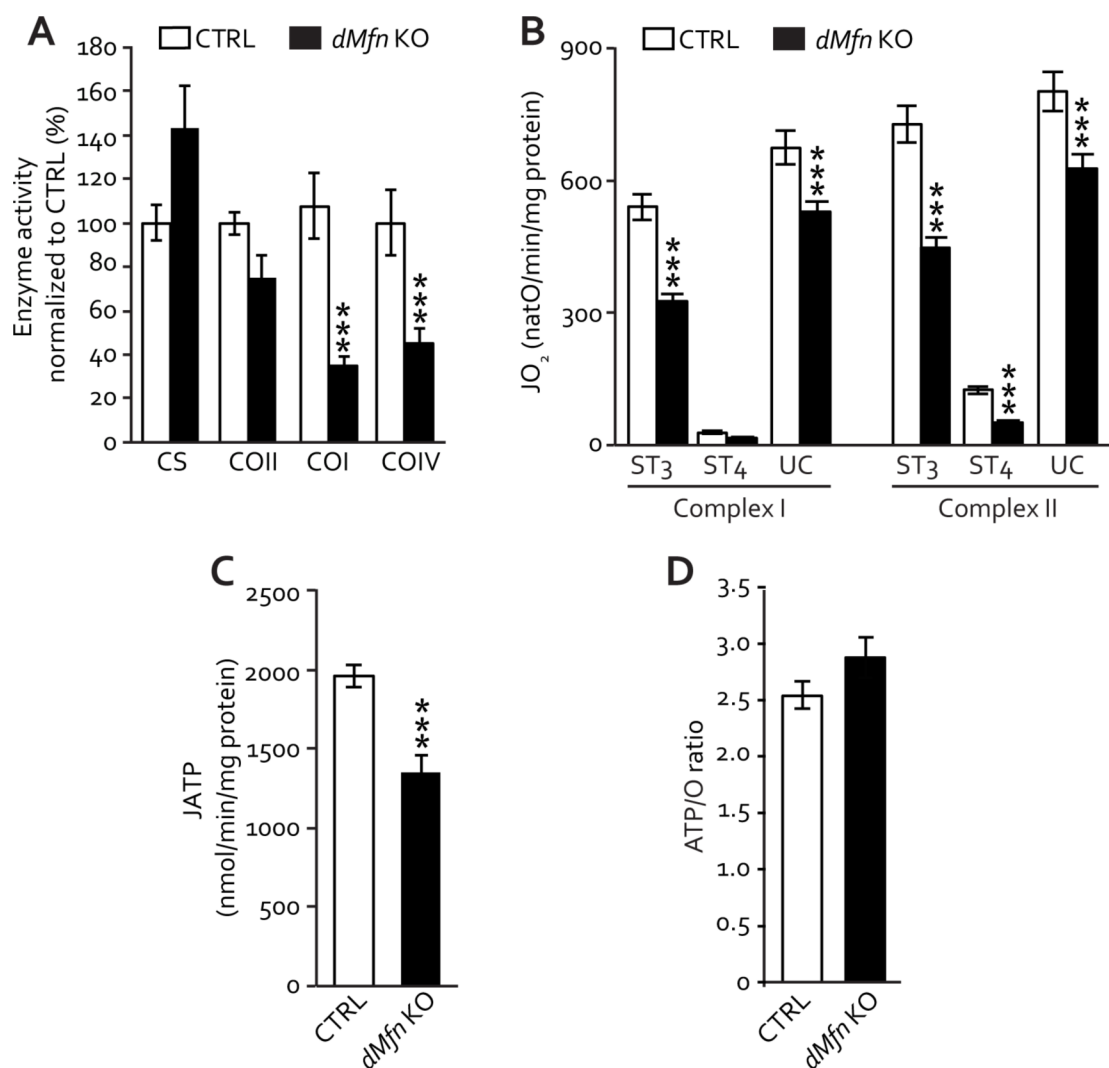


Figure 2.7 Heart *dMfn* KO animals exhibit mitochondria respiratory impairment

(A) Citrate synthase (CS) and respiratory chain enzyme activity (CI, CII, and CIV) was evaluated from isolated heart mitochondria from control (n=10) and *dMfn* KO (n=10) animals at 5 weeks of age. (B) Oxygen consumption rate of heart mitochondria isolated from control and *dMfn* KO animals at 5 weeks of age, n=10 for both genotypes. Mitochondrial respiration was assessed under phosphorylating (ST₃), non-phosphorylating (ST₄), and uncoupled (UC) conditions using complex I substrates (pyruvate, glutamate, malate) and complex II substrates (succinate). (C) Mitochondrial ATP synthesis rate of isolated heart mitochondria under phosphorylating conditions in presence of succinate and rotenone, determined in control and *dMfn* KO animals at 5 weeks of age, n=10 for both genotypes. (D) Oxidative phosphorylation yield (ATP synthesized per oxygen consumed) assessed in presence of succinate, rotenone and ADP, in heart mitochondria isolated from control and *dMfn* KO animals at 5 weeks of age (n=10 for each genotype). Error bars indicate \pm SEM. Student T-test; ***, P < 0.001.

2.5 *dMfn* KO heart mitochondria have mevalonate pathway defects

Coenzyme Q (CoQ) is a hydrophobic electron carrier between complex I-III and II-III of the respiratory chain. Previous research on single *Mfn1* and *Mfn2* knockouts animals and MEFs uncovered that MFN2 is required for OXPHOS activity by maintaining mitochondrial CoQ levels (Mourier et al., 2015). Although loss of MFN1 leads to a decrease in proteins associated with CoQ synthesis, the CoQ levels remained unaltered (Mourier et al., 2015). To determine whether loss of both mitofusins exacerbates the CoQ phenotype of single mitofusin KOs, we assessed hydrogen peroxide production and CoQ abundance in fusion-deficient heart and MEFs.

Mitochondrial peroxidic yield in *dMfn* KO heart mitochondria under phosphorylating conditions was similar to control (Figure 2.8A and B). In contrast, under non-phosphorylating conditions peroxidic yield was increased in *dMfn* KO heart mitochondria (Figure 2.8A and B). As complex I is a major site for ROS production, reverse electron flow from complex II to I was assessed. *dMfn* KO heart mitochondria were found to generate less hydrogen peroxide by reverse electron flow (Figure 2.8C and D). This finding suggests that the CoQ levels may be affected. Next, the abundance of CoQ₉ and CoQ₁₀ were determined by UPLC-MS/MS in *dMfn* KO heart mitochondria. Mutant animals had nearly 50 % CoQ₉, the most abundant form of CoQ in mice (Figure 2.9A). This finding was corroborated in cultured cells. Both *dMfn* KO and *Opaz1* KO MEFs showed CoQ_{9/10} depletion, to a similar degree as *Mfn2* KO MEFs (Figure 2.9B). Proteomic analysis comparing control and *dMfn* KO SILAC-labeled cells revealed several biological processes and pathways involved in cellular functions up regulated in *dMfn* KO MEFs (cell cycle, cytoskeleton organization). The majority of proteins downregulated were linked to mitochondrial function, corroborating the OXPHOS defect observed in *dMfn* KO heart mitochondria (Figure 2.9C). Interestingly, several proteins (IDI1, FDPS, MVD, and MVK) that require the mevalonate pathway backbone (terpenoid, sterol, cholesterol synthesis) were also down regulated in *dMfn* KO MEFs (Figure 2.9C and D). In summary, loss of mitofusin1-2 is associated with CoQ depletion linked to defects in its biosynthetic pathways. However, impaired mitochondrial respiration was driven primarily by loss of respiratory components rather than CoQ depletion.

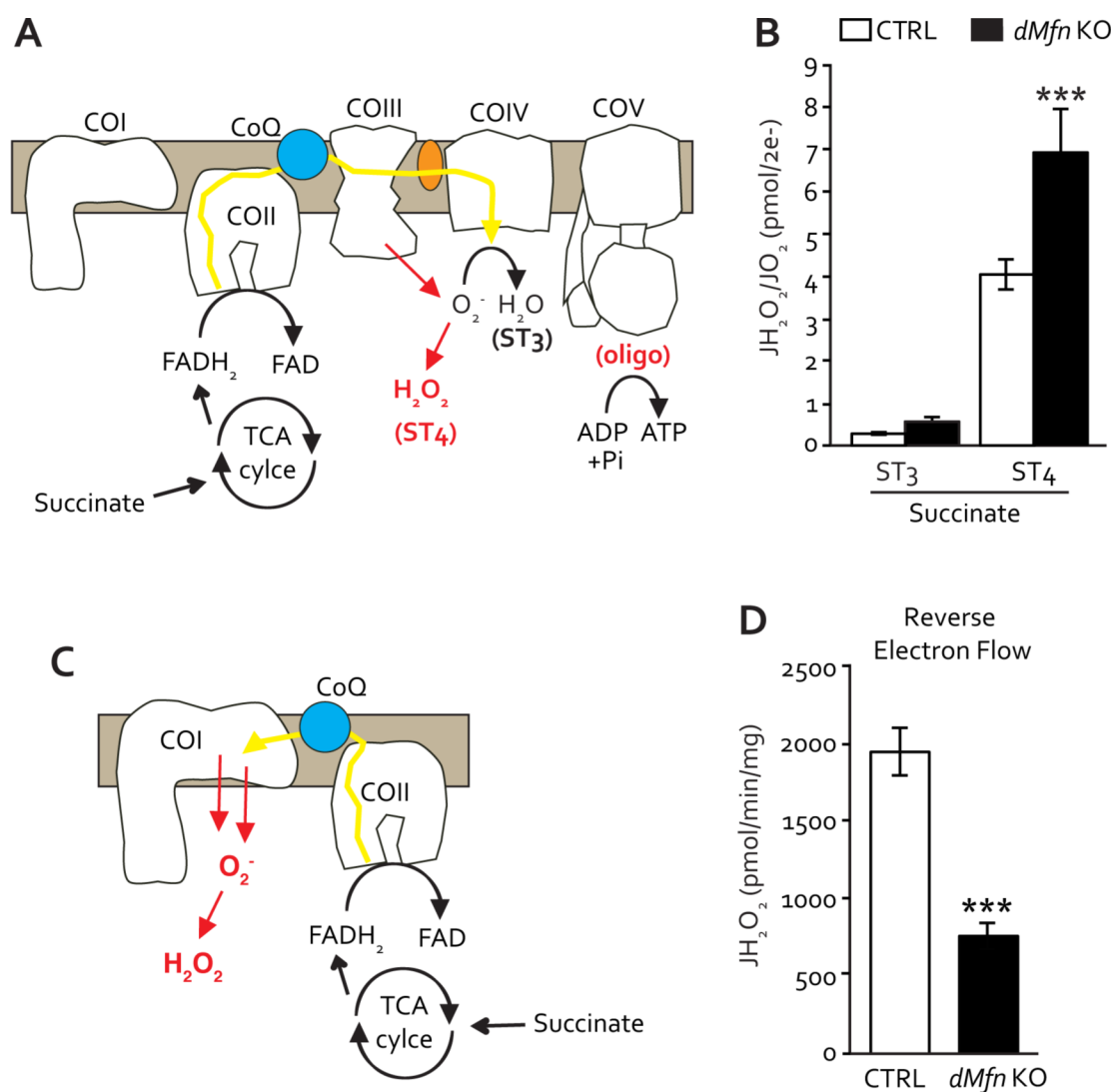


Figure 2.8 *dmfn* KO animals produce less ROS at the level of complex I

(A) Simplified scheme of hydrogen peroxide production with complex II substrate under phosphorylating (ST₃) and non-phosphorylating (ST₄) conditions. (B) Peroxidic yield (ratio between the hydrogen peroxide production and oxygen consumption flux) assessed in heart mitochondria isolated from control (n=5) and *dmfn* KO (n=3) animals at 5 weeks of age. The ratio was accessed in the presence of succinate, rotenone under phosphorylating (ST₃) and non-phosphorylating with the addition of oligomycin (ST₄). (C) Simplified scheme of hydrogen peroxide production by reverse electron flow (complex II to I) under non-phosphorylating (ST₄) conditions. (D) Hydrogen peroxide produced by the complex I through reverse electron flow in the presence of succinate under non-phosphorylating conditions in heart mitochondria isolated from control (n=5) and *dmfn* KO (n=3) animals at 5 weeks of age. Error bars indicate \pm SEM. Student T-test; ***, $P < 0.001$.

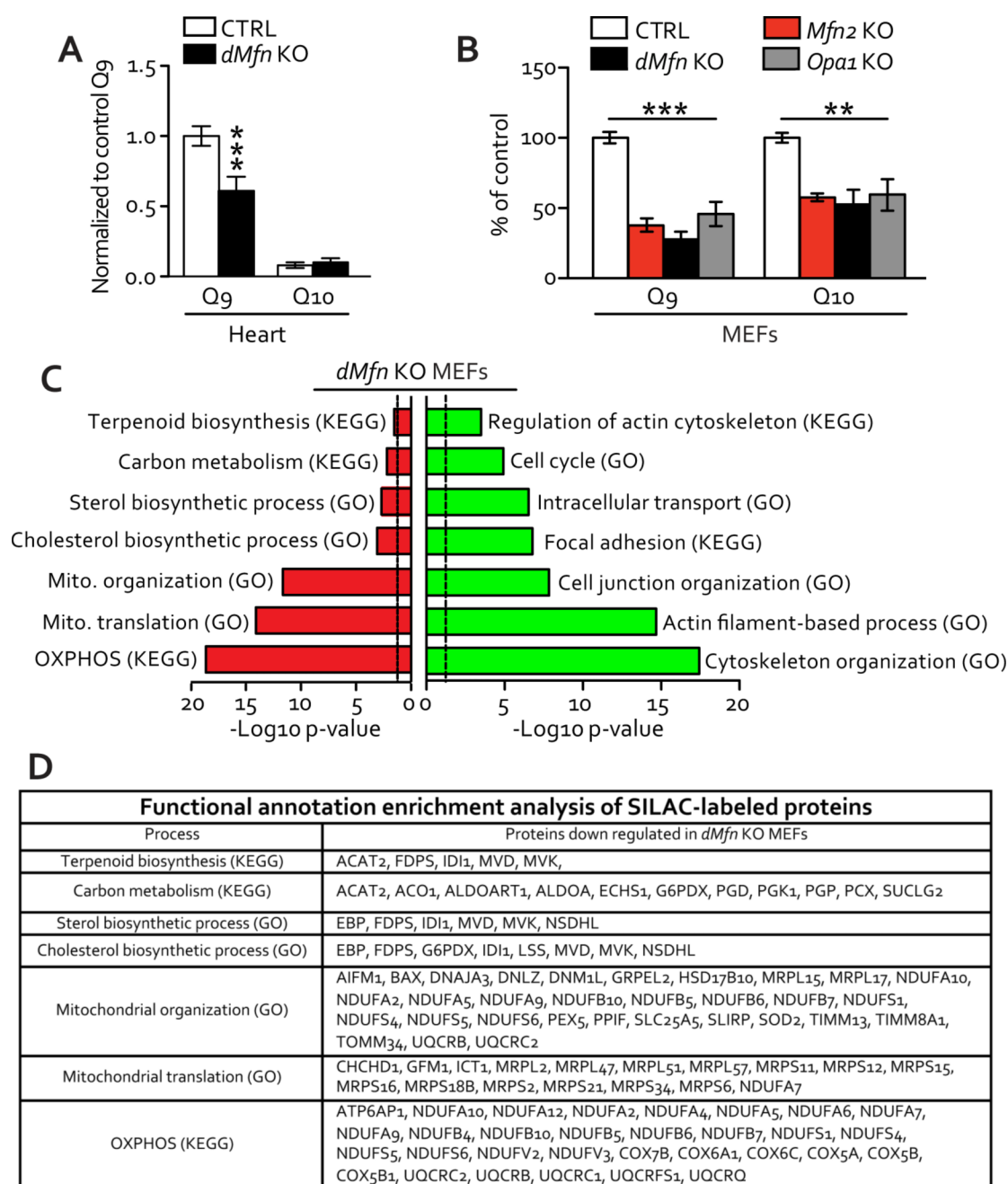


Figure 2.9 *dMfn* KO animals and MEFs exhibit CoQ depletion

(A) Coenzyme Q quantification of heart tissue from control and *dMfn* KO animals at 5-6 weeks of age, $n=4$ for both genotypes. (B) Quinone quantification of whole cell extracts isolated from control, *Mfn2* KO, *dMfn* KO, *Opa1* KO MEFs grown for one week in DMEM media supplemented with 1 % dialyzed FBS, Pen/Strep, NEAA, and uridine ($n=5$ for each genotype). (C) Functional annotation enrichment analysis of SILAC-labeled proteins found down regulated (red) and up regulated (green) in *dMfn* KO MEFs from 6 biological samples. Only functional categories that pass the 0.05 adjusted FDR (Benjamini) are annotated and presented as $-\text{Log}_{10}$ of the p-value. The broken dash-line shows the 0.05 threshold p-value. (D) List of down regulated proteins found enriched in each GO biological process category or KEGG pathway, related to (C). Error bars indicate \pm SEM. Student T-test; **, $P < 0.01$; ***, $P < 0.001$.

2.6 Loss of OMM fusion does not increase mtDNA deletions or point mutations

A prevailing theory in the field is that mitochondrial fusion plays a role in mtDNA stability (Chen et al., 2010; Viscomi and Zeviani, 2017). To examine the integrity of mtDNA, a sensitive read-out for mtDNA deletions was performed Illumina sequencing. With this technique we were able to analyze the frequency of mtDNA breakpoints, a signature of mtDNA deletions. We found no difference in the incidence of mtDNA deletions between control and *dMfn* KO animals (Figure 2.10A and B). In comparison, high levels of mtDNA rearrangements were detected in the deleter mouse (Figure 2.10C), which harbors a patient mutation in the DNA helicase *twinkle* (A360T) that leads to accumulation of mtDNA deletions (Tynismaa et al., 2005). Moreover, mtDNA mutation load analysis revealed no significant difference between control and *dMfn* KO heart tissue (Figure 2.10D). Together, these data suggest that OMM fusion is not required to ensure the integrity of mtDNA in heart tissue.

2.7 Loss of OMM fusion results in mtDNA depletion

Loss of OMM or IMM fusion has been associated with a dramatic decrease in mtDNA copy number (Chen et al., 2010; Papanicolaou et al., 2012). Southern blot analysis of mtDNA in heart tissue showed mtDNA levels depleted by 50 % in *dMfn* KO animals (Figure 2.11A and B). This reduction in mtDNA was confirmed by qPCR analysis of heart tissue, where a similar reduction in mtDNA levels was observed (Figure 2.11C). Furthermore, mtDNA depletion was far more drastic in *dMfn* KO MEFs as determined by qPCR and image analysis of mtDNA foci (Figure 12B-D). These results indicate that mitochondrial fusion plays a prominent role in maintaining mtDNA levels.

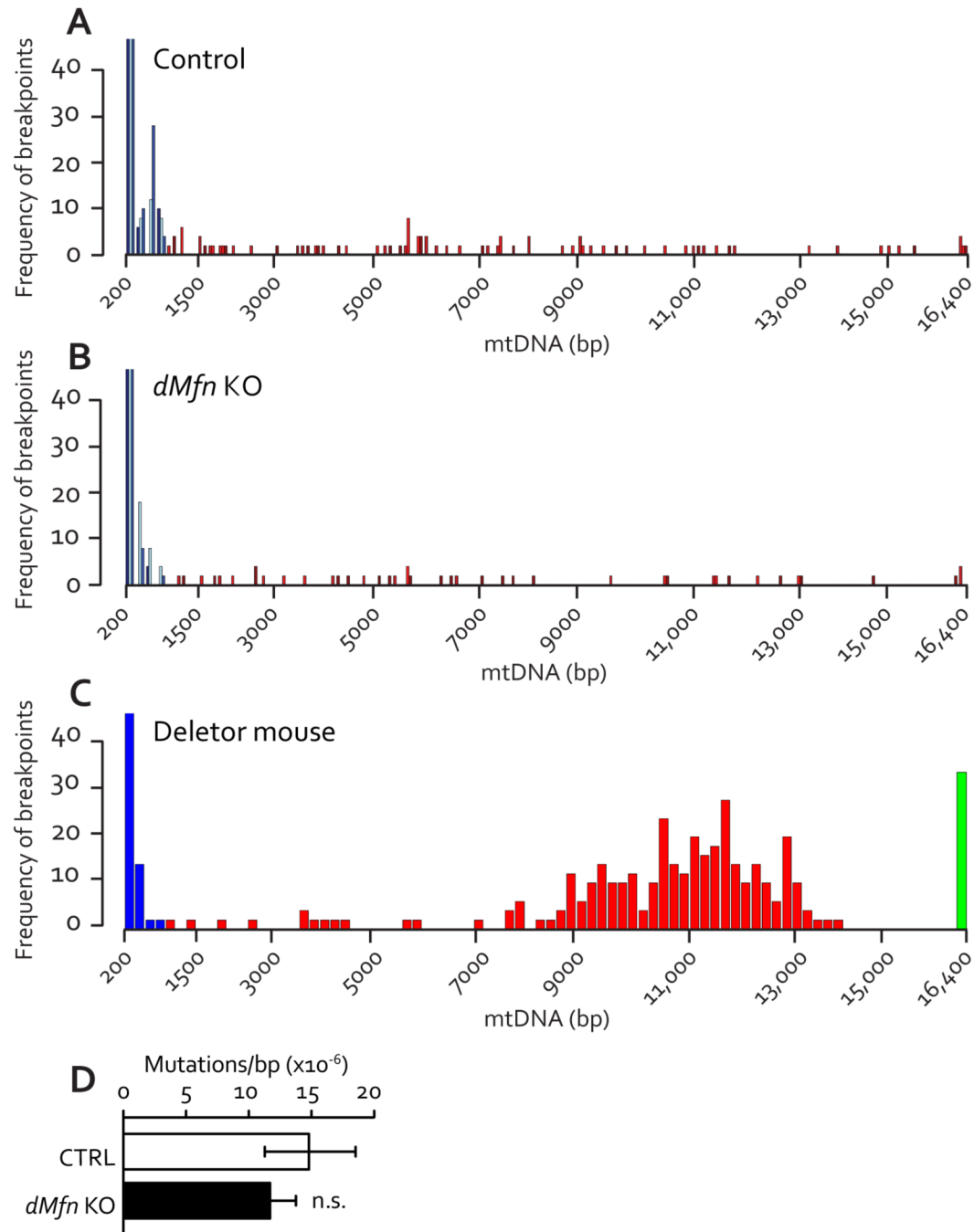


Figure 2.10 Loss of OMM fusion does not increase mtDNA deletions or point mutations

(A) Analysis of mitochondrial DNA deletion frequency from hearts of control (A), *dMfn* KO (B), and Deletor (C) animals at 5 weeks of age as determined by Illumina sequencing (n=3 for control and *dMfn* KO, n=1 Deletor mouse). Each graph shows all reads from individual animals with an incorrect long or short insert size, which are plotted as bins along the x-axis. The frequency of detected breakpoints is plotted on the y-axis. Blue bins represent variations in the fragment size and not deletion breakpoints and red bins denote deletions larger than 600 bases. In the deletor mice, a green bin at position 16,400 kb signifies deletion breakpoints encompassing the first and last positions of the reference sequence, leading to difficulties in assessing the true size of the deletion. Shades of blue and red indicate different individual animals within a group. (D) Mitochondrial DNA mutation load analysis in heart from control and *dMfn* KO animals at 5-6 weeks of age, n=3 for both genotypes. Error bars indicate \pm SEM. n.s., no statistical significance.

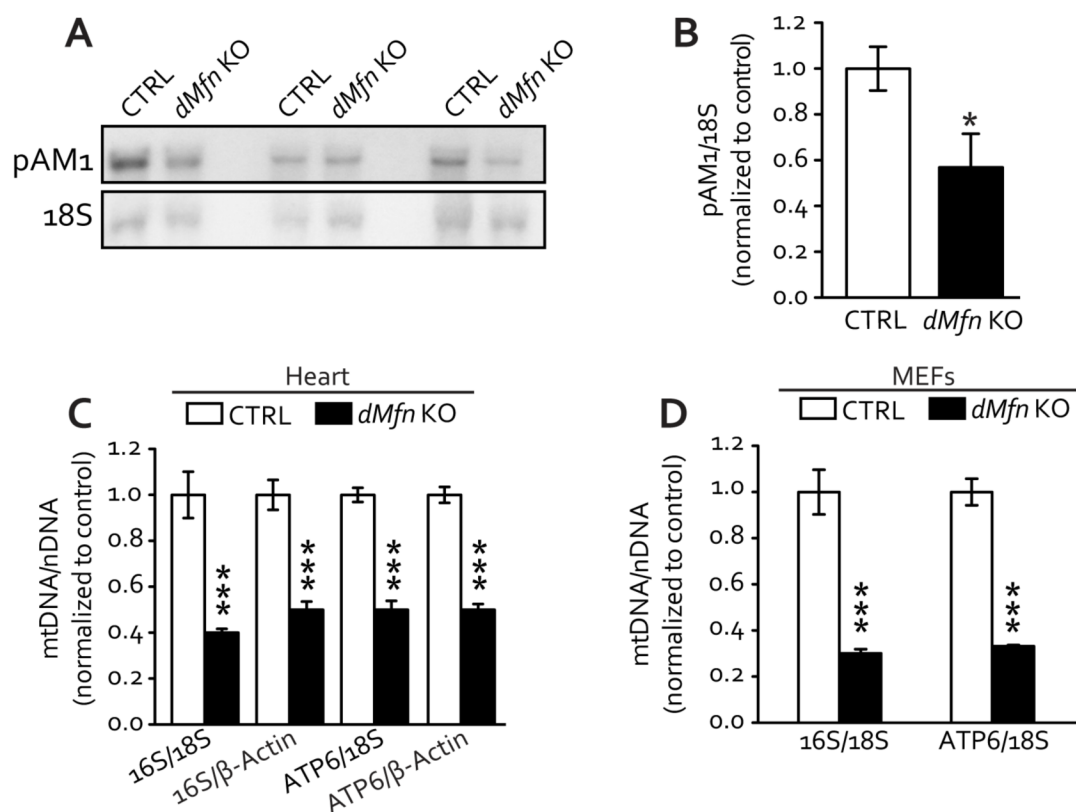


Figure 2.11 Confocal and STED microscopy resolution comparison of mtDNA foci

(A) Southern blot of control and *dMfn* KO total heart DNA samples ($n=3$ for each genotype) at 5 weeks of age. Linearized mtDNA was probed with pAM₁ (mouse mtDNA sequence). (B) Quantification of mtDNA levels by Southern blot analyses of control and *dMfn* KO heart DNA samples ($n=3$ for each genotype) at 5 weeks of age, related to (A). The mtDNA levels (pAM₁) were normalized to nuclear DNA (18S). (C) Quantitative PCR analysis of mtDNA copy number (16S and ATP6) normalized to nuclear DNA (β -Actin and 18S) from heart samples of control and *dMfn* KO at 5 weeks of age ($n=5$ of for each genotype). (D) Quantitative PCR analysis of mtDNA copy number (16S and ATP6) normalized to nuclear DNA (18S) from control and *dMfn* KO MEFs, $n=4$ of for each genotype. Error bars indicate \pm SEM. Student T-test; *, $P < 0.05$; ***, $P < 0.001$

2.8 Loss of OMM fusion leads to nucleoid clustering

Hundreds to thousands of nucleoids can be found in a different cell types and are typically found evenly distributed (Kukat et al., 2011). The mechanism and the complete set of proteins involved in nucleoid distribution remain elusive. To determine if mitochondrial fusion plays a role in mtDNA distribution, an immunofluorescence approach was implemented to examine nucleoid distribution in heart and MEFs. Confocal microscopy of heart sections immunostained with anti-DNA antibodies showed nucleoid foci in high abundance and evenly distributed in control animals (Figure 2.12A). In contrast, nucleoids were visibly reduced and often found as enlarged foci in *dMfn* KO heart sections (Figure 2.12A). These enlarged nucleoid foci were more prominent in *dMfn* KO MEFs (Figure 2.12B).

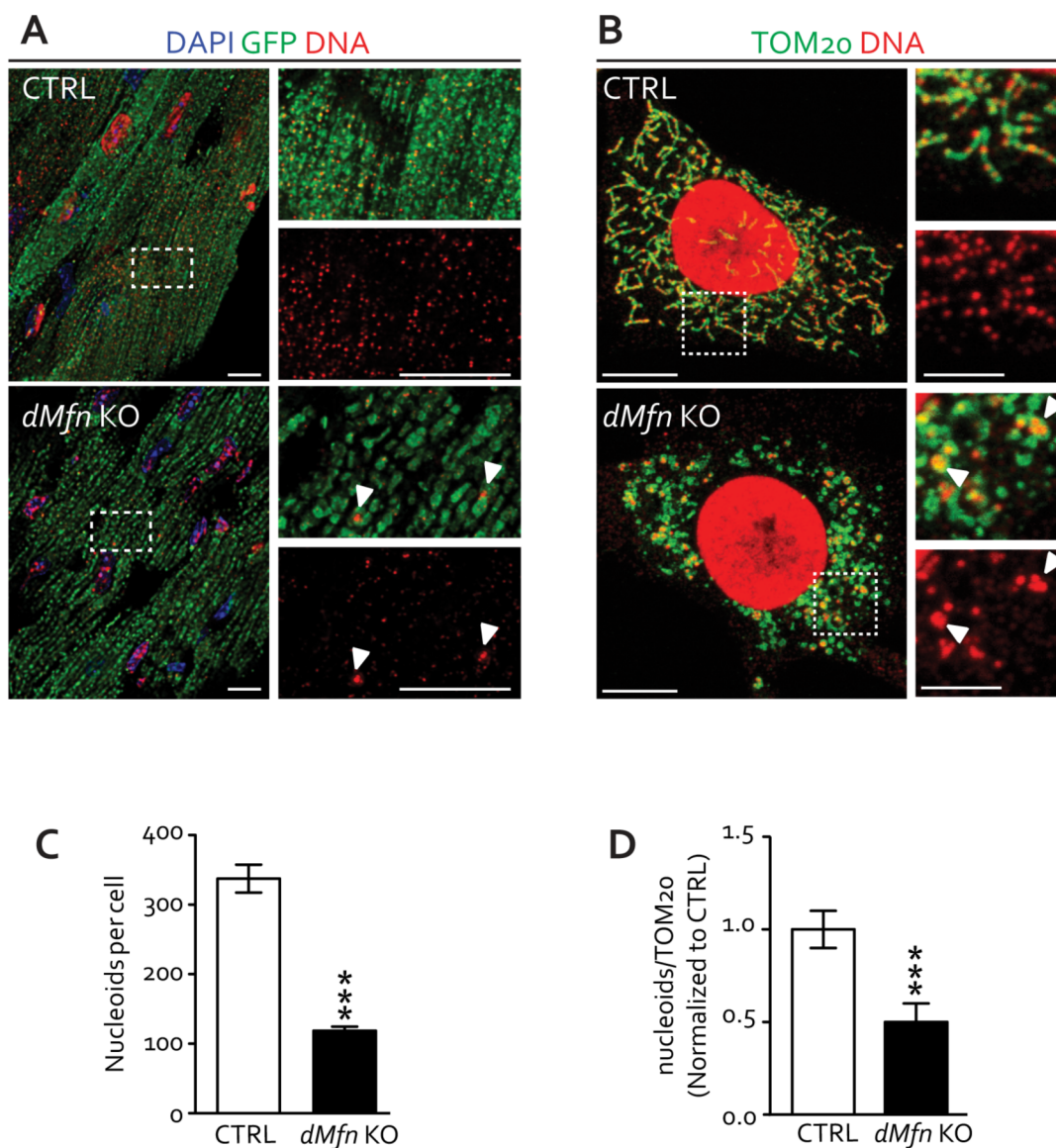


Figure 2.12 Confocal microscopy resolves mtDNA as enlarged molecules in *dMfn* KO heart and MEFs

(A) Representative confocal microscopy images of heart sections from control and *dMfn* KO animals at 4 weeks of age. Tissue samples were decorated with anti-GFP and anti-DNA antibodies, followed by DAPI staining. Dashed boxes specify area of magnification shown in the panels to the right. Scale bars represent 10 μ m. Staining patterns were determined in two independent experiments per genotype. (B) Confocal microscopy images of control and *dMfn* KO MEFs immunostained to detect TOM20 protein and mtDNA. Dashed boxes specify area of magnification shown in the panels to the right. Scale bars, main image 10 μ m, zoom-in 5 μ m. Three independent experiments per genotype. White arrows point to examples of enlarged mtDNA foci. (C) Quantification of nucleoids per cell from control and *dMfn* KO MEFs. Total nucleoids were counted from stacked confocal images decorated with anti-DNA antibodies. In total, 3 independent experiments were performed for each genotype and 9-11 cells measured per experiment. (D) Quantification of nucleoids per mitochondrial surface area (TOM20) from control and *dMfn* KO MEFs. Total nucleoids and the mitochondrial surface area were determined from stacked confocal images. In total, 3 independent experiments were performed for each genotype and 9-11 cells measured per experiment. Error bars indicate \pm SEM. Student T-test; ***, $P < 0.001$.

Confocal microscopy has a theoretical resolution limit of about 200 nm, thus the enlarged nucleoid foci observed through this method is not representative of the actual size. Stimulated emission depletion (STED) microscopy enables a resolution limit of about 50 nm with standard immunostaining procedures and we therefore performed STED microscopy to resolve the true diameter of these enlarged nucleoid foci in *dMfn* KOs. The diameter of nucleoids was previously determined by super-resolution microscopy to be about 100 nm (Brown et al., 2011; Kukat et al., 2011). Dual confocal and STED imaging of mtDNA immunostained with anti-DNA antibodies showed that small nucleoid foci as seen by confocal microscopy were single nucleoid foci also by STED microscopy (Figure 2.13A). In contrast, enlarged nucleoid foci observed by confocal microscopy were resolved into multiple clustered nucleoids by STED microscopy (Figure 2.13A). Thus, implementation of super-resolution microscopy allowed us to see the actual number of nucleoids and to distinguish between clustered and single nucleoids.

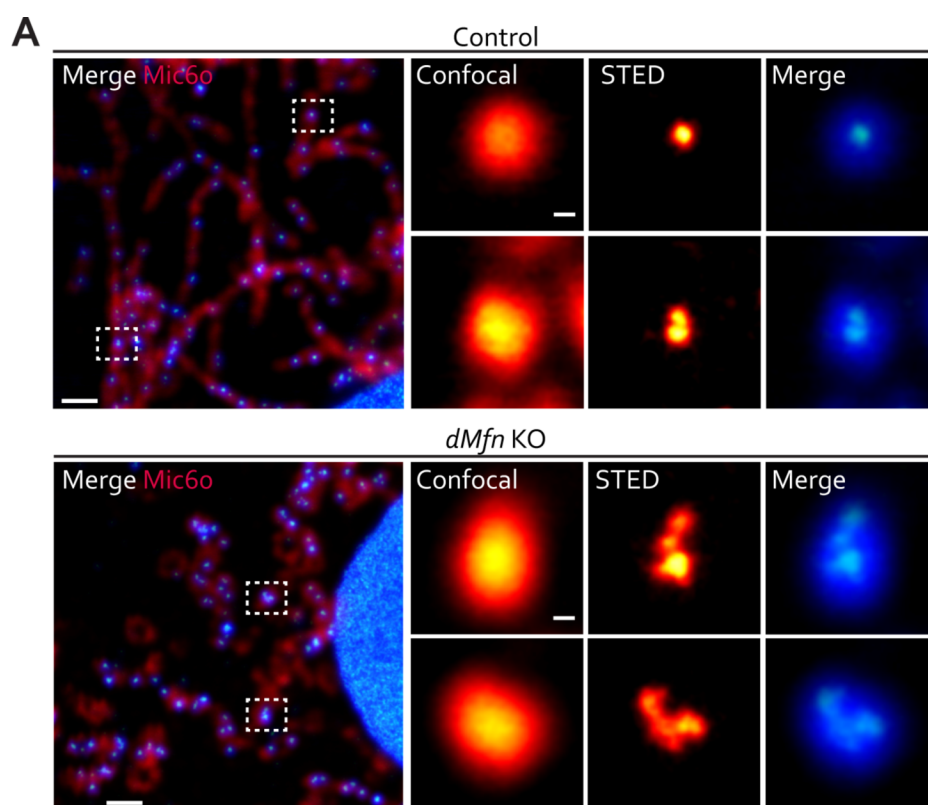


Figure 2.13 Comparison of mtDNA foci by confocal and STED microscopy

(A) Representative confocal and STED microscopy images of mtDNA foci immunostained with anti-dsDNA and anti-Mic60 antibodies from control and *dMfn* KO MEFs (left). Zoom-in of dash boxes showing mtDNA foci (right). Scale bars represents 1 μ m (left) and 100 nm (right).

The appearance of nucleoid clustering in *dMfn* KO MEFs was further corroborated by chemically staining mtDNA with picogreen (Figure 14A and B). The pattern obtained by picogreen staining of nucleoids was identical to the pattern obtained by anti-DNA antibody staining, whereby clustered nucleoids could be resolved into multiple single nucleoids STED microscopy.

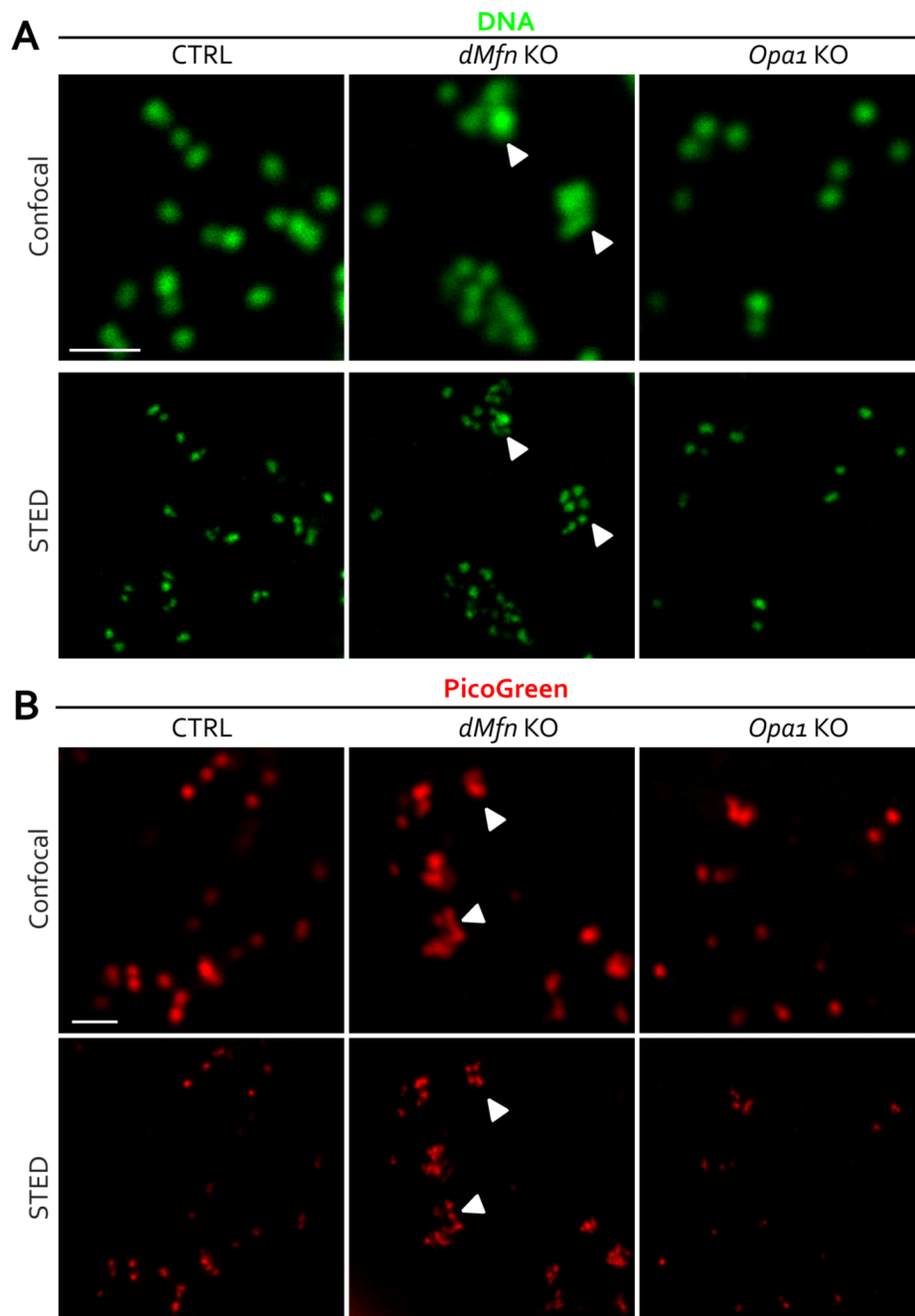


Figure 2.14 mtDNA clustering is present in OMM, but not IMM fusion-deficient MEFs
 (A) Representative images of control, *dMfn* KO, *Opa1* KO MEFs and labeled with anti-DNA antibodies and imaged by confocal and STED microscopy. (B) Representative images of control, *dMfn* KO, *Opa1* KO MEFs labeled with PicoGreen and imaged by confocal and STED microscopy. Scale bars are 1 μ m. Arrows indicate clustered mtDNA.

The appearance of clustered nucleoids in *dMfn* KOs prompted us to determine if other fusion-deficient models display clustering. Interestingly, only the absence of OMM fusion induced mtDNA clustering, because the mtDNA foci appeared normal in IMM fusion-deficient MEFs (Figure 2.14A and B). Further analysis showed single *Mfn1* KOs displaying a similar nucleoid diameter as control MEFs (Figure 2.15A and B).

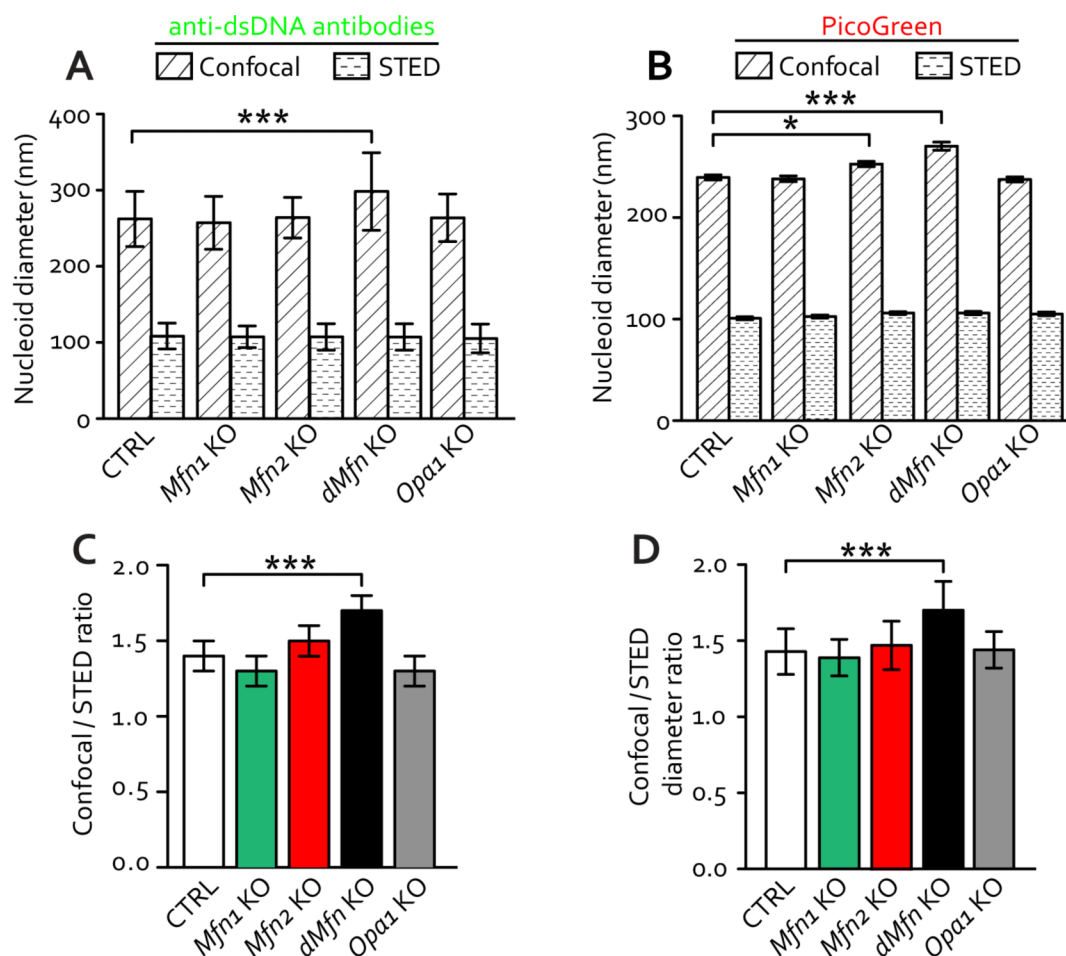


Figure 2.15 Loss of outer membrane fusion does not alter nucleoid diameter

(A) Quantification of average nucleoid diameters in confocal and STED acquired images after labeling with anti-DNA antibodies in control, *Mfn1* KO, *Mfn2* KO, *dMfn* KO, and *Opa1* KO MEFs. The nucleoid diameters were measured at full width at half maximum on 100 nucleoids from each genotype. (B) Quantification of average diameter of PicoGreen-labeled nucleoids in control, *Mfn1* KO, *Mfn2* KO, *dMfn* KO, and *Opa1* KO MEFs. The nucleoid diameters were measured at full width at half maximum on 100 nucleoids from each genotype. (C) Quantification of the ratio between the nucleoid diameters observed by confocal and STED images acquired after anti-DNA labeling in control, *Mfn1* KO, *Mfn2* KO, *dMfn* KO, and *Opa1* KO MEFs, $n=12$ for all genotypes. (D) The ratio between confocal and STED nucleoid diameters after PicoGreen labeling of control, *Mfn1* KO, *Mfn2* KO, *dMfn* KO, and *Opa1* KO MEFs, $n > 35$ with an average of 45-130 nucleoids per section. The confocal/STED ratio is an indication of the degree of nucleoid clustering. For (A) and (C), errors bars indicate standard error of the mean. For (B) and (D), errors bars indicate standard deviation of the mean. One-way ANOVA using Turkey's multiple comparison test; ***, $P < 0.001$.

Moreover, single *Mfn2* KO showed a small, but significant, increase in nucleoid diameter with picogreen staining and confocal imaging (Figure 2.15A and B). For control and all fusion-deficient models the STED-determined nucleoid diameter when labeled with picogreen or anti-DNA antibodies was calculated to be about 100 nm (Figure 2.15A and B). Analysis of the confocal/STED diameter ratio indicated that *dMfn* KO MEFs contained a higher degree of nucleoid clustering than other fusion-deficient cell models (Figure 2.15C and D). This finding was further emphasized in the gaussian distribution of STED-determined nucleoid diameters (Figure 2.16A), where nearly 40 % of nucleoids in *dMfn* KO MEFs were clustered (Figure 2.16B). These findings suggest that OMM fusion proteins play an important role in nucleoid distribution, whereas IMM fusion has no such effect.

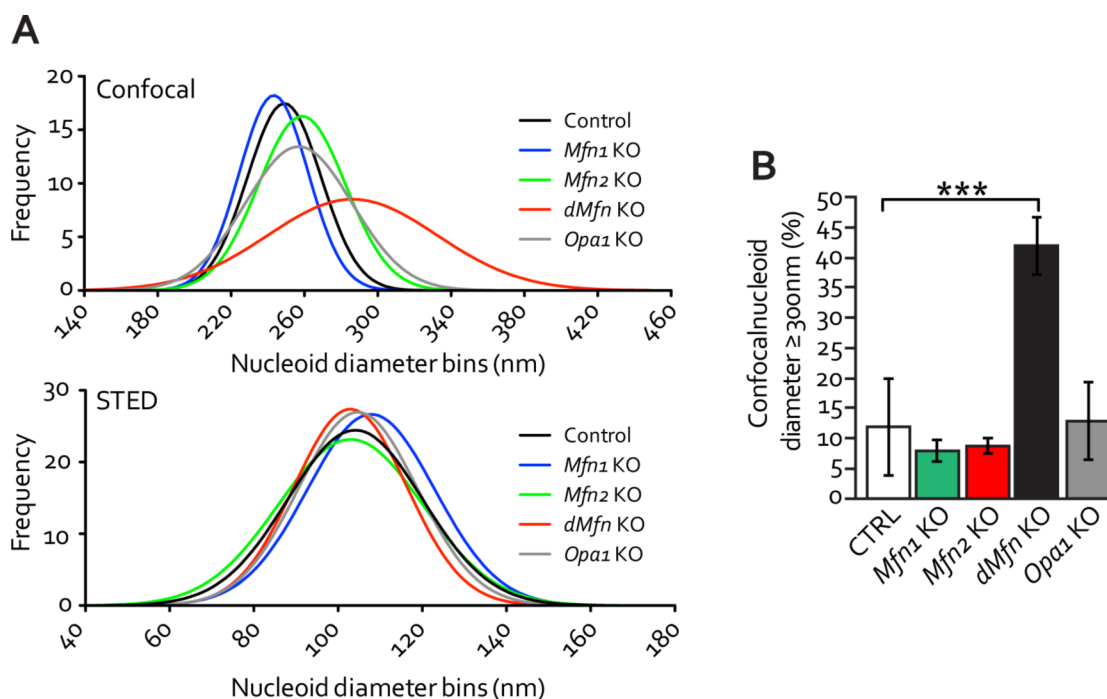


Figure 2.16 Loss of outer membrane fusion results in mitochondrial nucleoid clustering

(A) Gaussian distribution of PicoGreen-labeled nucleoid diameters determined from confocal and STED images using control, *Mfn1* KO, *Mfn2* KO, *dMfn* KO, and *Opa1* KO MEFs. (B) Quantification of PicoGreen-labeled nucleoids with a diameter ≥ 300 nm, related to (A), error bars indicate \pm SEM. Student T-test; ***, $P < 0.001$.

2.9 Loss of OMM fusion does not affect mtDNA compaction

Immunofluorescence analysis revealed that *dMfn* KO MEFs display nucleoid clustering without alteration in nucleoid diameter. However, this former set of analysis does not address directly the state of the mtDNA topology in the nucleoids. Through a combined biochemical and molecular approach, we investigated whether the enlarged nucleoids could be explained by the presence of physically interlocked mtDNA molecules. Total DNA from heart tissue was resolved in its native state on an agarose gel and subjected to Southern blotting to visualize mtDNA topologies. We treated control DNA with various enzymes to validate the identity of each topological species; *SacI* cuts mtDNA once and produces a linear fragment, *Nt.BbvCI* nicks dsDNA, topoisomerase I relaxes supercoils, topoisomerase II uncoils catenanes, and gyrase forms supercoiled circles (Figure 2.17A). In the control, mtDNA is primarily present as relaxed circles, while the other topological species are in low abundance (Figure 2.17A). With regards to *dMfn* KO animals, the topologies of mtDNA were similar to the topologies in control samples. This shows that nucleoid clustering is not due to physical tethering of mtDNA as there is no increase in catenated species.

Lastly, TFAM is the main mitochondrial protein that is always bound to mtDNA and it packages mtDNA into nucleoids. Therefore, we qualitatively assessed nucleoids for the presence of TFAM to rule out issues in mtDNA compaction. Fixed cultured MEFs were immunostained against DNA and TFAM and imaged by confocal microscopy. In control and fusion-deficient MEFs, we observed that TFAM as expected is present on every molecule of mtDNA (Figure 2.17B). Moreover, enlarged nucleoids showed larger TFAM foci, in agreement with the fact that enlarge nucleoids are composed of multiple nucleoids. All together, these data suggest OMM fusion does not affect mtDNA compaction, but rather plays a role in nucleoid distribution.

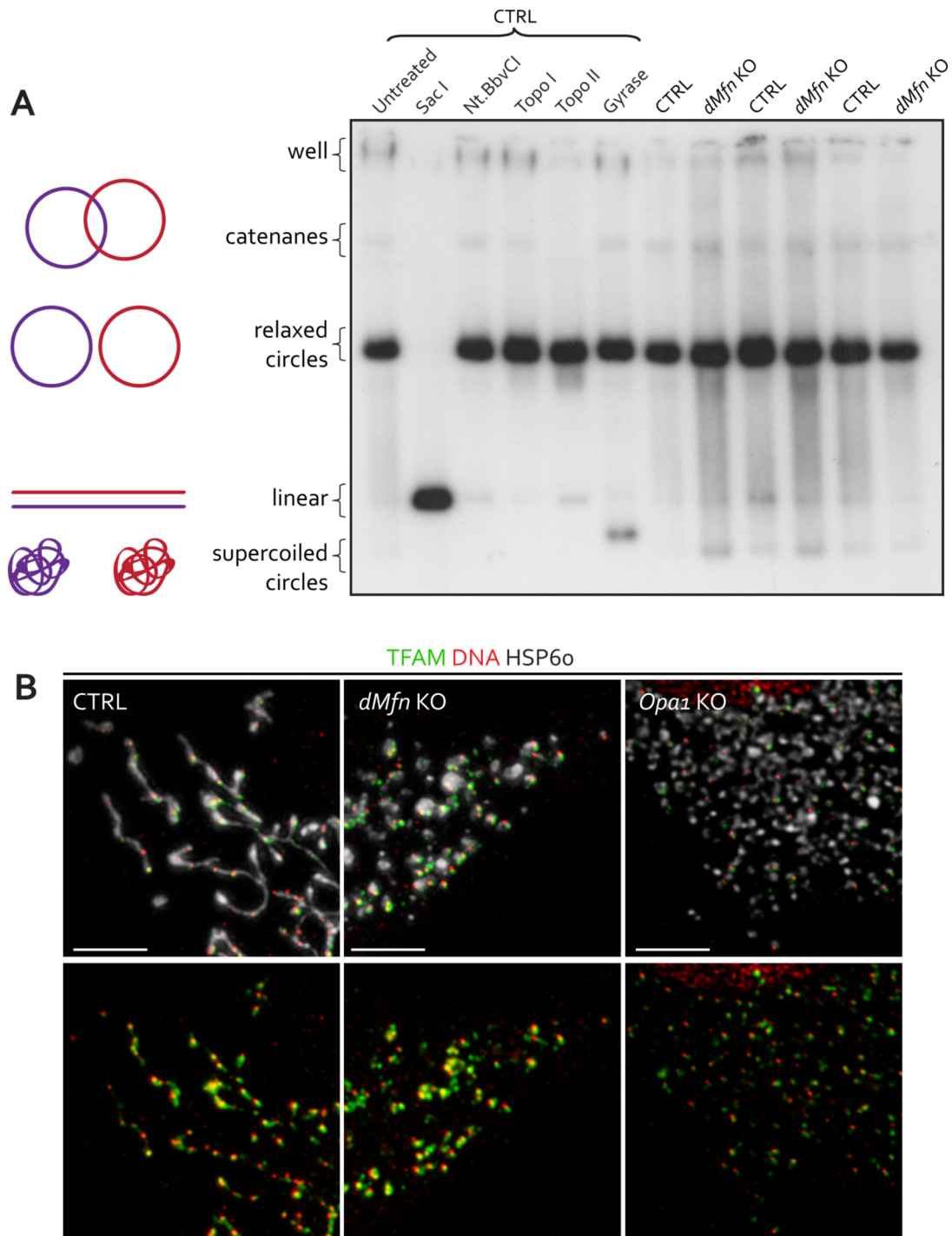


Figure 2.17 Loss of OMM fusion does not affect compaction of nucleoids

(A) mtDNA topology gel using total DNA from heart tissue of 3-week old control ($n=3$) and *dMfn* KO ($n=3$) mice. The high molecular weight portion of the gel is shown. Control mtDNA was either untreated or treated with *SacI*, *Nt.BbvCI*, topoisomerase I (Topo I), topoisomerase II (Topo II), or DNA gyrase enzymes to distinguish the various mtDNA topologies. Mitochondrial DNA was probed with pAM₁ (mouse mtDNA sequence). (B) Representative image of control, *dMfn* KO, and *Opa1* KO MEFs decorated with anti-TFAM, anti-DNA and anti-HSP6o antibodies from 3 independent experiments. Scale bar is 5 μm .

2.10 Loss of OMM fusion does not affect mt-transcription activity

The basal mt-transcription initiation machinery composed of POLRMT, TFB₂M, and TFAM is crucial for mitochondrial gene expression (Gustafsson et al., 2016). Mitochondrial DNA transcription and replication are coupled processes, whereby mt-transcription generates the RNA primer for mtDNA replication. Previously characterized animal models with defects in mt-transcription in heart tissue were associated with a loss of mtDNA (Larsson et al., 1998; Kühl et al., 2016). To investigate the origin of mtDNA depletion upon loss of fusion, mitochondrial gene expression was assessed in fusion-deficient heart tissue and MEFs.

Western blot analysis of isolated heart mitochondria found steady-state levels of TFAM and TFB₂M that were similar to control levels, while POLRMT protein levels were highly increased in *dMfn* KO animals (Figure 2.18). Interestingly, despite having sufficient transcription machinery proteins, *dMfn* KO animals compared to control animals contained less mt-transcripts from both the light and heavy strands as determined by northern blots (Figure 2.19). However, the decrease in mitochondrial transcripts was not as profound as in heart specific *Polrmt* KO animals, an indication that mt-transcription activity is not fully abolished.

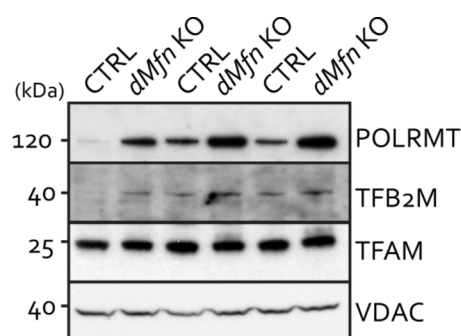


Figure 2.18 Dramatic increase in POLRMT upon the loss of OMM fusion

Steady-state levels of proteins involved in mt-transcription from heart mitochondria from control and *dMfn* KO animals at 5 weeks of age (n=3 for each genotype) as determined by western blot analysis.

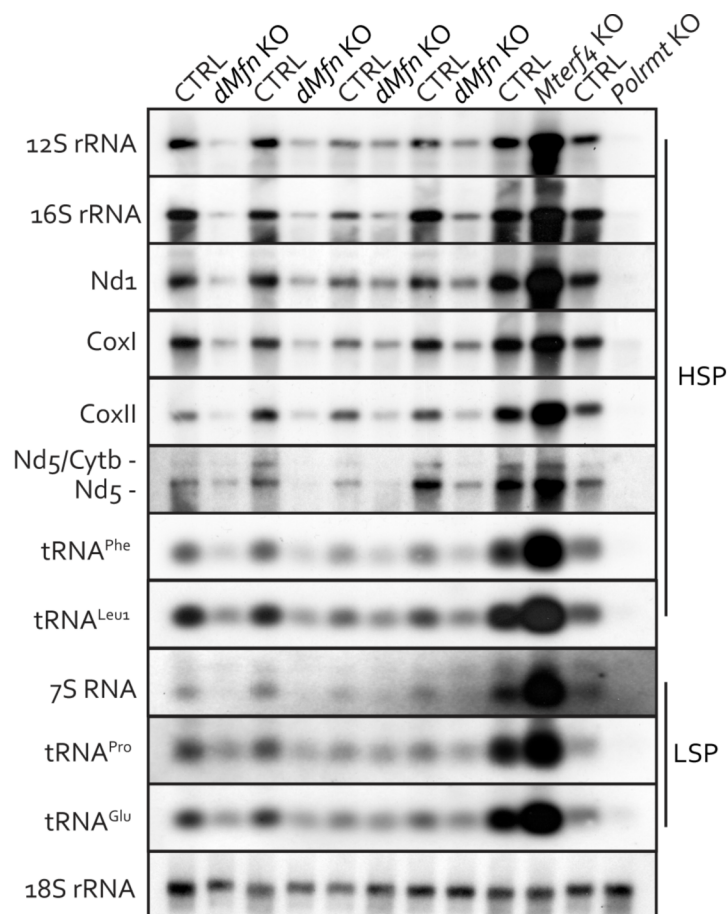


Figure 2.19 Loss of OMM fusion results in a reduction of mt-transcripts

Northern blot analysis of mitochondrial transcripts in heart tissue from the heavy and light strand promoter (HSP and LSP) of control and *dMfn* KO animals at 5 weeks of age (n=4 for each genotype). *Mterf4* and *Polrmt* heart knockouts were included as controls for increase and decrease of levels of mt-transcripts, respectively.

To functionally assess total mt-transcription, an *in organello* assay using isolated heart mitochondria was performed to follow *de novo* synthesis of mt-transcripts. Compared to controls, *dMfn* KO heart mitochondria produced overall considerably less mt-transcripts (Figure 2.20A and C). Taking into account the mtDNA depletion in *dMfn* KOs, the activity of mt-transcription per mtDNA template was similar between control and *dMfn* KO animals (Figure 2.20B and D). These analyses show that mt-transcription activity is unaffected and limited by mtDNA copy number.

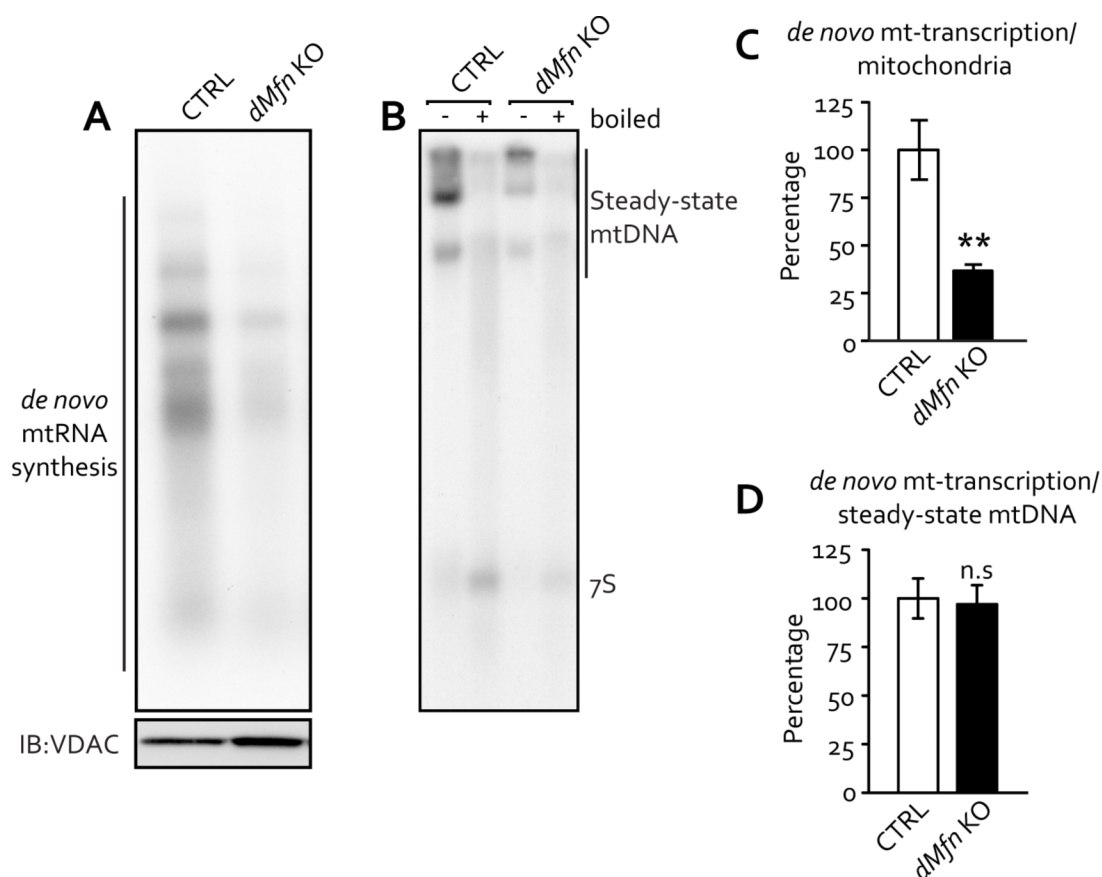


Figure 2.20 Mitochondrial fusion is dispensable for mt-transcription

(A) Representative image of a mitochondrial *de novo* transcription assay and (B) Southern blot analysis with the same isolated heart mitochondria. For Southern blot, mtDNA was visualized with 7S DNA probe. Mitochondrial VDAC levels were determined by western blot analysis and used as loading control. Multiple control (n=6) and *dMfn* KO (n=5) heart mitochondrial samples were analyzed at 4 weeks of age. (C) Quantification of mitochondrial *de novo* transcription related to VDAC protein levels in control (n=6) and *dMfn* heart KO (n=5) mitochondria, related to (A). (D) Quantification of mitochondrial *de novo* transcription relative to the steady-state levels of mtDNA of control (n=6) and *dMfn* KO (n=5) heart mitochondria, related to (A and B). Error bars indicate \pm SEM. Student T-test; **, $P < 0.01$. n.s., no significant difference.

This finding was further investigated at the level of individual nucleoids in MEFs through immunofluorescence approaches. Fluorescence *in situ* hybridization (FISH) was applied to detect the mtDNA-encoded *Cox1* mRNA on fixed MEFs. This FISH probe was detected only in mitochondria, was insensitive to DNase treatment, and highly specific for *Cox1* mRNA (Figure 2.21A). The *Cox1* mRNA FISH staining pattern was present as distinct foci in very close proximity to nucleoids (Figure 2.21B). *Cox1* mRNA was abundant in control MEFs, while *dMfn* KO MEFs *Cox1* mRNA was less abundant (Figure 2.21B and C), consistent with Northern blot analysis. However, analysis of individual nucleoids revealed that nearly every nucleoid was positive for *Cox1* mRNA in both control and *dMfn* KO MEFs (Figure 2.21B and D).

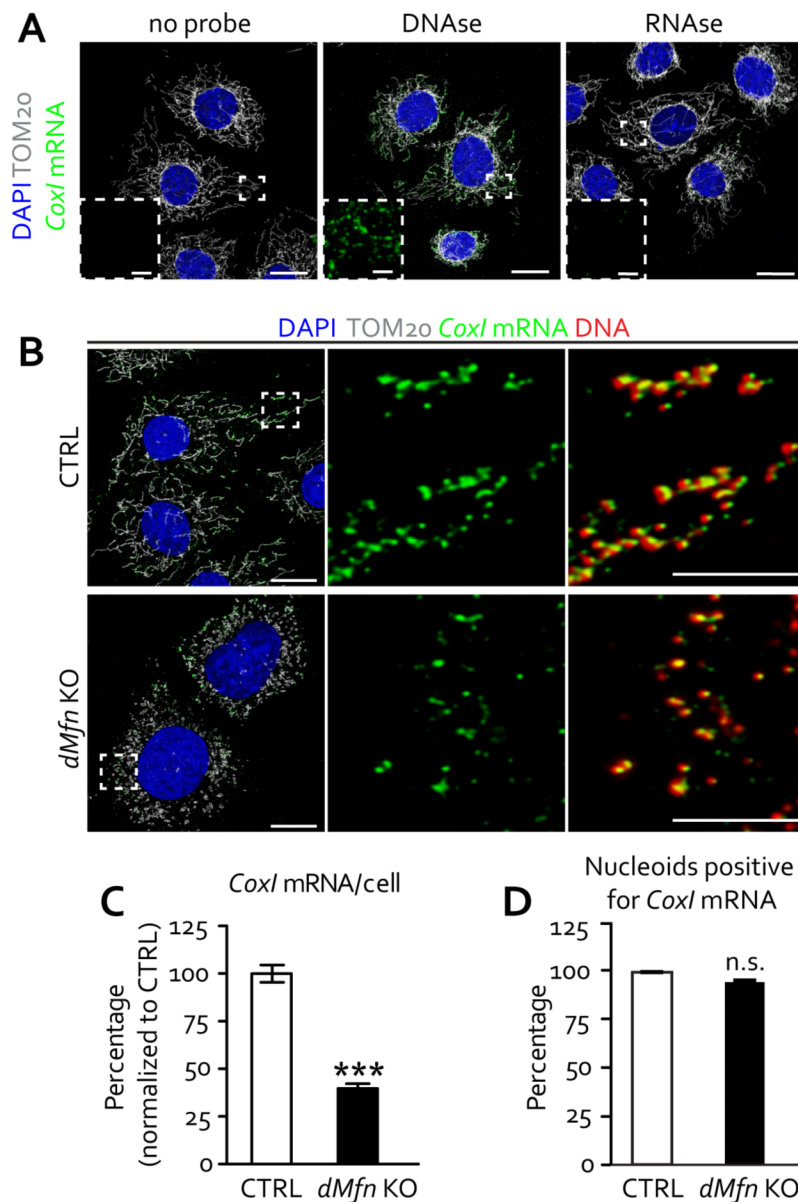


Figure 2.21 Steady-state *Cox1* mRNA follow mtDNA levels

(A) Representative confocal images of fluorescence in situ hybridization (FISH) in control MEFs visualizing the mitochondrial *Cox1* mRNA and immunocytochemistry to detect the TOM20 protein. DNase and RNase treatment verified the specificity of *Cox1* mRNA probe. Scale bars represent 10 μm , zoom-in scale bar is 1.6 μm . (B) Representative confocal images of mitochondrial *Cox1* mRNA visualized by FISH, followed by immunocytochemistry to detect mtDNA and TOM20 protein in control and *dMfn* KO MEFs. Scale bars, 5 μm . (n=5 per genotype). (C) Quantification of *Cox1* mRNA in control (n=17) and *dMfn* KO (n=15) from stacked confocal images. (D) Quantification of nucleoids positive for *Cox1* mRNA from stacked confocal images of control (n=15) and *dMfn* KO (n=14) MEFs. Error bars indicate \pm SEM. Student T-test; ***, $P < 0.001$; n.s, no significant difference.

Since FISH analysis of *CoxI* mRNA is not reflective of ongoing mt-transcription, *de novo* mt-transcript production was evaluated in cultured cells. We incubated cells with the uridine analog Bromouridine (BrU) and its incorporation into nascent mRNA was assessed by immunofluorescence. The immunofluorescence signal of BrU was detected in the nucleus and mitochondria. The staining pattern of BrU within mitochondria was punctuated and always found in the presence of the mt-mRNA binding protein LRPPRC (Figure 2.22A). In line with FISH analysis of *CoxI* mRNA, BrU incorporation was severely decreased in both OMM and IMM fusion-deficient *dMfn* KO and *Opa1* KO MEFs (Figure 2.22B and C). Moreover, in both control and fusion-deficient MEFs the majority of nucleoids were positive for BrU, suggesting that BrU was incorporated into nascent mitochondrial mRNA (Figure 2.22B and D). Notably, clustered nucleoids in *dMfn* KO MEFs exhibited higher abundance of BrU-incorporated mRNA (Figure 2.22B). Altogether, these results suggest that, although mt-transcription is proportional to the number mtDNA template, it is not impaired by loss of mitochondrial fusion and that clustered nucleoids also are transcribed.

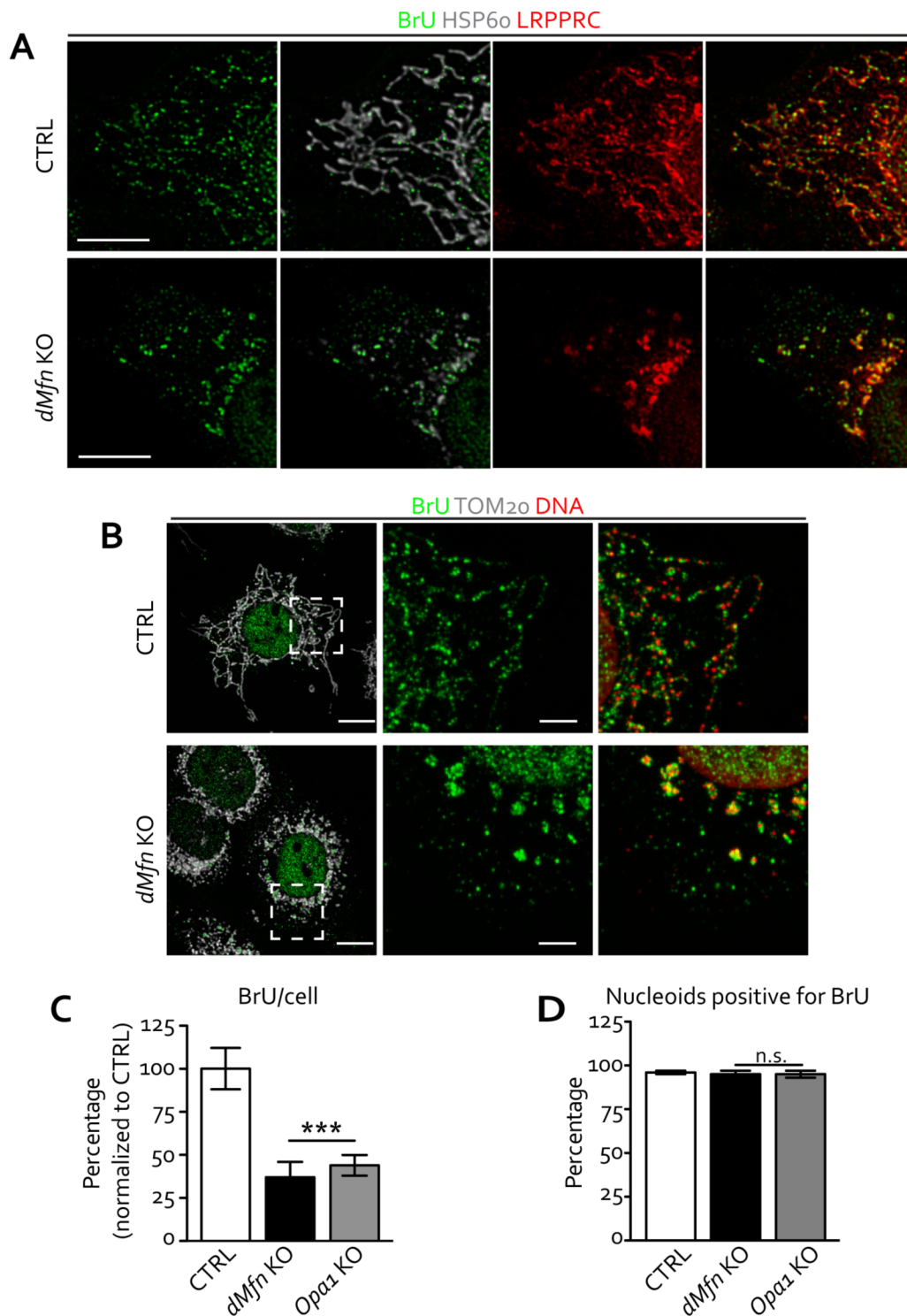


Figure 2.22 Newly synthesized mt-transcripts follow mtDNA levels

(A) Representative confocal images of BrU-labeled mRNA and the mitochondrial proteins LRPPRC and HSP6o in control and *dMfn* KO MEFs. Scale bars represent 5 μ m. Staining patterns were determined in three independent experiments for each genotype. (B) Representative confocal images of BrU-labeled mRNA, DNA and TOM2o protein in control and *dMfn* KO MEFs. Dashed boxes specify the areas of magnification shown to the right. Scale bars represent 10 μ m (main image) or 5 μ m (zoom images). Staining patterns were determined in five independent experiments per genotype. (C) Quantification of BrU-labeled mRNAs from stacked confocal images of control (n=15) and *dMfn* KO (n=15) MEFs. (D) Quantification of nucleoids positive for BrU from stacked confocal images of control (n=15), *dMfn* KO (n=18), and *Opz1* KO (n=15) MEFs. Error bars indicate \pm SEM. Student T-test; ***, $P < 0.001$; n.s, no significant difference.

2.11 Loss of mitochondrial fusion affects replisome composition

Initiation of mtDNA replication is dependent on mt-transcription to form the RNA primer (Kühl et al., 2016). However, our findings presented above exclude impaired transcription as a cause for the observed mtDNA depletion in *dMfn* KO hearts. Faithful replication of mtDNA requires a dedicated protein replisome. We therefore proceeded to investigate replisome abundance and activity. The mitochondrial replisome is composed POLRMT, POL γ , TWNK, and SSBP1.

Western blot analysis revealed significant changes in the composition of the replisome in isolated mitochondria from *dMfn* KO and *Opa1* KO MEFs (Figure 2.23A). In fusion-deficient MEFs, the steady-state levels of PolyA were reduced by nearly 50 % compared to controls, while the levels of TWNK were not significantly altered (Figure 2.23B). Since a western blot analysis on denatured proteins cannot evaluate whether replisome proteins are engaged with mtDNA, a glycerol gradient with an iodixanol pad was utilized to enrich for nucleoids and nucleoid-associated proteins under native conditions using isolated MEF mitochondria (Figure 2.23C). In all cell types, the vast majority of known nucleoid-associated proteins were enriched in fraction 1 of the gradient (Figure 2.23D). Importantly, southern blot analysis showed that mtDNA was found only in fraction 1. Proteins such as the OMM protein VDAC and matrix proteins LRPPRC and ATP5A were present in lighter-density fractions (Figure 2.23D). Quantitative analysis of protein abundance relative to mtDNA in fraction 1 revealed changes in the stoichiometry of replisome proteins. In *dMfn* KO and *Opa1* KO MEFs, the stoichiometry of replisome interacting with mtDNA were imbalanced, composed of less PolyA and increased levels of TWNK and SSBP1 proteins (Figure 2.23E and F).

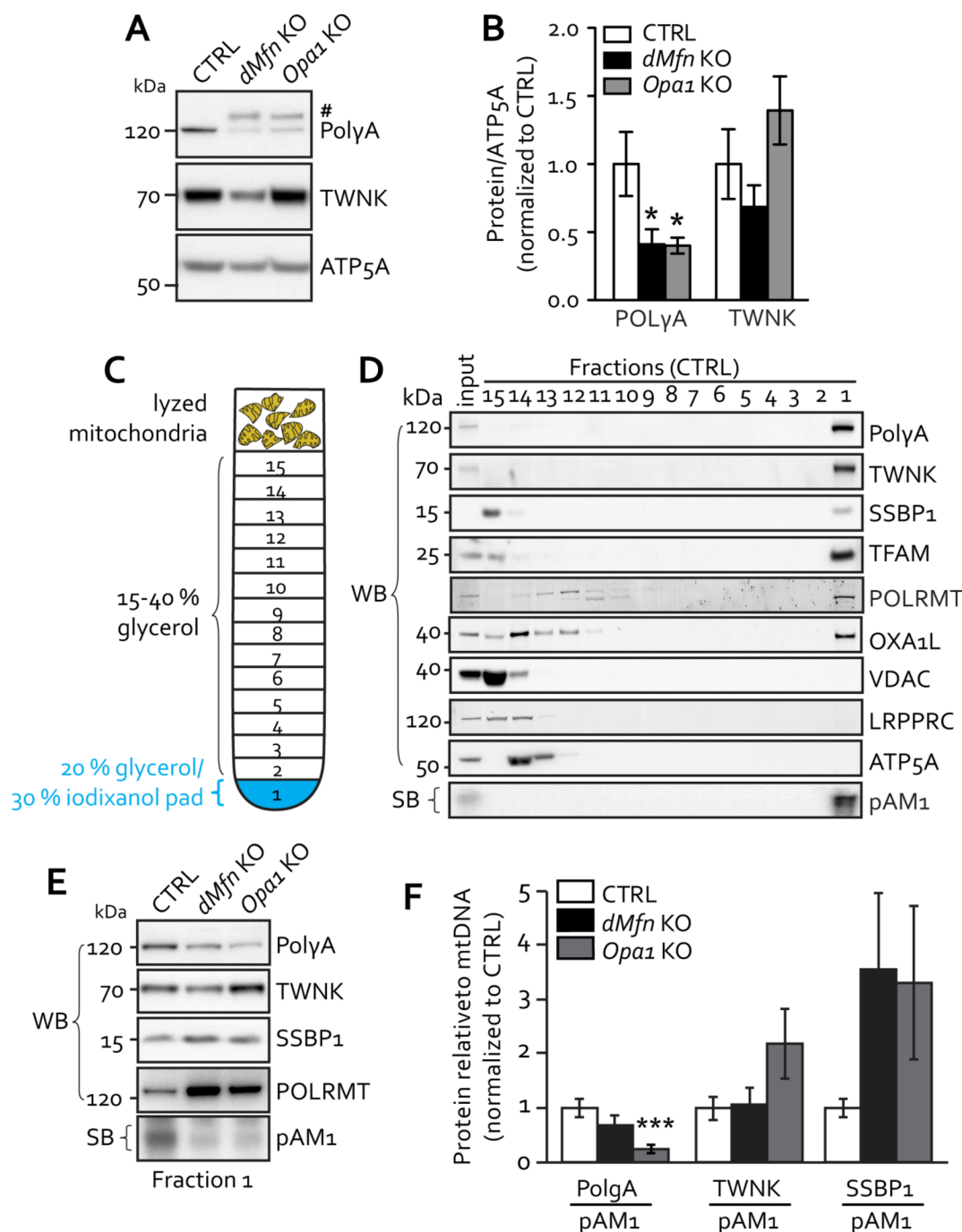


Figure 2.23 Loss of OMM fusion alters replisome stoichiometry

(A) Representative western blot of steady-state levels of replisome proteins of isolated mitochondria from control, *dMfn* KO, and *Opa1* KO MEFs, $n=4$ per genotype. # denotes cross-reactive band. (B) Quantitative analysis of protein abundance related to (A). Protein levels were normalized to VDAC, $n=4$ per genotype. (C) Schematic depiction of the glycerol density gradient with an iodixanol pad for nucleoid enrichment and lyzed mitochondrial layered on top of gradient. (D) Representative western blot analysis of glycerol gradient fractions from mitochondria isolated from control MEFs. Upper panel shows western blot analysis (WB) and lower panel shows Southern blot (SB) analysis to detect mtDNA by using the pAM1 probe. Three independent experiments were performed on controls. Similar enrichment in fraction 1 was also observed in *dMfn* KO and *Opa1* KO MEFs. (E) Representative western blot and southern blot analysis of enriched proteins in fraction 1 from isolated mitochondria of control, *dMfn* KO, and *Opa1* KO MEFs, $n=3$ per genotype. (F) Quantitative analysis related to (E) of enriched proteins relative to mtDNA levels in fraction 1 from isolated mitochondria of control, *dMfn* KO, and *Opa1* KO MEFs, $n=3$ per genotype. Error bars indicate \pm SEM. Student T-test; * $P < 0.05$; *** $P < 0.001$.

To further validate these findings, individual nucleoids were examined for the presence of replisome proteins through immunocytochemistry and confocal microscopy. Immunostaining of SSBP1 and mtDNA in control and *dMfn* KO MEFs revealed three populations of SSBP1: free SSBP1, SSBP1 partially overlapping with mtDNA, and SSBP1 completely overlapping with mtDNA. In control MEFs, 29 % of SSBP1 was present as distinct foci free of mtDNA and 29% co-localizing with mtDNA (Figure 2.24A and B). In contrast, *dMfn* KO MEFs exhibited a shift towards more SSBP1 co-localizing with mtDNA (38 %) resulting in less free SSBP1 (20 %) (Figure 2.24A and B). This finding is in agreement with other results showing enrichment of SSBP1 in nucleoid fractions in fusion-deficient MEFs (Figure 2.23F). Similar immunofluorescence analyses were attempted for PolyA or TWNK; however, numerous commercially available antibodies or custom-made antibodies failed to specifically detect endogenous PolyA or TWNK. Altogether, these data show that mitochondrial fusion plays a role in maintaining a balanced replisome.

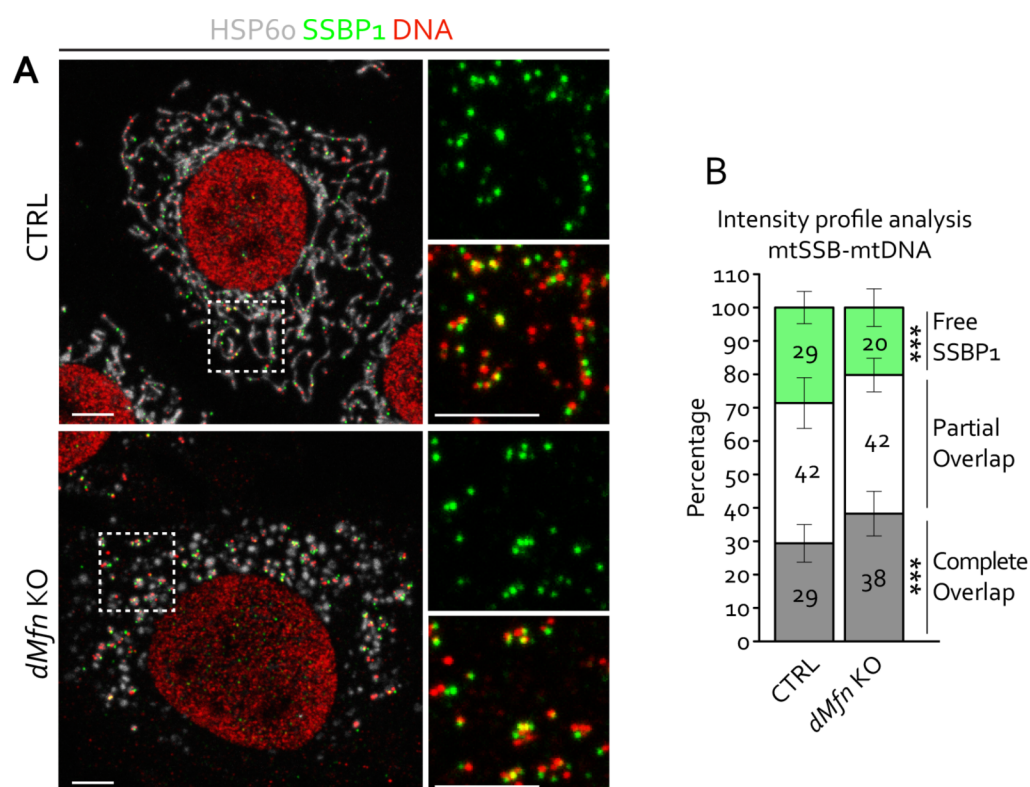


Figure 2.24 SSBP1 interaction with mtDNA increases upon loss of OMM fusion

(A) Representative confocal image of control and *dMfn* KO MEFs immunostained with anti-SSBP1 and anti-dsDNA antibodies, $n=3$ for each genotype. Scale bars represent 5 μm . (B) Line scan analysis based on intensity profiles of SSBP1 and mtDNA of control and *dMfn* KO MEFs, $n=3$ for each genotype, 7-10 cells analyzed per n . Error bars indicate \pm SEM. Student T-test; ***, $P < 0.001$.

2.12 Mitochondrial fusion is required to sustain high rates of mtDNA replication

In order to maintain high mtDNA copy number, a cell must contain a mechanism that coordinates the balance between abortive and genome-length mtDNA replication. In addition to replication, regulation of mtDNA stability is an important factor controlling copy number. To date, very little is known about how mtDNA replication is organized and regulated *in vivo*. Since we found that fusion-deficient MEFs have an imbalance in replisome factors, we assessed whether this functionally perturbs mtDNA replication activity.

The ability to replicate mtDNA was investigated under conditions that activate mtDNA synthesis. This can be achieved by depletion of mtDNA with ethidium bromide (EtBr) followed by monitoring of the repopulation of mtDNA over time. Control MEFs treated with EtBr for 6 days underwent a rapid depletion of mtDNA, while both *dMfn* and *Opa1* KO MEFs lost mtDNA at a slower rate (Figure 2.25A). Moreover, EtBr treatment caused fragmentation of mitochondria in control cells (Figure 2.25B) and in all genotypes about 25% of the population showed complete loss of mtDNA (ρ^0) (Figure 2.25C). The residual amount of mtDNA remaining after 6 days of EtBr treatment was significantly less in control MEFs (0.5 %) compared to *dMfn* and *Opa1* KO MEFs (5.3 % and 3.0 %, respectively) (Figure 2.25B). Interestingly, the loss of mtDNA in *Mfn1* and *Mfn2* KO MEFs was similar to control MEFs (1.0 % and 0.3 %, respectively) (Figure 2.25D). In the recovery phase, EtBr was removed from the culture medium in order to assess mtDNA repopulation of cells. During this phase, control and *Mfn2* KO MEFs displayed an accelerated rate of mtDNA recovery (Figure 2.25A). In contrast, *dMfn* and *Opa1* KO MEFs lagged dramatically behind in mtDNA synthesis. In fact, control MEFs were more productive with far less mtDNA templates, reaching a 150 fold increase of mtDNA in the repletion phase, whereas *dMfn* and *Opa1* KO MEFs, despite having more mtDNA templates after the depletion phase, displayed only 10-25 fold increase in mtDNA copy number (Figure 2.25E). Surprisingly, *Mfn1* KO MEFs also showed impaired mtDNA recovery with a 50 fold increase of mtDNA levels in the repletion phase (Figure 2.25E).

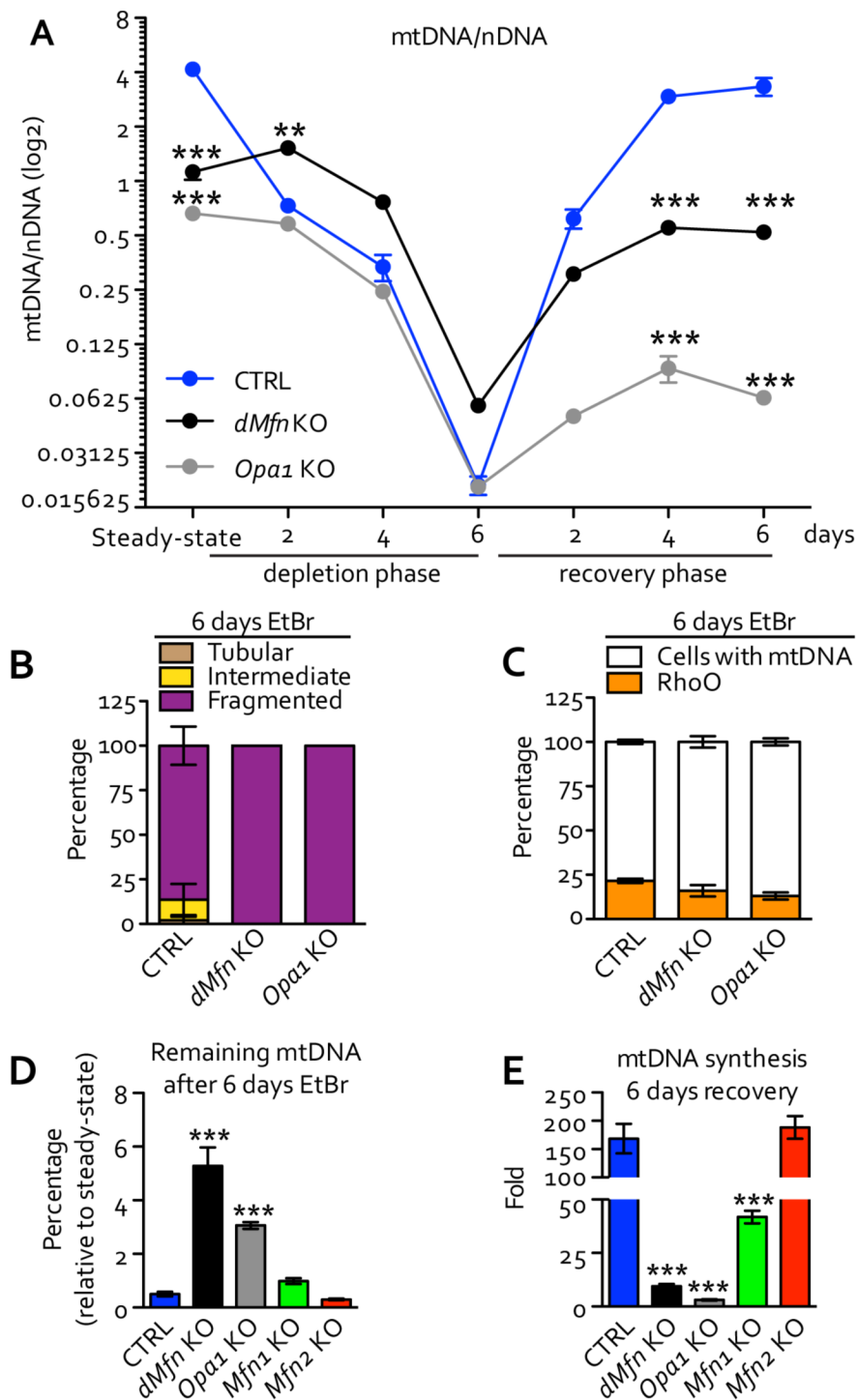


Figure 2.25 Loss of OMM fusion decreases mtDNA replication

(A) Quantitative PCR analysis of mtDNA copy number (ATP6) normalized to nuclear DNA (18S) of control, *dMfn* KO, and *Opa1* KO MEFs treated with 100 ng/ml EtBr and during recovery phase after EtBr treatment, $n=4-8$ replicates per genotype. (B) Image analysis of mitochondrial network morphology in control, *dMfn* KO, and *Opa1* KO MEFs after treatment of cell with 100 ng/ml EtBr for 6 days, $n=3$ per genotype, and 17-149 cells evaluated per n . Network morphology was visualized by immunocytochemistry using anti-TOM20 antibodies. (C) Image analysis for the presence or lack of mtDNA in control, *dMfn* KO, and *Opa1* KO MEFs after treatment of cell with 100 ng/ml EtBr for 6 days, $n=3$ per genotype, and 67-134 cells evaluated per n . MEFs were immunostained with anti-dsDNA and TOM20 antibodies. (D) Quantification of mtDNA levels in control, *dMfn* KO, *Opa1*, *Mfn1* KO, *Mfn2* KO MEFs after 6 days of treatment with 100 ng/ml EtBr, $n=4$ for all genotypes. (E) Quantification of the fold change of mtDNA during recovery phase after treatment with 100 ng/ml EtBr for 6 days in control, *dMfn* KO, *Opa1*, *Mfn1* KO, *Mfn2* KO MEFs, $n=4-8$ replicates per genotype. One-way ANOVA using Turkey's multiple comparison test; ***, $P < 0.001$.

Lastly, to rule out changes in the cellular dNTP pools as a cause for the limited capacity for mtDNA replication in fusion-deficient MEFs, we determined the abundance of dNTP pools by UPLC-MS. As a negative control, cellular purines (dGTP and dATP) levels were mildly depleted by treating control MEFs with 2 mM hydroxyurea for 30 hours. Hydroxyurea is well described to arrest DNA replication by inhibiting the ribonucleotide reductase enzyme that catalyzes the formation of dNTPs and NTPs. Quantification of cellular dNTP pools revealed no change in dNTPs in all fusion-deficient cell models, although *Mfn1* and *Opa1* KO MEFs showed a trend for increase levels (Figure 2.26A).

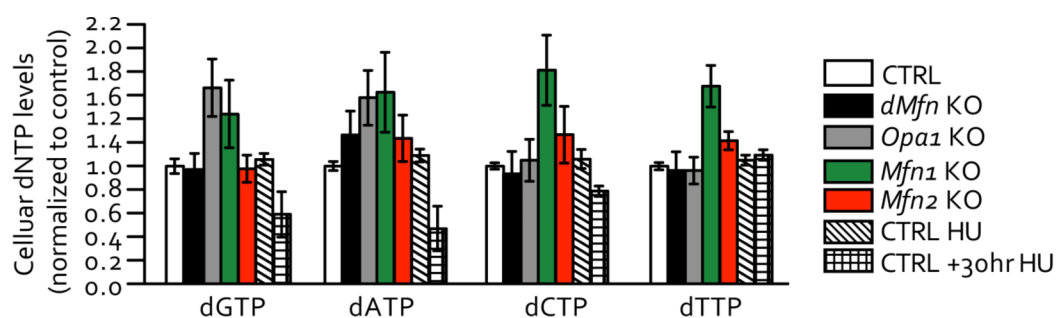


Figure 2.26 Loss of OMM fusion does not affect cellular dNTP pools

Quantification of cellular dNTPs by UPLC-MS from control (n=10), *dMfn* KO (n=11), *Opa1* KO (n=12), *Mfn1* KO (n=7), *Mfn2* KO (n=7), control without hydroxyurea treatment (-HU, n=3), and control MEFs treated for 30 hours with 2 mM hydroxyurea (+HU, n=3). Two-way ANOVA with Bonferroni multiple comparisons revealed no statistical significance between cell types or dNTP.

2.13 OMM fusion is necessary for postnatal mtDNA replication in the heart

In order to establish the relevance of the observed mtDNA replication defect and replisome imbalance in MEFs in a physiological context, we assessed various facets of mtDNA replication in *dMfn* KO animals. We examined the expansion of mtDNA copy number during postnatal heart development. In control mice, mtDNA levels gradually increased in the first few weeks after birth and between the 3rd and 4th week the mtDNA copy number is substantially increased by almost 10-fold (Figure 2.27A). In contrast, although *dMfn* KO animals are born with similar levels of mtDNA in heart, loss of mitochondrial fusion renders their mitochondria incompetent to synthesize mtDNA and they therefore develop severe mtDNA depletion by 4 weeks of age (Figure 2.27A). At this same age, *dMfn* KO heart mitochondria display an

imbalance of replisome factors (Figure 2.27B). Like fusion-deficient MEFs, the imbalance of replisome factors was characteristic by a decreased PolyA protein relative to TWNK protein levels in *dMfn* KO heart mitochondria.

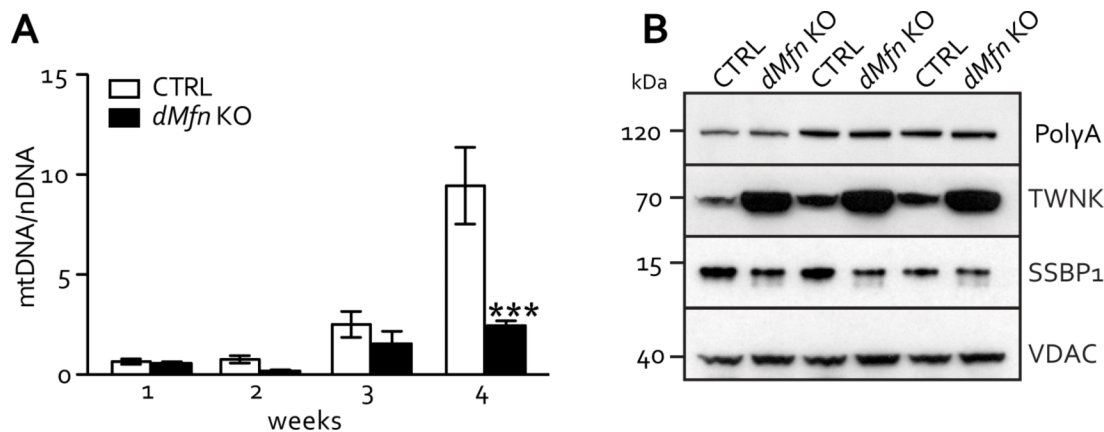


Figure 2.27 OMM fusion is necessary for postnatal mtDNA replication in the heart

(A) Quantitative PCR analysis of mtDNA copy number (ATP6) normalized to nuclear DNA (18S) in heart samples from control and *dMfn* KO at 1-4 weeks of age ($n=3-10$ per genotype). Two-way ANOVA using Bonferroni multiple comparison test; ***, $P < 0.001$. (B) Western blot showing the steady-state levels of replisome proteins in isolated heart mitochondria from control and *dMfn* KO mice at 5-6 weeks of age, $n=3$ per genotype.

The imbalance in replisome factors and inability to increase mtDNA copy number during post-natal development suggested a possible molecular impairment of mtDNA replication. Typically, more than 95 % of all initiated mtDNA replication events are prematurely terminated (abortive) after about 650 nucleotides to generate a short single-stranded species denoted 7S DNA (Gustafsson et al., 2016). There was no difference in steady-state levels of 7S DNA between control and *dMfn* KO animals by Southern blot (Figure 2.28A) or by qPCR analyses (Figure 2.28B). This finding was surprising since other mutant models exhibiting mtDNA depletion exhibit increased (*Mgme1* heart KO) or decreased (*Polrmt* heart KO) 7S DNA levels (Kühl et al., 2016; Matic et al., 2018).

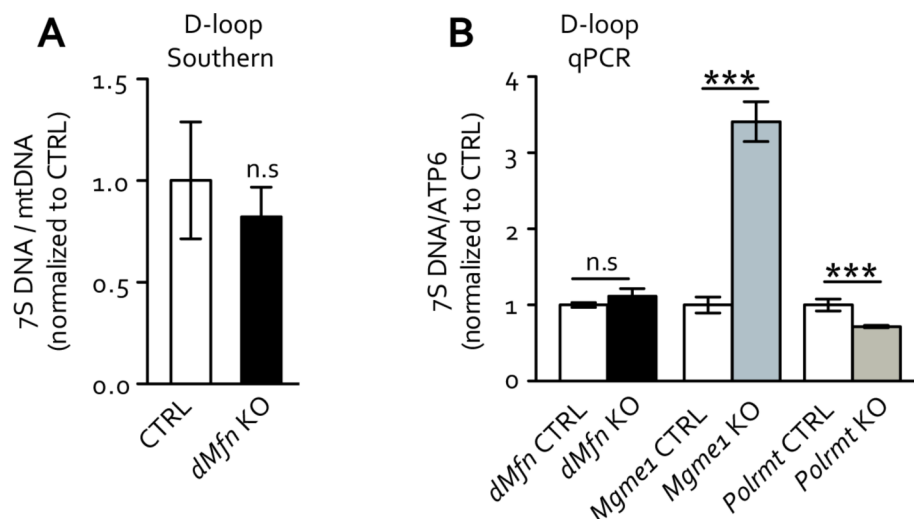


Figure 2.28 OMM fusion is necessary for postnatal mtDNA replication in the heart

(A) Southern blot quantification of relative 7S DNA levels in heart mitochondria from controls and *dMfn* KO mice, $n=4$ for both genotypes. (B) Quantitative PCR analysis of 7S DNA levels relative to mtDNA levels (ATP6) in heart tissue from control ($n=3$) and *dMfn* KO ($n=3$) at 3 weeks of age; control ($n=4$) and *Mgme1* KO ($n=4$) at 11 weeks of age; and control ($n=4$) and *Polrmt* KO ($n=4$) animals at 4 weeks of age. Error bars indicate \pm SEM. Student T-test; ***, $P < 0.001$; n.s, no significant difference.

Next, to functionally assess mtDNA replication activity in isolated heart mitochondria we performed *in organello* assays. Heart mitochondria were incubated with a radioactively labeled deoxynucleotide for two hours, which is the estimated time it takes for one molecule of mtDNA to be replicated (Berk and Clayton, 1974). Afterwards, mtDNA was isolated, subjected to Southern blotting, and newly replicated mtDNA and 7S DNA was visualized by capturing the ionizing radiation produced by the incorporated radioactive-deoxynucleotide. When isolated mtDNA is not boiled, 7S DNA remains attached to mtDNA and is seen together with full-length mtDNA on top of the gel. However, 7S DNA single stranded DNA can be separated by boiling isolated mtDNA. The higher molecular weight mtDNA is then observed on the top of the gel, whereas the smaller 7S DNA fragments migrate towards the bottom of the gel. Following mtDNA synthesis from initiation to completion, we found that most of the *de novo* mtDNA replication products in control heart mitochondria is 7S DNA. Although *dMfn* KO heart mitochondria appear to generate more mtDNA when comparing unboiled samples, analysis of boiled samples show smear of incomplete replication products surrounding the 7S DNA (Figure 2.29A and B). This finding suggests that *dMfn* KOs are able to initiate

mtDNA replication but fail to complete the replication cycles. Altogether, these data conclude that OMM fusion is necessary for maintaining the balance of replisome proteins, which allow for rapid mtDNA replication during postnatal development of the heart.

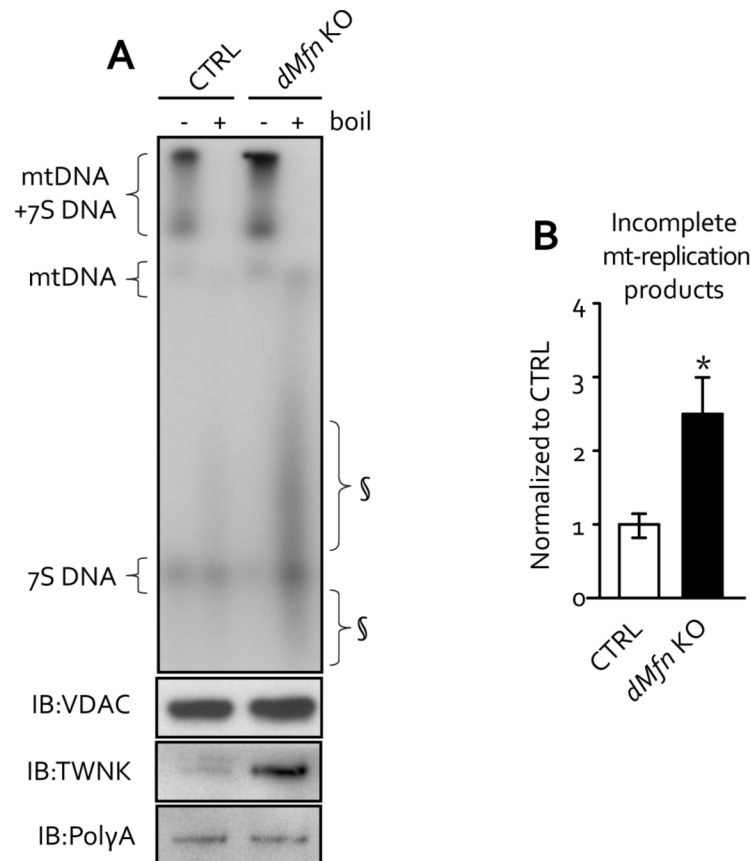


Figure 2.29 OMM fusion is necessary for faithful mtDNA replication

(A) Mitochondrial *de novo* replication assay in heart mitochondria from control (n=12) and *dMfn* KO (n=8) animals at 3-4 weeks of age. Below, immunoblotting (IB) against VDAC, TWNK, and Poly A protein levels. Incomplete mtDNA replication products (§) are indicated. (B) Quantification of relative abundance of incomplete mtDNA *de novo* replication products in control (n=6) and *dMfn* KO (n=7) heart mitochondria at 3-4 weeks of age. Error bars indicate \pm SEM. Student T-test; *, P < 0.05.

3.0 DISCUSSION

There are many copies of mitochondrial DNA in mammalian cells, which are expressed and maintained in order to ensure a functional OXPHOS system (Larsson et al., 1994). The regulation of mtDNA maintenance is multi-layered and involves various machinery acting on mtDNA transcription, mtDNA replication, nucleotide metabolism, mtDNA stability, and organelle quality control (Viscomi and Zeviani, 2017). To add to the complexity, remodeling of the mitochondrial network through fusion or fission of mitochondrial membranes can affect mtDNA integrity, maintenance, and its distribution (Mishra and Chan, 2014). The research presented in this thesis reports on an unexpected link between OMM fusion and replication and distribution of mtDNA in mammalian cells.

On mitochondrial form and function

It is generally assumed that the shape of the mitochondrial network reflects the functional state of mitochondria (Ryan and Hoogenraad, 2007; Westermann, 2012). Namely, a fragmented network is often interpreted as a sign of mitochondrial dysfunction, while a tubular network is attributed to functional mitochondria. This has been shown to be true in yeast (Rapaport et al., 1998; Shepard and Yaffe, 1999). In mammals this correlation doesn't always apply, possibly due to differences in the proteins regulating mitochondrial dynamics. We have shown that the absence of *Mfn2*, *Mfn1-2* or *Opa1* all exhibited fragmented mitochondria and display impaired mitochondrial respiration, with the exception of *Mfn1* KOs. Interestingly, mild respiratory dysfunction can also be observed in hyper-tubular mitochondrial network caused by the loss of *Drp1* in MEFs (Parone et al., 2008; Ishihara et al., 2015). Hence, form does not necessary follow function when it comes to mitochondria morphology.

On the bioenergetic role of mitochondrial fusion

Through our studies we demonstrate that loss mitochondrial fusion proteins can trigger mitochondrial respiratory dysfunction in two ways. Interestingly, heart *Mfn1* KO and *Mfn2* KO animals and MEFs exhibit a down-regulation in the biosynthetic pathway for CoQ, but only loss of MFN2 lead to CoQ depletion and respiratory dysfunction not attributed to changes in respiratory protein levels (Mourier et al., 2015; Silva Ramos et al., 2016). However, MFN2 associated OXPHOS defects have been reported in other tissues like brown adipose tissue and skeletal muscle (Sebastián et al., 2012; Boutant et al., 2017; Mahdaviani et al., 2017). It remains unclear how MFN2 contributes to the maintenance of mitochondrial CoQ pools. In fact, the majority of CoQ is produced in the IMM but can be found in nearly every cellular organelle. (Stefely and Pagliarini, 2017). Thus, taking into consideration reports describing MFN2 as a mitochondria-ER tether (de Brito and Scorrano, 2008) and studies finding newly synthesized CoQ₁₀ at mitochondrial associated membranes and the ER (Fernández-Ayala et al., 2005), it may be possible these two processes are physically linked. If true, MFN2 tethers may serve as important structural components for intra-organelle synthesis of CoQ. A recent study in budding yeast has also recognized a connection between CoQ biosynthesis and the MFN2 homolog Fzo1p, suggesting this relationship has been evolutionarily conserved (Stefely et al., 2016). Further studies are needed to understand how these sites are regulated, whether these sites facilitate import of intermediates or export of CoQ, and as well identifying the enzymes and substrates present at these sites. Alternatively, MFN2 and CoQ levels may be linked through glutathione redox cycles (GSH/GSSH) that activate mitochondrial fusion and which maybe mediated by semiquinone ROS production (Wang and Hekimi, 2016; Mattie et al., 2017). This possible MFN2-CoQ relationship remains to be investigated.

The second way mitochondrial fusion proteins mediate respiratory capacity is through maintenance of mtDNA. In line with previous studies, the complete loss of fusion (*dMfn* KO or *Opa1* KO) affected mtDNA copy number (Chen et al., 2010, 2011; Papanicolaou et al., 2012). As a consequence, we found that ATP production per oxygen consumed is limited to mtDNA levels. Although the absence of mitofusin1-2 or OPA1 presented CoQ deficiency, to a similar extent as loss of MFN2,

the respiratory impairment was driven by the partial collapse of the OXPHOS system due to mtDNA depletion rather than CoQ loss. This has several implications. It suggests that the combined loss of MFN1 and MFN2 does not have an additive effect to further reduce CoQ levels. Rather, it suggests the tethering properties of MFN2 play an important role in the synthesis of CoQ. Another conclusion drawn is that CoQ deficiency can occur as a secondary response to respiratory dysfunction as exemplified in *Opa1* KO MEFs. This finding is in agreement with other mutant animal models displaying CoQ loss associated with OXPHOS defects (Kühl et al., 2017). Moreover, since both loss of OMM and IMM fusion can elicit near identical bioenergetic impairments and mtDNA loss, it is unlikely that secondary role of OPA1 in cristae remodeling is the key mechanism driving OXPHOS dysfunction as previously proposed (Cogliati et al., 2013). Unexpectedly, the *dMfn* KO MEFs used by Cogliati and colleagues showed a contrasting bioenergetic profile and no growth defect on glucose and galactose medium. It is unclear why there is a discrepancy between these cell lines that share the same origin (the lab of David Chan, Caltech). However, a close inspection of the cristae morphology in two publications from this lab show *dMfn* KO MEFs exhibiting abnormal cristae (Gomes et al., 2011) and in a later study showing *dMfn* KO MEFs with no change in cristae shape (Cogliati et al., 2013). This suggests a shift in cell population likely occurred by clonal expansion and could explain the bioenergetic discrepancy. In summary, mitochondrial fusion proteins can influence respiratory function by either supporting CoQ synthesis or maintenance of mtDNA.

On mtDNA distribution

The research presented in this thesis show that OMM fusion proteins are important players to segregate mitochondrial nucleoids. Unexpectedly, nucleoid distribution was not dependent on IMM fusion. The majority of nucleoids in *Opa1* KO MEFs were distinctly present as single foci of similar size. This finding can mean two things. First, it could mean that mtDNA is not distributed throughout the mitochondrial network by IMM remodeling. This is supported by single molecule studies of TFAM that revealed constraint diffusion with the mitochondrial matrix, suggesting that nucleoids are not undergoing long-range redistribution (Busch et al., 2014). Second, it would also suggest that even mtDNA distribution throughout the mitochondrial network depends on proteins on the OMM. Indeed, it was shown that loss of DRP1 prevented mitochondrial division and induced massive aggregation of mtDNA (Ban-Ishihara et al., 2013; Ishihara et al., 2015). In comparison to *Drp1* KOs, mtDNA clustering in *dMfn* KOs was moderate.

In further support of the OMM as a mtDNA distribution center, newly synthesized mtDNA molecules were found to be segregated at ER-OMM contact sites (Lewis et al., 2016). Mitofusins may be involved in this process by establishing ER-mitochondria tethers. However, since loss of *Mfn2* only mildly induced clustering, it is still not clear if this is the underlying mechanism. Moreover, it remains to be investigated if losing ER-mitochondria contact sites would induce mtDNA clustering. One study on acute disruption of ER shape, that shifted the proportion of ER tubules into sheet-like structures, reported no mtDNA aggregation (Lewis et al., 2016). This experimental approach however might not have disrupted contact sites. Additionally, since changes in cholesterol content can also induce mtDNA clustering, studies looking at cholesterol content in *dMfn* KOs would also be warranted because the biosynthetic pathway for cholesterol is down-regulated in this model. Overall, from these and previous studies it is becoming evident that an important mtDNA distribution platform resides on the OMM, which rely on fusion and fission proteins.

On mtDNA integrity

We demonstrate that the profound mtDNA depletion is not explained by genome instability. *dMfn* heart KO animals neither showed a difference in mtDNA mutation load nor did they exhibit a greater abundance of mtDNA deletions. These findings go against a popular theory that fusion stabilizes mtDNA by preventing mutagenesis. This hypothesis is based on a previous report showing that skeletal muscle *dMfn* KO mice accumulate point mutations and deletions of mtDNA (Chen et al., 2010). However, this theory is unsatisfactory because the absolute levels of point mutations and deletions were extremely low ($2-3 \times 10^{-6}$ and 1×10^{-6} , respectively). Assuming that about $\sim 10^3$ mtDNA copies are present per nucleus in skeletal muscle cells, then only $1:10^3$ of the nuclear domains in skeletal muscle will contain a deletion or a point mutation of mtDNA. These low levels of mtDNA point mutations and deletions are insufficient to account for mtDNA loss or respiratory dysfunction. In comparison, the mutator mouse (POLG γ exonuclease mutant) harbors about 1×10^{-3} point mutations which is sufficient to cause OXPHOS dysfunction (Trifunovic et al., 2004). It is unlikely that the tissue-specific expression levels of mitofusins could account for the discrepancy between the studies. In both heart and skeletal muscle the RNA expression of *Mfn1* is low (7.7 and 5.5 RPKM, respectively), while *Mfn2* is very high in both tissues (89.9 and 71.1 RPKM, respectively). Interestingly, some adult patients with *Mfn2* or *Opa1* mutations were reported to have mtDNA deletions (Lodi et al., 2011; Rouzier et al., 2012). Although the determination of mtDNA deletions in these patients was not based on DNA sequencing but rather PCR, this finding would suggest a causal link between aging and formation of mtDNA deletions. Thus, it is possible that fusion-deficient animals do not live long enough to generate and accumulate mtDNA deletions, while human patients do. Further studies with animal models carrying human mutations in fusion proteins would help to determine if mitochondria genome stability depends on mitochondrial fusion proteins during aging.

On mtDNA depletion and premature death

We report that conditional heart *dMfn* KO animals suffer from severe mtDNA depletion and die prematurely between 5-6 weeks of age. This is in stark contrast to single mitofusin1 and 2 heart KO animals that have no change mtDNA copy number and have a normal life span (Mourier et al., 2015). However, the lifespan was similar to *dMfn* skeletal muscle KO animals that live up to 6-8 weeks (Chen et al., 2010). Other mutant mice displaying severe mtDNA loss also die around the same age as *dMfn* KO animals, such as *Polrmt* heart KO animals which live up to 6 weeks (Kühl et al., 2016). Some mutant mice die earlier, like *Tk2* whole body KO animals die at around 2 weeks of age (Zhou et al., 2008). Interestingly, *Opa1* skeletal muscle KO animals die the earliest, 9 days after birth (Tezze et al., 2017). However, not all mutant mice displaying mtDNA depletion die within the first month; *Tfam* heart KO animals die between 10-12 weeks of age, *Twnk* heart KO animals die at 19 weeks, and *Mgme1* whole body KO animals do not die prematurely (Hansson et al., 2004; Milenkovic et al., 2013; Matic et al., 2018). The early premature death of fusion-deficient animals further emphasizes the important of these proteins in mtDNA maintenance.

On mtDNA replication

The link between mitochondria fusion and mtDNA maintenance was first made in the budding yeast. The yeast homolog of *Opa1*, *Mgm1*, was named mitochondrial genome maintenance because loss of this protein caused complete loss of mtDNA (Jones and Fangman, 1992; Guan et al., 1993). In mammals, IMM and OMM fusion are equally important to maintain mitochondrial DNA copy number. In agreement with previous reports, the absence of mitofusins in mouse heart tissue leads to a strong reduction in mtDNA copy number (Chen et al., 2010; Papanicolaou et al., 2012). In our studies to uncover the molecular basis of mtDNA depletion upon the loss mitochondrial fusion, we were able to rule out certain factors. We found that mitochondrial fusion is dispensable for mt-transcription. Transcription activity was normal and reflective of total mtDNA template in *dMfn* KO animals and MEFs. Moreover, mtDNA clustering had no effect on transcription activity. Since *Drp1* KO animals exhibit massive nucleoid clustering without affecting mtDNA levels, we can

infer that moderate nucleoid clustering would not prevent mtDNA from being replicated in *dMfn* KO animals. Additionally, replication of mtDNA would not be impaired by a lack of dNTPs, as these were present in normal abundance. These findings would strongly argue that loss of mitochondrial fusion specifically affects mtDNA replication at the molecular level.

We show that OMM fusion ensures that the mtDNA replication is functional by maintaining a balanced replisome. This is well in line with previous *in vitro* studies that have shown that a balanced replisome composition is essential for efficient mtDNA replication (Farge et al., 2007; Fusté et al., 2014; Korhonen et al., 2004; Roos et al., 2013). Consistent with these data, mtDNA depletion phenotypes have also been reported *in vivo* when replisome proteins have been overexpressed or knocked-out in animals (Hance et al., 2005; Humble et al., 2013; Lefai et al., 2000; Martínez-Azorín et al., 2008; Milenkovic et al., 2013; Tynismaa et al., 2004). The presence of an imbalance replisome prevented high rates of mtDNA synthesis and resulted in the generation of incomplete replication products. How mitochondrial fusion ensures a balance replisome remains to be further examined. One possibility can be that content mixing induced by mitochondrial fusion may increase the half-life of replisome factors. In summary, we report an unexpected link between mitochondrial fusion and mammalian mtDNA replication, whereby mitochondrial fusion coordinates and promotes high rates of mtDNA replication by maintaining a balance replisome.

4.0 REFERENCES

- Abrahams, J.P., Leslie, A.G.W., Lutter, R., and Walker, J.E. (1994). Structure at 2.8 Å resolution of F₁-ATPase from bovine heart mitochondria. *Nature* *370*, 621–628.
- Akman, G., Desai, R., Bailey, L.J., Yasukawa, T., Dalla, I.R., Durigon, R., Holmes, J.B., Moss, C.F., Mennuni, M., Houlden, H., et al. (2016). Pathological ribonuclease H1 causes R-loop depletion and aberrant DNA segregation in mitochondria., Pathological ribonuclease H1 causes R-loop depletion and aberrant DNA segregation in mitochondria. *Proc. Natl. Acad. Sci. U. S. Am. Proc. Natl. Acad. Sci. U. S. Am.* *113*, 113, E4276, E4276-85.
- Allen, J.F. (2015). Why chloroplasts and mitochondria retain their own genomes and genetic systems: Colocation for redox regulation of gene expression. *Proc. Natl. Acad. Sci.* *112*, 10231–10238.
- Ameur, A., Stewart, J.B., Freyer, C., Hagström, E., Ingman, M., Larsson, N.-G., and Gyllenstein, U. (2011). Ultra-Deep Sequencing of Mouse Mitochondrial DNA: Mutational Patterns and Their Origins. *PLoS Genet* *7*, e1002028.
- Anderson, S., Bankier, A.T., Barrell, B.G., Bruijn, M.H.L. de, Coulson, A.R., Drouin, J., Eperon, I.C., Nierlich, D.P., Roe, B.A., Sanger, F., et al. (1981). Sequence and organization of the human mitochondrial genome. *Nature* *290*, 457–465.
- Ashburner, M., Ball, C.A., Blake, J.A., Botstein, D., Butler, H., Cherry, J.M., Davis, A.P., Dolinski, K., Dwight, S.S., Eppig, J.T., et al. (2000). Gene Ontology: tool for the unification of biology. *Nat. Genet.* *25*, 25–29.
- Ban, T., Ishihara, T., Kohno, H., Saita, S., Ichimura, A., Maenaka, K., Oka, T., Mihara, K., and Ishihara, N. (2017). Molecular basis of selective mitochondrial fusion by heterotypic action between OPA1 and cardiolipin. *Nat. Cell Biol.* *19*, 856.
- Ban-Ishihara, R., Ishihara, T., Sasaki, N., Mihara, K., and Ishihara, N. (2013). Dynamics of nucleoid structure regulated by mitochondrial fission contributes to cristae reformation and release of cytochrome c. *Proc. Natl. Acad. Sci.* *110*, 11863–11868.
- Berg, J.M., Tymoczko, J.L., and Stryer, L. (2002). Glucose Can Be Synthesized from Noncarbohydrate Precursors. *Biochem.* 5th Ed.
- Berk, A.J., and Clayton, D.A. (1974). Mechanism of mitochondrial DNA replication in mouse L-cells: Asynchronous replication of strands, segregation of circular daughter molecules, aspects of topology and turnover of an initiation sequence. *J. Mol. Biol.* *86*, 801–824.
- Bibb, M.J., Van Etten, R.A., Wright, C.T., Walberg, M.W., and Clayton, D.A. (1981). Sequence and gene organization of mouse mitochondrial DNA. *Cell* *26*, 167–180.
- Björkholm, P., Harish, A., Hagström, E., Ernst, A.M., and Andersson, S.G.E. (2015). Mitochondrial genomes are retained by selective constraints on protein targeting. *Proc. Natl. Acad. Sci.* *112*, 10154–10161.
- Bleazard, W., McCaffery, J.M., King, E.J., Bale, S., Mozdy, A., Tieu, Q., Nunnari, J., and Shaw, J.M. (1999). The dynamin-related GTPase Dnm1 regulates mitochondrial fission in yeast. *Nat. Cell Biol.* *1*, 298–304.
- Bogenhagen, D., and Clayton, D.A. (1977). Mouse L cell mitochondrial DNA molecules are selected randomly for replication throughout the cell cycle. *Cell* *11*, 719–727.
- Bogenhagen, D., and Clayton, D.A. (1978). Mechanism of mitochondrial DNA replication in mouse L-cells: Kinetics of synthesis and turnover of the initiation sequence. *J. Mol. Biol.* *119*, 49–68.
- Bonifacino, J.S., and Glick, B.S. (2004). The Mechanisms of Vesicle Budding and Fusion. *Cell* *116*, 153–166.
- Boutant, M., Kulkarni, S.S., Joffraud, M., Ratajczak, J., Valera-Alberni, M., Combe, R., Zorzano, A., and Cantó, C. (2017). Mfn2 is critical for brown adipose tissue thermogenic function. *EMBO J.* *36*, 1543–1558.
- Boyer, P.D. (1975). A model for conformational coupling of membrane potential and proton translocation to ATP

- synthesis and to active transport. *FEBS Lett.* **58**, 1–6.
- Boyer, P.D. (1993). The binding change mechanism for ATP synthase — Some probabilities and possibilities. *Biochim. Biophys. Acta BBA - Bioenerg.* **1140**, 215–250.
- Brandt, T., Cavellini, L., Kühlbrandt, W., and Cohen, M.M. (2016). A mitofusin-dependent docking ring complex triggers mitochondrial fusion in vitro. *ELife* **5**.
- de Brito, O.M., and Scorrano, L. (2008). Mitofusin 2 tethers endoplasmic reticulum to mitochondria. *Nature* **456**, 605–610.
- Brown, T.A., Cecconi, C., Tkachuk, A.N., Bustamante, C., and Clayton, D.A. (2005). Replication of mitochondrial DNA occurs by strand displacement with alternative light-strand origins, not via a strand-coupled mechanism. *Genes Dev.* **19**, 2466–2476.
- Brown, T.A., Tkachuk, A.N., Shtengel, G., Kopek, B.G., Bogenhagen, D.F., Hess, H.F., and Clayton, D.A. (2011). Superresolution Fluorescence Imaging of Mitochondrial Nucleoids Reveals Their Spatial Range, Limits, and Membrane Interaction. *Mol. Cell Biol.* **31**, 4994–5010.
- Busch, K.B., Kowald, A., and Spelbrink, J.N. (2014). Quality matters: how does mitochondrial network dynamics and quality control impact on mtDNA integrity? *Philos. Trans. R. Soc. B Biol. Sci.* **369**.
- Cannon, B., and Nedergaard, J. (2008). Studies of Thermogenesis and Mitochondrial Function in Adipose Tissues. In *Adipose Tissue Protocols*, (Humana Press), pp. 109–121.
- Cao, L., Shitara, H., Horii, T., Nagao, Y., Imai, H., Abe, K., Hara, T., Hayashi, J.-I., and Yonekawa, H. (2007). The mitochondrial bottleneck occurs without reduction of mtDNA content in female mouse germ cells. *Nat. Genet.* **39**, 386–390.
- Cao, Y.-L., Meng, S., Chen, Y., Feng, J.-X., Gu, D.-D., Yu, B., Li, Y.-J., Yang, J.-Y., Liao, S., Chan, D.C., et al. (2017). MFN1 structures reveal nucleotide-triggered dimerization critical for mitochondrial fusion. *Nature* **542**, 372–376.
- Carrodeguas, J.A., Pinz, K.G., and Bogenhagen, D.F. (2002). DNA Binding Properties of Human pol γ B. *J. Biol. Chem.* **277**, 50008–50014.
- Cerritelli, S.M., Frolova, E.G., Feng, C., Grinberg, A., Love, P.E., and Crouch, R.J. (2003). Failure to Produce Mitochondrial DNA Results in Embryonic Lethality in Rnaseh1 Null Mice. *Mol. Cell* **11**, 807–815.
- Chatre, L., and Ricchetti, M. (2013). Prevalent coordination of mitochondrial DNA transcription and initiation of replication with the cell cycle. *Nucleic Acids Res.* **41**, 3068–3078.
- Chen, H., Detmer, S.A., Ewald, A.J., Griffin, E.E., Fraser, S.E., and Chan, D.C. (2003). Mitofusins Mfn1 and Mfn2 coordinately regulate mitochondrial fusion and are essential for embryonic development. *J. Cell Biol.* **160**, 189–200.
- Chen, H., Vermulst, M., Wang, Y.E., Chomyn, A., Prolla, T.A., McCaffery, J.M., and Chan, D.C. (2010). Mitochondrial Fusion Is Required for mtDNA Stability in Skeletal Muscle and Tolerance of mtDNA Mutations. *Cell* **141**, 280–289.
- Chen, Y., Liu, Y., and Dorn, G.W. (2011). Mitochondrial Fusion is Essential for Organelle Function and Cardiac Homeostasis. *Circ. Res.* **109**, 1327–1331.
- Cherepanov, D.A., Mulkidjanian, A.Y., and Junge, W. (1999). Transient accumulation of elastic energy in proton translocating ATP synthase. *FEBS Lett.* **449**, 1–6.
- Cipolat, S., de Brito, O.M., Dal Zilio, B., and Scorrano, L. (2004). OPA1 requires mitofusin 1 to promote mitochondrial fusion. *Proc. Natl. Acad. Sci. U. S. A.* **101**, 15927–15932.
- Cogliati, S., Frezza, C., Soriano, M.E., Varanita, T., Quintana-Cabrera, R., Corrado, M., Cipolat, S., Costa, V., Casarin, A., Gomes, L.C., et al. (2013). Mitochondrial Cristae Shape Determines Respiratory Chain Supercomplexes Assembly and Respiratory Efficiency. *Cell* **155**, 160–171.
- Cortopassi, G.A., and Arnheim, N. (1990). Detection of a specific mitochondrial DNA

- deletion in tissues of older humans. *Nucleic Acids Res.* *18*, 6927–6933.
- Del Dotto, V., Mishra, P., Vidoni, S., Fogazza, M., Maresca, A., Caporali, L., McCaffery, J.M., Cappelletti, M., Baruffini, E., Lenaers, G., et al. (2017). OPA1 Isoforms in the Hierarchical Organization of Mitochondrial Functions. *Cell Rep.* *19*, 2557–2571.
- Desai, R., Frazier, A.E., Durigon, R., Patel, H., Jones, A.W., Dalla Rosa, I., Lake, N.J., Compton, A.G., Mountford, H.S., Tucker, E.J., et al. (2017). ATAD3 gene cluster deletions cause cerebellar dysfunction associated with altered mitochondrial DNA and cholesterol metabolism. *Brain* *140*, 1595–1610.
- Doda, J.N., Wright, C.T., and Clayton, D.A. (1981). Elongation of displacement-loop strands in human and mouse mitochondrial DNA is arrested near specific template sequences. *Proc. Natl. Acad. Sci. U. S. A.* *78*, 6116–6120.
- Dufour, E., Terzioglu, M., Sterky, F.H., Sørensen, L., Galter, D., Olson, L., Wilbertz, J., and Larsson, N.-G. (2008). Age-associated mosaic respiratory chain deficiency causes trans-neuronal degeneration. *Hum. Mol. Genet.* *17*, 1418–1426.
- Durigon, R., Mitchell, A.L., Jones, A.W., Manole, A., Mennuni, M., Hirst, E.M., Houlden, H., Maragni, G., Lattante, S., Doronzio, P.N., et al. (2018). LETM1 couples mitochondrial DNA metabolism and nutrient preference. *EMBO Mol. Med.* e8550.
- Falkenberg, M. (2018). Mitochondrial DNA replication in mammalian cells: overview of the pathway. *Essays Biochem.* EBC20170100.
- Falkenberg, M., Larsson, N.-G., and Gustafsson, C.M. (2007). DNA Replication and Transcription in Mammalian Mitochondria. *Annu. Rev. Biochem.* *76*, 679–699.
- Farge, G., Pham, X.H., Holmlund, T., Khorostov, I., and Falkenberg, M. (2007). The accessory subunit B of DNA polymerase γ is required for mitochondrial replisome function. *Nucleic Acids Res.* *35*, 902–911.
- Farge, G., Holmlund, T., Khvorostova, J., Rofougaran, R., Hofer, A., and Falkenberg, M. (2008). The N-terminal domain of TWINKLE contributes to single-stranded DNA binding and DNA helicase activities. *Nucleic Acids Res.* *36*, 393–403.
- Farmer, T., Naslavsky, N., and Caplan, S. (2018). Tying trafficking to fusion and fission at the mighty mitochondria. *Traffic* *19*, 569–577.
- Farr, C.L., Wang, Y., and Kaguni, L.S. (1999). Functional Interactions of Mitochondrial DNA Polymerase and Single-stranded DNA-binding Protein TEMPLATE-PRIMER DNA BINDING AND INITIATION AND ELONGATION OF DNA STRAND SYNTHESIS. *J. Biol. Chem.* *274*, 14779–14785.
- Fernández-Ayala, D.J.M., Brea-Calvo, G., López-Lluch, G., and Navas, P. (2005). Coenzyme Q distribution in HL-60 human cells depends on the endomembrane system. *Biochim. Biophys. Acta BBA - Biomembr.* *1713*, 129–137.
- Fernández-Millán, P., Lázaro, M., Cansiz-Arda, Ş., Gerhold, J.M., Rajala, N., Schmitz, C.-A., Silva-Espiña, C., Gil, D., Bernadó, P., Valle, M., et al. (2015). The hexameric structure of the human mitochondrial replicative helicase Twinkle. *Nucleic Acids Res.* *43*, 4284–4295.
- Fisher, R.P., Lisowsky, T., Parisi, M.A., and Clayton, D.A. (1992). DNA wrapping and bending by a mitochondrial high mobility group-like transcriptional activator protein. *J. Biol. Chem.* *267*, 3358–3367.
- Friedman, J.R., Lackner, L.L., West, M., DiBenedetto, J.R., Nunnari, J., and Voeltz, G.K. (2011). ER Tubules Mark Sites of Mitochondrial Division. *Science* *334*, 358–362.
- Gerhold, J.M., Cansiz-Arda, Ş., Löhmus, M., Engberg, O., Reyes, A., Rennes, H., van Sanz, A., Holt, I.J., Cooper, H.M., and Spelbrink, J.N. (2015a). Human Mitochondrial DNA-Protein Complexes Attach to a Cholesterol-Rich Membrane Structure. *Sci. Rep.* *5*, 15292.
- Gerhold, J.M., Cansiz-Arda, Ş., Löhmus, M., Engberg, O., Reyes, A., van Rennes, H., Sanz, A., Holt, I.J., Cooper, H.M., and Spelbrink, J.N. (2015b). Human Mitochondrial DNA-Protein Complexes Attach to a Cholesterol-Rich Membrane Structure. *Sci. Rep.* *5*.

- Gilkerson, R.W., Selker, J.M.L., and Capaldi, R.A. (2003). The cristal membrane of mitochondria is the principal site of oxidative phosphorylation. *FEBS Lett.* *546*, 355–358.
- Gomes, L.C., Benedetto, G.D., and Scorrano, L. (2011). During autophagy mitochondria elongate, are spared from degradation and sustain cell viability. *Nat. Cell Biol.* *13*, 589–598.
- Gray, M.W. (2015). Mosaic nature of the mitochondrial proteome: Implications for the origin and evolution of mitochondria. *Proc. Natl. Acad. Sci. U. S. A.* *112*, 10133–10138.
- Gray, M.W., Burger, G., and Lang, B.F. (1999). Mitochondrial Evolution. *Science* *283*, 1476–1481.
- Griparic, L., Wel, N.N. van der, Orozco, I.J., Peters, P.J., and Blik, A.M. van der (2004). Loss of the Intermembrane Space Protein Mgm1/OPA1 Induces Swelling and Localized Constrictions along the Lengths of Mitochondria. *J. Biol. Chem.* *279*, 18792–18798.
- Guan, K., Farh, L., Marshall, T.K., and Deschenes, R.J. (1993). Normal mitochondrial structure and genome maintenance in yeast requires the dynamin-like product of the MGM1 gene. *Curr. Genet.* *24*, 141–148.
- Gustafsson, C.M., Falkenberg, M., and Larsson, N.-G. (2016). Maintenance and Expression of Mammalian Mitochondrial DNA. *Annu. Rev. Biochem.* *85*, null.
- Hales, K.G., and Fuller, M.T. (1997). Developmentally Regulated Mitochondrial Fusion Mediated by a Conserved, Novel, Predicted GTPase. *Cell* *90*, 121–129.
- Hance, N., Ekstrand, M.I., and Trifunovic, A. (2005). Mitochondrial DNA polymerase gamma is essential for mammalian embryogenesis. *Hum. Mol. Genet.* *14*, 1775–1783.
- Hansson, A., Hance, N., Dufour, E., Rantanen, A., Hultenby, K., Clayton, D.A., Wibom, R., and Larsson, N.-G. (2004). A switch in metabolism precedes increased mitochondrial biogenesis in respiratory chain-deficient mouse hearts. *Proc. Natl. Acad. Sci.* *101*, 3136–3141.
- Herrmann, G.J., Thatcher, J.W., Mills, J.P., Hales, K.G., Fuller, M.T., Nunnari, J., and Shaw, J.M. (1998). Mitochondrial Fusion in Yeast Requires the Transmembrane GTPase Fzo1p. *J. Cell Biol.* *143*, 359–373.
- Herrmann, J.M., and Köhl, R. (2007). Catch me if you can! Oxidative protein trapping in the intermembrane space of mitochondria. *J. Cell Biol.* *176*, 559–563.
- Hillen, H.S., Morozov, Y.I., Sarfallah, A., Temiakov, D., and Cramer, P. (2017). Structural Basis of Mitochondrial Transcription Initiation. *Cell* *171*, 1072–1081.e10.
- Holt, I.J., Harding, A.E., and Morgan-Hughes, J.A. (1988). Deletions of muscle mitochondrial DNA in patients with mitochondrial myopathies. *Nature* *331*, 717–719.
- Hu, J., Dong, L., and Outten, C.E. (2008). The Redox Environment in the Mitochondrial Intermembrane Space Is Maintained Separately from the Cytosol and Matrix. *J. Biol. Chem.* *283*, 29126–29134.
- Huang, D.W., Sherman, B.T., and Lempicki, R.A. (2008). Systematic and integrative analysis of large gene lists using DAVID bioinformatics resources. *Nat. Protoc.* *4*, 44–57.
- Huang, G., Massoudi, D., Muir, A.M., Joshi, D.C., Zhang, C.-L., Chiu, S.Y., and Greenspan, D.S. (2017). WBSR16 Is a Guanine Nucleotide Exchange Factor Important for Mitochondrial Fusion. *Cell Rep.* *20*, 923–934.
- Humble, M.M., Young, M.J., Foley, J.F., Pandiri, A.R., Travlos, G.S., and Copeland, W.C. (2013). Polg2 is essential for mammalian embryogenesis and is required for mtDNA maintenance. *Hum. Mol. Genet.* *22*, 1017–1025.
- Ignatenko, O., Chilov, D., Paetau, I., Miguel, E., Jackson, C.B., Capin, G., Paetau, A., Terzioglu, M., Euro, L., and Suomalainen, A. (2018). Loss of mtDNA activates astrocytes and leads to spongiform encephalopathy. *Nat. Commun.* *9*, 70.
- Ingerman, E., Perkins, E.M., Marino, M., Mears, J.A., McCaffery, J.M., Hinshaw, J.E., and Nunnari, J. (2005). Dnm1 forms spirals

- that are structurally tailored to fit mitochondria. *J. Cell Biol.* *170*, 1021–1027.
- Ishihara, N., Fujita, Y., Oka, T., and Mihara, K. (2006). Regulation of mitochondrial morphology through proteolytic cleavage of OPA1. *EMBO J.* *25*, 2966–2977.
- Ishihara, N., Nomura, M., Jofuku, A., Kato, H., Suzuki, S.O., Masuda, K., Otera, H., Nakanishi, Y., Nonaka, I., Goto, Y.-I., et al. (2009). Mitochondrial fission factor Drp1 is essential for embryonic development and synapse formation in mice. *Nat. Cell Biol.* *11*, 958–966.
- Ishihara, T., Ban-Ishihara, R., Maeda, M., Matsunaga, Y., Ichimura, A., Kyogoku, S., Aoki, H., Katada, S., Nakada, K., Nomura, M., et al. (2015). Dynamics of Mitochondrial DNA Nucleoids Regulated by Mitochondrial Fission Is Essential for Maintenance of Homogeneously Active Mitochondria during Neonatal Heart Development. *Mol. Cell. Biol.* *35*, 211–223.
- Jones, B.A., and Fangman, W.L. (1992). Mitochondrial DNA maintenance in yeast requires a protein containing a region related to the GTP-binding domain of dynamin. *Genes Dev.* *6*, 380–389.
- Kanehisa, M., and Goto, S. (2000). KEGG: Kyoto Encyclopedia of Genes and Genomes. *Nucleic Acids Res.* *28*, 27–30.
- Kaufman, B.A., Durisic, N., Mativetsky, J.M., Costantino, S., Hancock, M.A., Grutter, P., and Shoubbridge, E.A. (2007). The Mitochondrial Transcription Factor TFAM Coordinates the Assembly of Multiple DNA Molecules into Nucleoid-like Structures. *Mol. Biol. Cell* *18*, 3225–3236.
- Kaupilla, J.H.K., Bonekamp, N.A., Mourier, A., Isokallio, M.A., Just, A., Kaupilla, T.E.S., Stewart, J.B., and Larsson, N.-G. (2018). Base-excision repair deficiency alone or combined with increased oxidative stress does not increase mtDNA point mutations in mice. *Nucleic Acids Res.* *46*, 6642–6669.
- Keeling, P.J., and Palmer, J.D. (2008). Horizontal gene transfer in eukaryotic evolution. *Nat. Rev. Genet.* *9*, 605–618.
- Kiselycznyk, C., and Holmes, A. (2011). All (C57BL/6) Mice are not Created Equal. *Front. Neurosci.* *5*.
- Kolesar, J.E., Wang, C.Y., Taguchi, Y.V., Chou, S.-H., and Kaufman, B.A. (2013). Two-dimensional intact mitochondrial DNA agarose electrophoresis reveals the structural complexity of the mammalian mitochondrial genome. *Nucleic Acids Res.* *41*, e58.
- Korhonen, J.A., Gaspari, M., and Falkenberg, M. (2003a). TWINKLE Has 5' → 3' DNA Helicase Activity and Is Specifically Stimulated by Mitochondrial Single-stranded DNA-binding Protein. *J. Biol. Chem.* *278*, 48627–48632.
- Korhonen, J.A., Gaspari, M., and Falkenberg, M. (2003b). TWINKLE Has 5' → 3' DNA Helicase Activity and Is Specifically Stimulated by Mitochondrial Single-stranded DNA-binding Protein. *J. Biol. Chem.* *278*, 48627–48632.
- Koshiba, T., Detmer, S.A., Kaiser, J.T., Chen, H., McCaffery, J.M., and Chan, D.C. (2004). Structural Basis of Mitochondrial Tethering by Mitofusin Complexes. *Science* *305*, 858–862.
- Kühl, I., Kukat, C., Ruzzenente, B., Milenkovic, D., Mourier, A., Miranda, M., Koolmeister, C., Falkenberg, M., and Larsson, N.-G. (2014). POLRMT does not transcribe nuclear genes. *Nature* *514*, E7–E11.
- Kühl, I., Miranda, M., Posse, V., Milenkovic, D., Mourier, A., Siira, S.J., Bonekamp, N.A., Neumann, U., Filipovska, A., Polosa, P.L., et al. (2016). POLRMT regulates the switch between replication primer formation and gene expression of mammalian mtDNA. *Sci. Adv.* *2*, e1600963.
- Kühl, I., Miranda, M., Atanassov, I., Kuznetsova, I., Hinze, Y., Mourier, A., Filipovska, A., and Larsson, N.-G. (2017). Transcriptomic and proteomic landscape of mitochondrial dysfunction reveals secondary coenzyme Q deficiency in mammals. *ELife* *6*, e30952.
- Kukat, C., Wurm, C.A., Spähr, H., Falkenberg, M., Larsson, N.-G., and Jakobs, S. (2011). Super-resolution microscopy reveals that mammalian mitochondrial nucleoids have a uniform size and frequently contain a single

- copy of mtDNA. *Proc. Natl. Acad. Sci.* *108*, 13534–13539.
- Kukat, C., Davies, K.M., Wurm, C.A., Spähr, H., Bonekamp, N.A., Köhl, I., Joos, F., Polosa, P.L., Park, C.B., Posse, V., et al. (2015). Cross-strand binding of TFAM to a single mtDNA molecule forms the mitochondrial nucleoid. *Proc. Natl. Acad. Sci. U. S. A.*
- Kurland, C.G., and Andersson, S.G.E. (2000). Origin and Evolution of the Mitochondrial Proteome. *Microbiol. Mol. Biol. Rev.* *64*, 786–820.
- Lagouge, M., Mourier, A., Lee, H.J., Spähr, H., Wai, T., Kukat, C., Silva Ramos, E., Motori, E., Busch, J.D., Siira, S., et al. (2015). SLIRP Regulates the Rate of Mitochondrial Protein Synthesis and Protects LRPPRC from Degradation. *PLoS Genet* *11*, e1005423.
- Langmead, B., Trapnell, C., Pop, M., and Salzberg, S.L. (2009). Ultrafast and memory-efficient alignment of short DNA sequences to the human genome. *Genome Biol.* *10*, R25.
- Larsson, N.-G. (2010). Somatic Mitochondrial DNA Mutations in Mammalian Aging. *Annu. Rev. Biochem.* *79*, 683–706.
- Larsson, N.G., Oldfors, A., Holme, E., and Clayton, D.A. (1994). Low Levels of Mitochondrial Transcription Factor A in Mitochondrial DNA Depletion. *Biochem. Biophys. Res. Commun.* *200*, 1374–1381.
- Larsson, N.G., Wang, J., Wilhelmsson, H., Oldfors, A., Rustin, P., Lewandoski, M., Barsh, G.S., and Clayton, D.A. (1998). Mitochondrial transcription factor A is necessary for mtDNA maintenance and embryogenesis in mice. *Nat. Genet.* *18*, 231–236.
- Lee, J.E., Westrate, L.M., Wu, H., Page, C., and Voeltz, G.K. (2016). Multiple dynamin family members collaborate to drive mitochondrial division. *Nature* *540*, 139–143.
- Lee, S., Sterky, F.H., Mourier, A., Terzioglu, M., Cullheim, S., Olson, L., and Larsson, N.-G. (2012). Mitofusin 2 is necessary for striatal axonal projections of midbrain dopamine neurons. *Hum. Mol. Genet.* *21*, 4827–4835.
- Lefai, E., Calleja, M., Ruiz de Mena, I., Lagina III, A.T., Kaguni, L.S., and Garesse, R. (2000). Overexpression of the catalytic subunit of DNA polymerase γ results in depletion of mitochondrial DNA in *Drosophila melanogaster*. *Mol. Gen. Genet. MGG* *264*, 37–46.
- Legesse-Miller, A., Massol, R.H., and Kirchhausen, T. (2003). Constriction and Dnm1p Recruitment Are Distinct Processes in Mitochondrial Fission. *Mol. Biol. Cell* *14*, 1953–1963.
- Lewis, S.C., Uchiyama, L.F., and Nunnari, J. (2016). ER-mitochondria contacts couple mtDNA synthesis with mitochondrial division in human cells. *Science* *353*, aaf5549.
- Li, H., and Durbin, R. (2010). Fast and accurate long-read alignment with Burrows–Wheeler transform. *Bioinformatics* *26*, 589–595.
- Li, H., Handsaker, B., Wysoker, A., Fennell, T., Ruan, J., Homer, N., Marth, G., Abecasis, G., and Durbin, R. (2009). The Sequence Alignment/Map format and SAMtools. *Bioinformatics* *25*, 2078–2079.
- Li, M., Schönberg, A., Schaefer, M., Schroeder, R., Nasidze, I., and Stoneking, M. (2010). Detecting Heteroplasmy from High-Throughput Sequencing of Complete Human Mitochondrial DNA Genomes. *Am. J. Hum. Genet.* *87*, 237–249.
- Lodi, R., Tonon, C., Valentino, M.L., Manners, D., Testa, C., Malucelli, E., Morgia, C.L., Barboni, P., Carbonelli, M., Schimpf, S., et al. (2011). Defective Mitochondrial Adenosine Triphosphate Production in Skeletal Muscle From Patients With Dominant Optic Atrophy Due to OPA1 Mutations. *Arch. Neurol.* *68*, 67–73.
- Losón, O.C., Song, Z., Chen, H., and Chan, D.C. (2013). Fis1, Mff, MiD49, and MiD51 mediate Drp1 recruitment in mitochondrial fission. *Mol. Biol. Cell* *24*, 659–667.
- Macao, B., Uhler, J.P., Siibak, T., Zhu, X., Shi, Y., Sheng, W., Olsson, M., Stewart, J.B., Gustafsson, C.M., and Falkenberg, M. (2015). The exonuclease activity of DNA polymerase γ is required for ligation during mitochondrial DNA replication. *Nat. Commun.* *6*.

- Mahdaviani, K., Benador, I.Y., Su, S., Gharakhanian, R.A., Stiles, L., Trudeau, K.M., Cardamone, M., Enríquez-Zarralanga, V., Ritou, E., Aprahamian, T., et al. (2017). Mfn2 deletion in brown adipose tissue protects from insulin resistance and impairs thermogenesis. *EMBO Rep.* *18*, 1123–1138.
- Mai, N., Chrzanowska-Lightowlers, Z.M.A., and Lightowlers, R.N. (2017). The process of mammalian mitochondrial protein synthesis. *Cell Tissue Res.* *367*, 5–20.
- Maier, U.-G., Zauner, S., Woehle, C., Bolte, K., Hempel, F., Allen, J.F., and Martin, W.F. (2013). Massively Convergent Evolution for Ribosomal Protein Gene Content in Plastid and Mitochondrial Genomes. *Genome Biol. Evol.* *5*, 2318–2329.
- Mandel, H., Szargel, R., Labay, V., Elpeleg, O., Saada, A., Shalata, A., Anbinder, Y., Berkowitz, D., Hartman, C., Barak, M., et al. (2001). The deoxyguanosine kinase gene is mutated in individuals with depleted hepatocerebral mitochondrial DNA. *Nat. Genet.* *29*, 337–341.
- Martin, M., Cho, J., Cesare, A.J., Griffith, J.D., and Attardi, G. (2005). Termination Factor-Mediated DNA Loop between Termination and Initiation Sites Drives Mitochondrial rRNA Synthesis. *Cell* *123*, 1227–1240.
- Matic, S., Jiang, M., Nicholls, T.J., Uhler, J.P., Dirksen-Schwandenland, C., Polosa, P.L., Simard, M.-L., Li, X., Atanassov, I., Rackham, O., et al. (2018). Mice lacking the mitochondrial exonuclease MGME1 accumulate mtDNA deletions without developing progeria. *Nat. Commun.* *9*, 1202.
- Mattie, S., Riemer, J., Wideman, J.G., and McBride, H.M. (2017). A new mitofusin topology places the redox-regulated C terminus in the mitochondrial intermembrane space. *J Cell Biol* jcb.201611194.
- McBride, H.M. (2018). Mitochondria and endomembrane origins. *Curr. Biol.* *28*, R367–R372.
- Milenkovic, D., Matic, S., Kühl, I., Ruzzenente, B., Freyer, C., Jemt, E., Park, C.B., Falkenberg, M., and Larsson, N.-G. (2013). TWINKLE is an essential mitochondrial helicase required for synthesis of nascent D-loop strands and complete mtDNA replication. *Hum. Mol. Genet.* *22*, 1983–1993.
- Misgeld, T., and Schwarz, T.L. (2017). Mitostasis in Neurons: Maintaining Mitochondria in an Extended Cellular Architecture. *Neuron* *96*, 651–666.
- Mishra, P., and Chan, D.C. (2014). Mitochondrial dynamics and inheritance during cell division, development and disease. *Nat. Rev. Mol. Cell Biol.* *15*, 634–646.
- Mishra, P., Carelli, V., Manfredi, G., and Chan, D.C. (2014). Proteolytic Cleavage of Opa1 Stimulates Mitochondrial Inner Membrane Fusion and Couples Fusion to Oxidative Phosphorylation. *Cell Metab.* *19*, 630–641.
- Mishra, P., Varuzhanyan, G., Pham, A.H., and Chan, D.C. (2015). Mitochondrial Dynamics Is a Distinguishing Feature of Skeletal Muscle Fiber Types and Regulates Organellar Compartmentalization. *Cell Metab.* *22*, 1033–1044.
- Mitchell, P. (1961). Coupling of Phosphorylation to Electron and Hydrogen Transfer by a Chemi-Osmotic type of Mechanism. *Nature* *191*, 144–148.
- Moraes, C.T., DiMauro, S., Zeviani, M., Lombes, A., Shanske, S., Miranda, A.F., Nakase, H., Bonilla, E., Werneck, L.C., Servidei, S., et al. (1989). Mitochondrial DNA Deletions in Progressive External Ophthalmoplegia and Kearns-Sayre Syndrome. *N. Engl. J. Med.* *320*, 1293–1299.
- Mourier, A., Ruzzenente, B., Brandt, T., Kühlbrandt, W., and Larsson, N.-G. (2014). Loss of LRPPRC causes ATP synthase deficiency. *Hum. Mol. Genet.* ddt652.
- Mourier, A., Motori, E., Brandt, T., Lagouge, M., Atanassov, I., Galinier, A., Rappl, G., Brodesser, S., Hultenby, K., Dieterich, C., et al. (2015). Mitofusin 2 is required to maintain mitochondrial coenzyme Q levels. *J. Cell Biol.* *208*, 429–442.
- Nass, M.M.K., and Nass, S. (1963). INTRAMITOCHONDRIAL FIBERS WITH DNA CHARACTERISTICS I. Fixation and Electron Staining Reactions. *J. Cell Biol.* *19*, 593–611.

- Neupert, W. (2012). SnapShot: Mitochondrial Architecture. *Cell* 149, 722-722.e1.
- Nicholls, D.G., and Ferguson, S.J. (2013a). 9 - Cellular Bioenergetics. In *Bioenergetics (Fourth Edition)*, D.G. Nicholls, and S.J. Ferguson, eds. (Boston: Academic Press), pp. 255-302.
- Nicholls, D.G., and Ferguson, S.J. (2013b). 5 - Respiratory Chains. In *Bioenergetics (Fourth Edition)*, D.G. Nicholls, and S.J. Ferguson, eds. (Boston: Academic Press), pp. 91-157.
- Nicholls, T.J., Nadalutti, C.A., Motori, E., Sommerville, E.W., Gorman, G.S., Basu, S., Hoberg, E., Turnbull, D.M., Chinnery, P.F., Larsson, N.-G., et al. (2018). Topoisomerase 3 α Is Required for Decatenation and Segregation of Human mtDNA. *Mol. Cell* 69, 9-23.e6.
- Nikkanen, J., Forsström, S., Euro, L., Paetau, I., Kohnz, R.A., Wang, L., Chilov, D., Viinamäki, J., Roivainen, A., Marjamäki, P., et al. (2016). Mitochondrial DNA Replication Defects Disturb Cellular dNTP Pools and Remodel One-Carbon Metabolism. *Cell Metab.* 23, 635-648.
- Ojala, D., Montoya, J., and Attardi, G. (1981). tRNA punctuation model of RNA processing in human mitochondria. *Nature* 290, 470-474.
- Olafsson, S., Whittington, D., Murray, J., Regnier, M., and Moussavi-Harami, F. (2017). Fast and sensitive HPLC-MS/MS method for direct quantification of intracellular deoxyribonucleoside triphosphates from tissue and cells. *J. Chromatogr. B* 1068-1069, 90-97.
- Ong, S.-E., and Mann, M. (2006). A practical recipe for stable isotope labeling by amino acids in cell culture (SILAC). *Nat. Protoc.* 1, 2650-2660.
- Otera, H., Wang, C., Cleland, M.M., Setoguchi, K., Yokota, S., Youle, R.J., and Mihara, K. (2010). Mff is an essential factor for mitochondrial recruitment of Drp1 during mitochondrial fission in mammalian cells. *J. Cell Biol.* 191, 1141-1158.
- Ozawa, T., Yoneda, M., Tanaka, M., Ohno, K., Sato, W., Suzuki, H., Nishikimi, M., Yamamoto, M., Nonaka, I., and Horai, S. (1988). Maternal inheritance of deleted mitochondrial DNA in a family with mitochondrial myopathy. *Biochem. Biophys. Res. Commun.* 154, 1240-1247.
- Palmer, C.S., Osellame, L.D., Laine, D., Koutsopoulos, O.S., Frazier, A.E., and Ryan, M.T. (2011). MiD49 and MiD51, new components of the mitochondrial fission machinery. *EMBO Rep.* 12, 565-573.
- Papanicolaou, K.N., Kikuchi, R., Ngoh, G.A., Coughlan, K.A., Dominguez, I., Stanley, W.C., and Walsh, K. (2012). Mitofusins 1 and 2 Are Essential for Postnatal Metabolic Remodeling in Heart. *Circ. Res.* 111, 1012-1026.
- Parone, P.A., Cruz, S.D., Tondera, D., Mattenberger, Y., James, D.I., Maechler, P., Barja, F., and Martinou, J.-C. (2008). Preventing Mitochondrial Fission Impairs Mitochondrial Function and Leads to Loss of Mitochondrial DNA. *PLOS ONE* 3, e3257.
- Payne, B.A.I., Wilson, I.J., Yu-Wai-Man, P., Coxhead, J., Deehan, D., Horvath, R., Taylor, R.W., Samuels, D.C., Santibanez-Koref, M., and Chinnery, P.F. (2013). Universal heteroplasmy of human mitochondrial DNA. *Hum. Mol. Genet.* 22, 384-390.
- Pinto, A.R., Ilinykh, A., Ivey, M.J., Kuwabara, J.T., D'Antoni, M.L., Debuque, R., Chandran, A., Wang, L., Arora, K., Rosenthal, N., et al. (2016). Revisiting Cardiac Cellular Composition. *Circ. Res.* 118, 400-409.
- Posse, V., and Gustafsson, C.M. (2017). Human Mitochondrial Transcription Factor B2 Is Required for Promoter Melting during Initiation of Transcription. *J. Biol. Chem.* 292, 2637-2645.
- Posse, V., Shahzad, S., Falkenberg, M., Hällberg, B.M., and Gustafsson, C.M. (2015). TEFM is a potent stimulator of mitochondrial transcription elongation in vitro. *Nucleic Acids Res.* 43, 2615-2624.
- Rajala, N., Gerhold, J.M., Martinsson, P., Klymov, A., and Spelbrink, J.N. (2014). Replication factors transiently associate with mtDNA at the mitochondrial inner membrane to facilitate replication. *Nucleic Acids Res.* 42, 952-967.

- Ramachandran, A., Basu, U., Sultana, S., Nandakumar, D., and Patel, S.S. (2017). Human mitochondrial transcription factors TFAM and TFB2M work synergistically in promoter melting during transcription initiation. *Nucleic Acids Res.* *45*, 861–874.
- Rapaport, D., Brunner, M., Neupert, W., and Westermann, B. (1998). Fzo1p Is a Mitochondrial Outer Membrane Protein Essential for the Biogenesis of Functional Mitochondria in *Saccharomyces cerevisiae*. *J. Biol. Chem.* *273*, 20150–20155.
- Ringel, R., Sologub, M., Morozov, Y.I., Litonin, D., Cramer, P., and Temiakov, D. (2011). Structure of human mitochondrial RNA polymerase. *Nature* *478*, 269–273.
- Robberson, D.L., and Clayton, D.A. (1972). Replication of Mitochondrial DNA in Mouse L Cells and Their Thymidine Kinase-Derivatives: Displacement Replication on a Covalently-Closed Circular Template. *Proc. Natl. Acad. Sci. U. S. A.* *69*, 3810–3814.
- Roos, S., Macao, B., Fusté, J.M., Lindberg, C., Jemt, E., Holme, E., Moslemi, A.-R., Oldfors, A., and Falkenberg, M. (2013). Subnormal levels of POLyA cause inefficient initiation of light-strand DNA synthesis and lead to mitochondrial DNA deletions and autosomal dominant progressive external ophthalmoplegia. *Hum. Mol. Genet.* *22*, 2411–2422.
- Rötig, A., and Poulton, J. (2009). Genetic causes of mitochondrial DNA depletion in humans. *Biochim. Biophys. Acta BBA - Mol. Basis Dis.* *1792*, 1103–1108.
- Rouzier, C., Bannwarth, S., Chaussonot, A., Chevrollier, A., Verschueren, A., Bonello-Palot, N., Fragaki, K., Cano, A., Pouget, J., Pellissier, J.-F., et al. (2012). The MFN2 gene is responsible for mitochondrial DNA instability and optic atrophy 'plus' phenotype. *Brain* *135*, 23–34.
- Ruzzenente, B., Metodiev, M.D., Wredenberg, A., Bratic, A., Park, C.B., Cámara, Y., Milenkovic, D., Zickermann, V., Wibom, R., Hultenby, K., et al. (2012). LRPPRC is necessary for polyadenylation and coordination of translation of mitochondrial mRNAs. *EMBO J.* *31*, 443–456.
- Ryan, M.T., and Hoogenraad, N.J. (2007). Mitochondrial-Nuclear Communications. *Annu. Rev. Biochem.* *76*, 701–722.
- Saada, A., Shaag, A., Mandel, H., Nevo, Y., Eriksson, S., and Elpeleg, O. (2001). Mutant mitochondrial thymidine kinase in mitochondrial DNA depletion myopathy. *Nat. Genet.* *29*, 342–344.
- Santel, A., and Fuller, M.T. (2001). Control of mitochondrial morphology by a human mitofusin. *J. Cell Sci.* *114*, 867–874.
- Satoh, M., and Kuroiwa, T. (1991). Organization of multiple nucleoids and DNA molecules in mitochondria of a human cell. *Exp. Cell Res.* *196*, 137–140.
- Schon, E.A., Rizzuto, R., Moraes, C.T., Nakase, H., Zeviani, M., and DiMauro, S. (1989). A direct repeat is a hotspot for large-scale deletion of human mitochondrial DNA. *Science* *244*, 346–349.
- Sebastián, D., Hernández-Alvarez, M.I., Segalés, J., Sorianoello, E., Muñoz, J.P., Sala, D., Waget, A., Liesa, M., Paz, J.C., Gopalacharyulu, P., et al. (2012). Mitofusin 2 (Mfn2) links mitochondrial and endoplasmic reticulum function with insulin signaling and is essential for normal glucose homeostasis. *Proc. Natl. Acad. Sci.*
- Shepard, K.A., and Yaffe, M.P. (1999). The yeast dynamin-like protein, Mgm1p, functions on the mitochondrial outer membrane to mediate mitochondrial inheritance. *J. Cell Biol.* *144*, 711–720.
- Shoubridge, E.A., Karpati, G., and Hastings, K.E.M. (1990). Deletion mutants are functionally dominant over wild-type mitochondrial genomes in skeletal muscle fiber segments in mitochondrial disease. *Cell* *62*, 43–49.
- Signes, A., and Fernandez-Vizarra, E. (2018). Assembly of mammalian oxidative phosphorylation complexes I–V and supercomplexes. *Essays Biochem.* *62*, 255–270.
- Silva Ramos, E., Larsson, N.-G., and Mourier, A. (2016). Bioenergetic roles of mitochondrial fusion. *Biochim. Biophys. Acta BBA - Bioenerg.* *1857*, 1277–1283.

- Smirnova, E., Shurland, D.-L., Ryazantsev, S.N., and Blik, A.M. van der (1998). A Human Dynamin-related Protein Controls the Distribution of Mitochondria. *J. Cell Biol.* *143*, 351–358.
- Spelbrink, J.N., Toivonen, J.M., Hakkaart, G.A.J., Kurkela, J.M., Cooper, H.M., Lehtinen, S.K., Lecrenier, N., Back, J.W., Speijer, D., Foury, F., et al. (2000). In Vivo Functional Analysis of the Human Mitochondrial DNA Polymerase POLG Expressed in Cultured Human Cells. *J. Biol. Chem.* *275*, 24818–24828.
- Spelbrink, J.N., Li, F.-Y., Tiranti, V., Nikali, K., Yuan, Q.-P., Tariq, M., Wanrooij, S., Garrido, N., Comi, G., Morandi, L., et al. (2001). Human mitochondrial DNA deletions associated with mutations in the gene encoding Twinkle, a phage T7 gene 4-like protein localized in mitochondria. *Nat. Genet.* *28*, 223–231.
- Spiegel, R., Saada, A., Flannery, P.J., Burté, F., Soiferman, D., Khayat, M., Eisner, V., Vladovski, E., Taylor, R.W., Bindoff, L.A., et al. (2016). Fatal infantile mitochondrial encephalomyopathy, hypertrophic cardiomyopathy and optic atrophy associated with a homozygous OPA1 mutation. *J. Med. Genet.* *53*, 127–131.
- Spinelli, J.B., and Haigis, M.C. (2018). The multifaceted contributions of mitochondria to cellular metabolism. *Nat. Cell Biol.* *20*, 745–754.
- Stefely, J.A., and Pagliarini, D.J. (2017). Biochemistry of Mitochondrial Coenzyme Q Biosynthesis. *Trends Biochem. Sci.* *42*, 824–843.
- Stefely, J.A., Kwiecien, N.W., Freiberger, E.C., Richards, A.L., Jochem, A., Rush, M.J.P., Ulbrich, A., Robinson, K.P., Hutchins, P.D., Veling, M.T., et al. (2016). Mitochondrial protein functions elucidated by multi-omic mass spectrometry profiling. *Nat. Biotechnol.* *34*, 1191–1197.
- Sterky, F.H., Lee, S., Wibom, R., Olson, L., and Larsson, N.-G. (2011). Impaired mitochondrial transport and Parkin-independent degeneration of respiratory chain-deficient dopamine neurons in vivo. *Proc. Natl. Acad. Sci.* *108*, 12937–12942.
- Stewart, J.B., Freyer, C., Elson, J.L., Wredenberg, A., Cansu, Z., Trifunovic, A., and Larsson, N.-G. (2008). Strong Purifying Selection in Transmission of Mammalian Mitochondrial DNA. *PLoS Biol* *6*, e10.
- Štrajbl, M., Shurki, A., and Warshel, A. (2003). Converting conformational changes to electrostatic energy in molecular motors: The energetics of ATP synthase. *Proc. Natl. Acad. Sci. U. S. A.* *100*, 14834–14839.
- Suomalainen, A., Majander, A., Haltia, M., Somer, H., Lönnqvist, J., Savontaus, M.L., and Peltonen, L. (1992). Multiple deletions of mitochondrial DNA in several tissues of a patient with severe retarded depression and familial progressive external ophthalmoplegia. *J. Clin. Invest.* *90*, 61–66.
- Suzuki, T., Nagao, A., and Suzuki, T. (2011). Human Mitochondrial tRNAs: Biogenesis, Function, Structural Aspects, and Diseases. *Annu. Rev. Genet.* *45*, 299–329.
- Szyrach, G., Ott, M., Bonnefoy, N., Neupert, W., and Herrmann, J.M. (2003). Ribosome binding to the Oxa1 complex facilitates co-translational protein insertion in mitochondria. *EMBO J.* *22*, 6448–6457.
- Terzioglu, M., Ruzzenente, B., Harmel, J., Mourier, A., Jemt, E., López, M.D., Kukat, C., Stewart, J.B., Wibom, R., Meharg, C., et al. (2013). MTERF1 Binds mtDNA to Prevent Transcriptional Interference at the Light-Strand Promoter but Is Dispensable for rRNA Gene Transcription Regulation. *Cell Metab.* *17*, 618–626.
- Tezze, C., Romanello, V., Desbats, M.A., Fadini, G.P., Albiero, M., Favaro, G., Ciciliot, S., Soriano, M.E., Morbidoni, V., Cerqua, C., et al. (2017). Age-Associated Loss of OPA1 in Muscle Impacts Muscle Mass, Metabolic Homeostasis, Systemic Inflammation, and Epithelial Senescence. *Cell Metab.* *25*, 1374–1389.e6.
- Tilokani, L., Nagashima, S., Paupe, V., and Prudent, J. (2018). Mitochondrial dynamics: overview of molecular mechanisms. *Essays Biochem.* *62*, 341–360.
- Tiranti, V., Rocchi, M., DiDonato, S., and Zeviani, M. (1993). Cloning of human and rat cDNAs encoding the mitochondrial single-

- stranded DNA-binding protein (SSB). *Gene* 126, 219–225.
- Trifunovic, A., Wredenberg, A., Falkenberg, M., Spelbrink, J.N., Rovio, A.T., Bruder, C.E., Bohlooly-Y, M., Gidlof, S., Oldfors, A., Wibom, R., et al. (2004). Premature ageing in mice expressing defective mitochondrial DNA polymerase. *Nature* 429, 417–423.
- Trumpower, B.L. (1990). The protonmotive Q cycle. Energy transduction by coupling of proton translocation to electron transfer by the cytochrome bc₁ complex. *J. Biol. Chem.* 265, 11409–11412.
- Tyynismaa, H., Sembongi, H., Bokori-Brown, M., Granycome, C., Ashley, N., Poulton, J., Jalanko, A., Spelbrink, J.N., Holt, I.J., and Suomalainen, A. (2004). Twinkle helicase is essential for mtDNA maintenance and regulates mtDNA copy number. *Hum. Mol. Genet.* 13, 3219–3227.
- Tyynismaa, H., Mjosund, K.P., Wanrooij, S., Lappalainen, I., Ylikallio, E., Jalanko, A., Spelbrink, J.N., Paetau, A., and Suomalainen, A. (2005). Mutant mitochondrial helicase Twinkle causes multiple mtDNA deletions and a late-onset mitochondrial disease in mice. *Proc. Natl. Acad. Sci. U. S. A.* 102, 17687–17692.
- Uhler, J.P., Thörn, C., Nicholls, T.J., Matic, S., Milenkovic, D., Gustafsson, C.M., and Falkenberg, M. (2016). MGME1 processes flaps into ligatable nicks in concert with DNA polymerase γ during mtDNA replication. *Nucleic Acids Res.* 44, 5861–5871.
- Viscomi, C., and Zeviani, M. (2017). MtDNA-maintenance defects: syndromes and genes. *J. Inherit. Metab. Dis.* 40, 587–599.
- Wang, C., and Youle, R.J. (2009). The Role of Mitochondria in Apoptosis*. *Annu. Rev. Genet.* 43, 95–118.
- Wang, H., and Oster, G. (1998). Energy transduction in the F₁ motor of ATP synthase. *Nature* 396, 279–282.
- Wang, Y., and Hekimi, S. (2016). Understanding Ubiquinone. *Trends Cell Biol.* 26, 367–378.
- Wanrooij, S., and Falkenberg, M. (2010). The human mitochondrial replication fork in health and disease. *Biochim. Biophys. Acta BBA - Bioenerg.* 1797, 1378–1388.
- Wanrooij, P.H., Uhler, J.P., Shi, Y., Westerlund, F., Falkenberg, M., and Gustafsson, C.M. (2012). A hybrid G-quadruplex structure formed between RNA and DNA explains the extraordinary stability of the mitochondrial R-loop. *Nucleic Acids Res.* 40, 10334–10344.
- Weibel, E.R. (1979). *Stereological Methods: Practical methods for biological morphometry* (Academic Press).
- Westermann, B. (2012). Bioenergetic role of mitochondrial fusion and fission. *Biochim. Biophys. Acta BBA - Bioenerg.* 1817, 1833–1838.
- Wikström, M., Krab, K., and Sharma, V. (2018). Oxygen Activation and Energy Conservation by Cytochrome c Oxidase. *Chem. Rev.* 118, 2469–2490.
- Yang, C., Curth, U., Urbanke, C., and Kang, C. (1997). Crystal structure of human mitochondrial single-stranded DNA binding protein at 2.4 Å resolution. *Nat. Struct. Mol. Biol.* 4, 153–157.
- Yu, S.B., and Pekkurnaz, G. (2018). Mechanisms Orchestrating Mitochondrial Dynamics for Energy Homeostasis. *J. Mol. Biol.*
- Zeviani, M., Servidei, S., Gellera, C., Bertini, E., DiMauro, S., and DiDonato, S. (1989). An autosomal dominant disorder with multiple deletions of mitochondrial DNA starting at the D-loop region. *Nature* 339, 309–311.
- Zhou, X., Solaroli, N., Bjerke, M., Stewart, J.B., Rozell, B., Johansson, M., and Karlsson, A. (2008). Progressive loss of mitochondrial DNA in thymidine kinase 2-deficient mice. *Hum. Mol. Genet.* 17, 2329–2335.
- Zorova, L.D., Popkov, V.A., Plotnikov, E.Y., Silachev, D.N., Pevzner, I.B., Jankauskas, S.S., Babenko, V.A., Zorov, S.D., Balakireva, A.V., Juhaszova, M., et al. (2018). Mitochondrial membrane potential. *Anal. Biochem.* 552, 50–59.

5.0 MATERIAL AND METHODS

5.1 GENERATION AND MAINTENANCE OF MICE

5.1.1 Generation of mutant mice

Mice with loxP-flanked *Mfn1* and *Mfn2* genes were generated by Taconic Biosciences and previously described in (Lee et al., 2012). These mice have loxP sites flanking exon 3 of the *Mfn1* gene and exon 5 of the *Mfn2* gene and a neomycin resistance cassette flanked by Frt sites was introduced to select for homologous recombination. The neomycin resistance cassette was removed by mating transgenic mice with mice constitutively expressing Flp recombinase. Conditional *Mfn1* and *Mfn2* heart double knockout mice were generated by mating *Mfn1*^{loxP/loxP} and *Mfn2*^{loxP/loxP} mice with mice expressing the Cre-recombinase protein (*Mfn1*^{loxP/loxP} and *Mfn2*^{loxP/+}, *Cre*^{+/-}) in heart and skeletal muscle under the control of the muscle creatinine kinase promoter (*Ckmm*). Littermates or age-matched animals lacking the Cre-recombinase allele were used as controls. For certain imaging experiments, *Mfn1*^{loxP/loxP}, *Mfn2*^{loxP/+}, *Cre*^{+/-} mice were crossed with *Mfn1*^{loxP/loxP}, *Mfn2*^{loxP/loxP}, *Cre*^{-/-} mice, constitutively expressing a mitochondria-targeted yellow fluorescence protein protein (*YFP*^{Tg/Tg}) from the ROSA26 locus. YFP reporter mice were previously described in (Sterky et al., 2011).

5.1.2 Mouse husbandry

All inbred C57BL/6N mice were housed in the animal facility at the Max Planck Institute for Biology of Aging. The mouse facility maintained a 12 hour light/dark cycle with an ambient temperature of 21°C. All mice were approved and permitted by the Landesamt für Natur, Umwelt and Verbraucherschutz, Nordrhein-Westfalen, Germany. All animal work was performed following the guidelines of the Federation of European Laboratory Animal Science Associations (FELASA).

5.1.3 Mouse genotyping

Two-week old pups were genotyped by isolating DNA from ear clippings; see *phenol chloroform extraction* for details. DNA was subject to polymerase chain reaction

(PCR) to amplify a target genomic segment, see Table 1 for details. PCR primers were designed to detect the both wild type and loxP-flanked *Mfn1* or *Mfn2* alleles, the *Cre* transgene, or the *Yfp* transgene. See Table 2 for PCR primers used for genotyping. PCR products were subjected to gel electrophoresis using 1 % agarose gels (Thermo Fisher Scientific, 16500-500) containing ethidium bromide and visualized using a U:Genius gel documentation system (Integrated Scientific Solutions Inc.).

Table 1: PCR reaction mix and conditions

<i>Locus</i>	<i>Reagents</i>	<i>Volume (μl)</i>	<i>PCR conditions</i>
<i>Mfn1</i> or <i>Mfn2</i>	DNA	2	95°C, 3 minutes
	5x PCR buffer	6	
	dNTP mix (1.25 mM each)	5	95°C, 30 seconds
	For primer (10 pmol/μl)	0.6	60°C, 30 seconds
	Rev primer (10 pmol/μl)	0.6	72°C, 1 minutes
	Taq polymerase	0.15	(30 cycles)
	Water	15.56	
	<i>Total volume</i>	28	72°C, 5 minutes
<i>Cre</i>	DNA	1	95°C, 3 minutes
	5x PCR buffer	4	
	dNTP mix (1.25 mM each)	3.2	95°C, 30 seconds
	For primer (10 pmol/μl)	0.6	53°C, 30 seconds
	Rev primer (10 pmol/μl)	0.6	72°C, 45 seconds
	Taq polymerase	0.1	(30 cycles)
	Water	10.5	
	<i>Total volume</i>	20	72°C, 5 minutes
<i>ROSA26</i>	DNA	1	95°C, 3 minutes
	5x PCR buffer	4	
	dNTP mix (1.25 mM each)	3.2	95°C, 30 seconds
	Primer 1 (10 pmol/μl)	0.4	55°C, 30 seconds
	Primer 2 (10 pmol/μl)	0.4	72°C, 1 minutes
	Primer 3 (10 pmol/μl)	0.4	(30 cycles)
	Taq polymerase	0.1	
Water	10.5		
	<i>Total volume</i>	20	72°C, 5 minutes

Table 2: Primers for mouse genotyping

<i>Locus</i>	<i>Primers</i>	<i>PCR products</i>
<i>Mfn1</i>	For, 5' TCTCCCCACAACAGTTTTTACC 3'	Wild type allele, 342 bp
	Rev, 5' CAGCCTGTGCTACATGAAACC 3'	loxP allele, 499 bp
<i>Mfn2</i>	For, 5' CTGATGGGGTAGAAGAGATGG 3'	Wild type allele, 141 bp
	Rev, 5' CTTCAAGGTCAGGCAAAGG 3'	loxP allele, 298 bp
<i>Cre</i>	For, 5' CACGACCAAGTGACAGCAAT 3'	Cre allele, 371bp
	Rev, 5' AGAGACGGAAATCCATCGCT 3'	
<i>ROSA26</i>	Primer 1, 5' AAAGTCGCTCTGAGTTGTTAT 3'	Wild type allele, 583 bp
	Primer 2, 5' GCGAAGAGTTTGTCTCAACC 3'	loxP allele, 300 bp
	Primer 3, 5' GGAGCGGGAGAAATGGATATG 3'	

5.2 CELL MODELS AND MAINTENANCE

5.2.1 Cell Lines

Mfn1, *Mfn2*, *Mfn1-2* double knockout mouse embryonic fibroblasts (MEF) were originally generated and immortalized in the lab of Prof. Dr. David Chan at the California Institute of Technology (Chen et al., 2003, 2005). Based on the published literature related to generation of these cell lines (Chen et al., 2003), the wild-type *Mfn1* and *Mfn2* genomic locus were double crossover with a targeted construct resulting in the generation of a pre-mature stop codon in exon 3 and a neomycin-resistance cassette flanked by loxP sites was inserted. MEFs were prepared from embryonic day 10.5 and immortalized by infection with retrovirus expressing Simian vacuolating virus 40 large T antigen. Control and *Mfn1*, *Mfn2*, *dMfn*, and *Opal* knockout MEFs were obtained as a gift from Prof. Dr. Thomas Langer and Dr. Mafalda Escobar-Henriques from the University of Cologne.

5.2.2 Cell Culture

All cells were maintained at 37°C with 5 % CO₂ in DMEM GlutaMax media containing 25 mM glucose (Thermo Fisher Scientific, 31966-021) and supplemented with 10 % fetal bovine serum (Thermo Fisher Scientific, 10270-106), 100 U/ml penicillin and 100 µg/ml streptomycin (Thermo Fisher Scientific, 15070-063), 1x non-essential amino acids (Thermo Fisher Scientific, 11140-050), and 50 µg/ml uridine (Sigma-Aldrich, U3750). Cells were passaged when confluency in a flask reached 90 %. Typical viability of cells was between 96-98 %.

5.3 BIOENERGETIC METHODS

5.3.1 Isolation of heart mitochondria for bioenergetics

Functional assessment of mitochondria requires intact mitochondrial membranes and the coupling of the respiratory chain to proton translocation across the inner mitochondrial membrane. High-quality mitochondria were isolated from mouse heart by gentle hand-homogenization followed by differential centrifugation. First, mice were sacrificed by cervical dislocation, skin disinfected with 70 % ethanol, the heart quickly extracted, and washed in ice-cold PBS. Remaining blood inside the heart was gently squeezed out with forceps. Tissue was then minced and placed inside a 5 ml Potter S homogenizer (Sartorius) containing 5 ml of mitochondria isolation buffer (MIB, 310 mM sucrose, 20 mM Tris-HCl, and 1 mM EGTA). Tissue was hand homogenized slowly with two different pestles, a very loose pestle first and then a slightly loose pestle, both custom made. Homogenates were transferred into a 13 ml centrifuge tube. To separate mitochondria from nuclear and cytoplasmic fractions, homogenates were centrifuged for 10 minutes at 1,000x *g* and 4°C. Supernatants were transferred into a new 13 ml centrifuge tube and mitochondria pelleted by centrifugation at 4,500x *g* for 10 minutes at 4°C. Crude mitochondria were resuspended gently with cut pipette tips in MIB and transferred into a 1.5 ml microcentrifuge tube. During experiments mitochondria were kept on ice or when not in use stored at -80°C.

5.3.2 High-resolution respirometry: Mitochondria

Mitochondria respiration is measured by recording the oxygen consumption at complex IV, as oxygen is reduced into water. An Oroboros-2K equipped with a polarographic oxygen sensor (Oroboros Instruments) was used for high-resolution determination of respiration in isolated mitochondria.

The Oxygraph-2K was calibrated to atmospheric oxygen prior to measurement of biological samples according to manufactures instructions. On experimental days, chambers were washed three times with water and 2.1 ml of fresh respiration buffer (120 mM sucrose, 50 mM KCl, 20 mM Tris-HCl, 4 mM KH_2PO_4 , 2 mM MgCl_2 , and 1 mM EGTA, pH 7.2) was incubated at 37°C and air calibrated with constant stirring until oxygen and flux plots were stabilized. The following parameters were set for the instrument: oxygen gain sensor set to 2, stirrer speed set to 750 rpm, data recording intervals set to 2, and oxygen slope set to 15.

Mitochondrial respiration under phosphorylating, non-phosphorylating, and uncoupled states was performed sequentially on 30 μg of crude heart mitochondria. Complex I-driven respiration under phosphorylating conditions was assessed by adding 1 mM ADP (Sigma-Aldrich, A2754), 10 mM pyruvate (Sigma-Aldrich, P2256), 5 mM glutamate (Sigma-Aldrich, 49449), and 5 mM malate (Sigma-Aldrich, M1000). Complex II-driven respiration under phosphorylating conditions was assessed by adding 1 mM ADP, 10 mM succinate (Sigma-Aldrich, S3674), and 10 nM rotenone (Sigma-Aldrich, R8875). The non-phosphorylating state was evaluated by the addition of 2.5 $\mu\text{g}/\text{ml}$ oligomycin (Sigma-Aldrich, O4876). The maximum respiratory capacity of mitochondria was reached by uncoupling electron transfer from proton translocation by successive addition of CCCP (Sigma-Aldrich, C2759) up to 3 μM . Respiratory controls (the ratio of phosphorylating/non-phosphorylating flux) were > 10 for complex I-driven respiration and >5 for complex II-driven respiration based on control heart mitochondria. A respiratory control ratio >3 denotes coupled mitochondria.

5.3.3 High-resolution respirometry: Whole cells

Mitochondrial respiration in whole cells is determined in a similar matter as for isolated mitochondria using an Oxygraph-2K. MEFs were maintained for 5 to 6 days in DMEM GlutaMax containing 25 mM glucose and supplemented with 1 % dialyzed fetal bovine serum (Sigma-Aldrich, A3382001), 100 U/ml penicillin and streptomycin, 1x non-essential amino acids, and 50 µg/ml uridine. MEFs were passaged once during this equilibration phase. On experimental days, MEFs in log phase were washed with PBS, trypsinized with 1 ml of 0.25 % Trypsin-EDTA (Thermo Fisher Scientific, 25200056), diluted with culture medium, cells pelleted by centrifugation at 800xg for 5 minutes, and resuspended in 800 µl of culture medium. A cell count from a 1:10 dilution was performed using a Vi-Cell XR cell analyzer (Beckman Coulter).

Mitochondrial respiration under phosphorylating, non-phosphorylating, and uncoupled states was performed sequentially using 1 million viable cells. See *High-resolution respirometry: Mitochondria* for details on Oxygraph preparation. Before the addition of respiratory substrates, cells were permeabilized with 0.02 mg/ml Digitonin (Sigma-Aldrich, 300410)/ethanol (4 µl from 10 mg/ml stock). Complex II-driven mitochondrial respiration under phosphorylating conditions was assessed with 2.3 mM ADP (10 µl from 0.5 M stock), 19.5 mM succinate (20 µl from 1 M stock), and 4.8 mM glycerol-3-phosphate (20 µl from 0.5 M stock, Sigma-Aldrich, G7886). The non-phosphorylating state was evaluated by the addition of 0.25 µg/ml oligomycin (1 µl from 500 µg/ml stock) and the maximum respiratory capacity of mitochondria was reached by successive addition of CCCP up to 0.3 µM (1 µl steps using 0.1 mM CCCP stock). Respiratory controls (the ratio of phosphorylating/non-phosphorylating flux) were >5 for complex II-driven respiration based on control cells.

5.3.4 Mitochondrial ATP production

Through the oxidative phosphorylation system ADP and phosphate can be converted into ATP, a chemical form of cellular energy. Mitochondrial ATP production can be measured in isolated mitochondria after substrate feeding using a commercially available ATPlite 1step kit (PerkinElmer, 6016736). The oxygen

consumption and ATP synthesis rates in isolated heart mitochondria (65 μg) were simultaneously measured via complex I-driven respiration (1 mM ADP, 10 mM pyruvate, 5 mM glutamate, and 5 mM malate) or complex II-driven respiration (1 mM ADP, 2 mM succinate, and 10 nM rotenone). To determine the ATP content, aliquots were collected every 20 seconds, precipitated in 7 % HClO_4 and 25 mM EDTA, centrifuged at 16,000 g for 10 minutes, and neutralized with 2 M KOH and 0.3 M MOPS. The ATPlite 1step kit was used following manufacture's instructions to measure the ATP abundance. The non-oxidative ATP synthesis rate was determined in a parallel experiment using oligomycin.

5.3.5 Respiratory Chain Enzyme Activities

Enzymatic activity of respiratory chain complexes in isolated mitochondria was assessed through spectrophotometric analysis and through respirometry analysis. Complex I, II, and citrate synthase activity was determined using a spectrophotometer (UV-3600; Hitachi) at 37°C using 15-50 μg of heart isolated mitochondria in 1 ml of phosphate buffer (50 mM KH_2PO_4 , pH 7.4). Complex I, NADH dehydrogenase, activity was determined in the presence of 0.25 mM NADH, 0.25 mM decylubiquinone, and 1 mM KCN at 340 nm ($\epsilon = 6220 \text{ M}^{-1}\text{cm}^{-1}$). Rotenone was added to control for complex I specific activity. Complex II, succinate dehydrogenase, activity was determined in the presence of 40 mM succinate, 35 μM dichlorophenolindophenol (DCPIP), and 1 mM KCN at 600 nm ($\epsilon = 21,000 \text{ M}^{-1}\text{cm}^{-1}$). Citrate synthase activity was determined in the presence of 0.1 mM acetyl-CoA, 0.5 mM oxaloacetate, and 0.1 mM 5,5'-dithiobis-2-nitrobenzoic acid (DTNB) at 412 nm ($\epsilon = 13,600 \text{ M}^{-1}\text{cm}^{-1}$). Complex IV activity was assessed on 65 μg of isolated mitochondria in 2 ml of MIB. Oxygen consumption was recorded using an Oxygraph-2K in the presence of 0.2 mM TMPD, 1 mM ascorbate, and 0.5 μM Antimycin A. Once respiratory flux was stabilized KCN (2 mM final) was injected into chamber. Complex IV activity was calculated as the difference between TMPD/ascorbate flux minus residual flux after KCN addition.

5.4 PROTEIN BIOCHEMISTRY

5.4.1 Isolation of heart mitochondria

Mice were sacrificed by cervical dislocation, skin disinfected with 70 % ethanol, the heart quickly extracted, and washed in ice-cold PBS. The remaining blood inside the heart was gently squeezed out with forceps. Tissue was then minced and placed inside a 5 ml Potter S homogenizer (Sartorius) containing 5 ml of MIB. Tissue was homogenized using a Homgen plus homogenizer (Schuett-biotech) with a fitting pestle performing 16 strokes at 300 rpm. Homogenates were transferred into a 13 ml centrifuge tube and centrifuged for 10 minutes at 1,000x *g* and 4°C. Supernatants were transferred into a new 13 ml centrifuge tube and mitochondria pelleted by centrifugation at 10,000x *g* for 10 minutes at 4°C. Crude mitochondria were gently resuspend in MIB and transferred into a 1.5 ml microcentrifuge tube. During experiments, mitochondria were kept on ice or when not in use stored at -80°C.

5.4.2 Isolation of MEF mitochondria

Isolation of mitochondria from cells was achieved by hypotonic cell disruption, homogenization with a syringe and followed by differential centrifugation, as previous described in (Lee and Bogenhagen 2016) with minor modifications. Cells were grown on square dishes (Thermo Fisher Scientific, 166508) for 2-3 days with standard medium. Cells were scraped with ice-cold PBS and centrifuged at 500x *g* for 5 minutes at 4°C. Cells were resuspended in 3 ml of 1x mitochondria isolation buffer for cells (MSH, 210 mM mannitol, 70 mM sucrose, 2 mM EDTA, 20 mM HEPES (KOH) pH 8.0, 0.2 mg/ml BSA, 2 mM DTT, and 1x protease inhibitors (Sigma-Aldrich, 04693159001), and plasma membrane was permeabilized with 0.04 % Digitonin (12 µl from 10 % Digitonin stock) for 2-3 minutes on ice. Digitonin was diluted by adding 7 ml of 1x MSH buffer and cells pelleted at 1,200x *g* for 5 minutes at 4°C. Cells were resuspended in 3 ml 1x MSH and lysed using a 25-G needle (Braun, 4657519) for about 12 strokes. After lysis an additional 7 ml of 1x MSH was added to the samples. Homogenates were centrifuged at 900x *g* for 5 minutes at 4°C using a swing-out rotor. Supernatant was collected in a new 15 ml tube and centrifugation step repeated another 2x to remove as much of the nuclear and cytoplasmic debris.

Supernatants were then centrifuged at 15,000x *g* for 15 minutes at 4°C to pellet mitochondria.

Mitochondria were washed with 3 ml of isolation buffer with potassium chloride (1x MSH, 1 M KCl) to further remove nuclear DNA and cytoplasmic rRNA contamination. Mitochondria were pelleted by centrifugation at 15,000x *g* for 15 minutes at 4°C and resuspended in 1 ml of nuclease buffer (1 mM ADP, 5 mM glutamic acid, 5 mM malate, 10 mM NaOH, 0.25 mg/ml BSA, 1x MSH buffer, 1x protease inhibitors, 10 mM MgCl₂, 60 mM KCl, 1 mM K₂HPO₄, 2 mM DTT) containing 25 µl DNaseI (2 mg/ml stock, Sigma, 10104159001), 2 µl Turbo DNase (1x stock, Thermo Fisher Scientific, AM2238), and 5 µl of RNase A (Qiagen, 19101). Samples were incubated for 20 minutes at 37°C with 500 rpm on an orbital shaker. Reaction was stop by with 25 mM EDTA (50 µl of 0.5 M stock).

Mitochondria were subject to an additional purification step through sucrose gradient sedimentation. DNase/RNase treated mitochondria were layered on top of a sucrose gradient. A sucrose gradient was prepared in an Ultraclear tube (Beckman Coulter, 344059) and composed of two layers. The upper layer contained 6 ml of 1M sucrose (1 M sucrose, 20 mM HEPES pH 8.0, 2 mM EDTA, 2 mM DTT, and 1x protease inhibitor cocktail) and the lower layer was 3 ml of 1.7M sucrose (1.7 M sucrose, 20 mM HEPES (KOH) pH 8.0, 2 mM EDTA, 2 mM DTT, and 1x protease inhibitors). Samples were centrifuged at 25,000 rpm for 25 minutes at 4°C using a SW-41 Ti rotor. Mitochondria were collected from the 1.7 M / 1 M sucrose interface into a 1.5 ml microcentrifuge tube, diluted with 2-3 volumes of 0.5x MSH buffer, and centrifuged at 10,000x *g* for 10 minutes at 4°C. Mitochondria were washed with 1x MSH buffer and centrifuged again. Lastly, mitochondria were resuspended in 1x MSH buffer (50 µl per square plate). During experiments mitochondria were kept on ice or when not in use stored at -80°C.

5.4.3 DC Protein Assay

Protein concentrations of isolated mitochondria from whole tissue and whole cell extracts were determined using the commercially available DC (detergent compatible) protein assay from Bio-Rad (5000111). Each sample was prepared in a clear 96-well Flat-bottom plate (Greiner bio-one, 655101) as duplicates. A standard

protein curve ranging from 5 μg to 30 μg was prepared using a 10 $\mu\text{g}/\mu\text{l}$ BSA stock (New England BioLabs, B9000S). First, 0.5 μl of reagent S (surfactant solution) was combined with 1 ml of reagent A (alkaline copper tartrate solution). Then, 25 μl of reagent A/S was pipetted to each well. Next, 1 μl of undiluted sample was added to a designated well. The plate was gently vortexed, 200 μl of reagent B (Folin reagent) was added to each well, and incubated at room temperature for 15 minutes. Absorbance was recorded at 750 nm with an Infinite M200 Pro plate reader (Tecan). A linear regression analysis was performed on protein standards and used to calculate protein concentration of experimental samples.

5.4.4 Western Blot

The abundance of target proteins can be analyzed in a homogenate or extract by immunoblotting with specific antibodies that recognized a protein of interest. Heart tissue and whole cells were first lysed in RIPA buffer (150 mM NaCl, 1.0 % NP-40 (Sigma-Aldrich, I8896) or Triton X-100 (Sigma-Aldrich, T8787), 0.5 % sodium deoxycholate (Sigma-Aldrich, D6750), 0.1 % SDS (Roth, CN302), 50 mM Tris pH 8.0). After lysis, protein concentration was determined using DC protein assay and 25-100 μg of protein was resuspended in 2x NuPAGE LDS Sample Buffer (Thermo Fisher Scientific, NP0007) with 0.1 M DTT. Isolated mitochondria were prepared by first removing the storage buffer (MIB) by centrifugation at 10,000 $\times g$ for 5 minutes at 4°C, followed by resuspension in 2x NuPAGE LDS Sample Buffer with 0.1 M DTT. Proteins were separated by SDS-PAGE in 4-12 % Bis-Tris precast gels using a XCell SureLock cell (Thermo Fisher Scientific). Proteins were transferred onto a 0.45 μm PVDF membrane (GE Healthcare, 1060023), or in some cases 0.45 μm nitrocellulose membranes (GE Healthcare, 10600002), with 1x transfer buffer (38.6 mM Tris, 47.8 mM glycine, 20 % methanol) using a Criterion blotter (Bio-Rad). After transfer, membranes were washed in 1x TBS and then blocked in 3 % milk/TBS for 1 hour. Primary antibodies were applied overnight at 4°C. Membranes were then washed 3x with TBST (0.1 % Tween 20 (Sigma-Aldrich, P9416) /TBS) for 5 minutes, 1x with TBS for 5 minutes, and HRP-conjugated secondary antibodies applied at room temperature. See Table 3 for complete list of primary and secondary antibodies used. Afterwards, membranes were washed again 3x with TBST and 1x with TBS.

Detection of HRP-conjugated secondary antibodies was achieved using Amersham ECL western blotting detection reagent (GE Healthcare, RPN2106) and Amersham Hyperfilm ECL (GE Healthcare, 28906836). For certain experiments, after primary antibody incubation PVDF membranes were decorated with near-infrared fluorescence-conjugated secondary antibodies (1:30,000 in BSA, Table 3) for 30 minutes at room temperature, washed 3x with TBST and 1x with TBS, and followed by fluorescence signal detection with an Odyssey imaging system.

Table 3: Primary and secondary antibodies used for immunoblotting

Protein target	Host	Source	Catalogue #	Dilution
Anti- β -Actin	Mouse	Abcam	ab8226	1:500
Anti-MFN1	Rabbit	Abcam	ab104274	1:500
Anti-MFN2	Mouse	Abcam	ab56889	1:500
Anti-OXPHOS cocktail	Mouse	Abcam	ab110413	1:1000
Anti-POLyA	Rabbit	Abcam	ab12899	1:250
Anti-TFAM	Rabbit	Abcam	ab131607	1:1000
Anti-VDAC	Mouse	Abcam	ab14734	1:1000
Anti-SSBP1	Rabbit	Sigma	HPA002866	1:500
Anti-TWNK	Rabbit	Custom-made, AfP	Milenkovic et al., 2013	1:100
Anti-TFB2M	Rabbit	Custom-made, AfP	Metodiev et al. 2009	1:100
Anti-POLRMT	Rabbit	Custom-made, AfP	Kühl et al., 2014	1:100
Anti-LRPPRC	Rabbit	Custom-made, AfP	Ruzzenente et al., 2012	1:100
Anti-NDFUA9	Mouse	Thermo Fisher Scientific	459100	1:1000
Anti-ATP5A	Mouse	Abcam	ab14748	1:1000
Anti-MTCO1	Mouse	Abcam	ab14705	1:1000
Anti-COIII Core2	Mouse	Abcam	ab14705	1:1000
Anti-SHD 70kDa Fp subunit	Mouse	Thermo Fisher Scientific	459200	1:1000
Anti-rabbit IgG - HRP	Donkey	GE Healthcare	NA9340V	1:10,000
Anti-mouse IgG -HRP	Sheep	GE Healthcare	NXA931	1:10,000
IRDye 800 conj. anti-rabbit	Donkey	Licor	925-32213	1:30,000
IRDye 800 conj. anti-mouse	Donkey	Licor	925-32212	1:30,000
Alexa Fluor 680 anti-mouse	Goat	Thermo Fisher Scientific	A27057	1:30,000
Alexa Fluor 680 anti-rabbit	Goat	Thermo Fisher Scientific	A21076	1:30,000

5.4.5 Blue Native PAGE Analyses

Analysis of protein complexes under native conditions was achieved by Blue Native PAGE electrophoresis, as previously described with minor modifications (Jha et al., 2016). Isolated mitochondria (50 μ g) were prepared by first removing the storage buffer (MIB) by centrifugation at 10,000x *g* for 5 minutes at 4°C. Mitochondria were then solubilized on ice for 15 minutes in 16 μ l of 1x NativePAGE sample buffer (Thermo Fisher Scientific, BN20032) containing 1 % DDM or 2 % Digitonin. Insoluble material was pelleted by centrifugation at 20,000x *g* for 30 minutes at 4°C. Next, 12 μ l of supernatant was collected and mixed with 0.5 μ l of NativePAGE 5 % G-250 sample additive (Invitrogen, BN20041). High molecular weight markers were prepared following manufactures instructions (GE Healthcare, 17-0445-01). Samples were separated on a 3-12 % NativePAGE Bis-Tris gel (Thermo Fisher Scientific, BN1001BOX). Initially, a dark blue cathode buffer (1x NativePAGE running buffer and 0.5x cathode additive; Invitrogen, BN2001 and BN2002) was added to the inner chamber of a XCell SureLock cell and ran for 30 minutes at 150 volts. Then, the dark blue cathode was removed by aspiration and exchanged with light blue cathode buffer (1x NativePAGE running buffer and 0.1x cathode additive) and separation was continued at 150 Volts until the blue front reach the bottom of the gel. The anode buffer (placed in the outside chamber of the XCell SureLock cell) consisted of 1x NativePAGE running buffer. DDM-treated samples were subjected to standard immunoblotting. To this end, proteins were transferred onto a PVDF membrane with BN-transfer buffer (47.9 mM Tris and 38.7 mM glycine) for 90 minutes at 400 mA and 4°C. Afterwards, residual Coomassie was removed by washing with methanol prior applying primary antibodies.

5.4.6 Glycerol Gradient Fractionation and Immunoblotting

Analysis of mitochondrial DNA-protein complexes can be achieved by glycerol gradient sedimentation followed by western and southern blotting. This protocol is adapted from (Lee and Bogenhagen 2016) with minor modifications. Crude mitochondria (250 μ g), which were DNaseI (Sigma-Aldrich, 10104159001) and RNase A (Qiagen, 19101) -treated and purified by sucrose gradient were used. The mitochondrial storage buffer (MIB) was removed by centrifugation at 10,000x *g* for

5 minutes at 4°C. Mitochondria were then lysed on ice in 83.3 µl (3 µg/µl), mitochondrial lysis buffer (MLB, 2 % Triton X-100, 100 mM HEPES (KOH) pH 8.0, 100 mM NaCl, 10 mM EDTA, 10 mM DTT, 1x Protease inhibitor cocktail without EDTA) for 15 minutes and two 8.3 µl aliquots (about 25 µg protein), from the total lysate, were collected as input samples for western and southern blotting. The remaining total lysate was carefully layered on top of the casted glycerol gradient. A 15-40 % glycerol gradient containing a 20 % glycerol / 30 % iodixanol pad at the bottom of gradient was casted. First, 5.5 ml of 15 % glycerol buffer (15 % glycerol in 1x MLB) was added onto a 14x89 mm Ultraclear tube (Beckman Coulter, 344059). Then, 5.5 ml of 40 % glycerol buffer (40 % glycerol in 1x MLB) was added with a syringe from the bottom of the tube, pushing the 15 % glycerol buffer upwards. Lastly, 500 µl of 20 % glycerol / 30 % iodixanol mixture was also added with a syringe to the bottom of the tube. Ultracentrifuge tubes were closed with SW 41 Ti long caps (Beranek Laborgeräte, 105-514-6) and gradient casted using a gradient master (model 107, Biocomp) with the following settings: 2 minutes and 31 seconds run time, 81.65 angle, and speed set to 14. Mitochondrial lysates were layered on top of the gradient, gradients balanced, and centrifuged at 151,000x g at 4°C for 4 hours. Gradient was manually fractionated in 750 µl increments from top to bottom using a 1 ml pipette. Fractions were filled up to 1 ml and divided in half for protein precipitation and DNA isolation.

Proteins were precipitated overnight at -20°C with 12 % trichloroacetic acid (Millipore 1.00807.1000) and 0.02 % sodium deoxycholate. The next day, samples were centrifuged at 20,000x g for 20 minutes at 4°C. Pellets were washed with 1 ml of acetone (Millipore 1.00014.1000), incubated on ice for 15 minutes, and centrifuged 20,000x g for 20 minutes at 4°C. After a second acetone wash, protein pellets were dried at room temperature and solubilized in 16 µl of 2x NuPAGE loading buffer containing 0.1 M DTT. See *Western blot* for further details on immunoblotting.

Mitochondrial DNA was isolated by phenol chloroform extraction. To each 500 µl fraction, 60 µl of 1 M Tris pH 8, 40 µl 3 % SDS, and 60 µl of 10 mg/ml Proteinase K was added and incubated overnight at 56°C. Then 600 µl of phenol chloroform was added and centrifuged at 5,000x g for 5 minutes. The upper phase

was aspirated into a 2 ml microcentrifuge tube and 60 μ l of 8 M potassium-acetate plus 2 μ l of GlycoBlue (Thermo Fisher Scientific, AM9515) was added and mixed by vortex. Then 1.5 ml of pure ethanol was added and samples incubated overnight at -20°C . Samples were tabletop centrifuged at max speed for 30 minutes at 4°C , pellet dried. DNA was resuspend in 15 μ l digestion buffer (1x Smartcut buffer) containing 1 μ l of SmaI-HF restriction enzyme (NEB, R3156S) and incubated for 1 hour at 37°C . Digested samples were prepared for agarose gel electrophoresis by adding 4 μ l of 6x DNA loading dye. See *Southern blot* for further details on how mtDNA was visualized.

5.5 MOLECULAR BIOLOGY METHODS

5.5.1 Northern blot

Total RNA was extracted from frozen ground heart tissue using the ToTALLY RNA isolation kit (Ambion, AM1910) or TRIzol reagent (Thermo Fisher Scientific, 15596026). Extracted RNA was subjected to DNase treatment following instructions from TURBO DNA-free™ kit (Thermo Fisher Scientific, AM1907). RNA sample loading buffer (Sigma, R1386) was added to RNA (1-2 µg), denatured for 20 minutes at 65°C, loaded onto a 1 or 1.8 % formaldehyde-MOPS agarose gel, and ran for 2 hours at 120 volts. Migration of RNA through the gel was checked with a UV transilluminator. RNA was transferred overnight onto a 15 x 15 cm Hybond-N+ membrane (GE Healthcare, RPN203B). The membrane was first incubated in MilliQ water for 15 minutes, and both gel and membrane were incubated in 20x saline-sodium citrate (SSC) buffer for 20 minutes prior to transfer assembly.

Gel to membrane transfer assembly was as follows. A large glass dish was filled with 20x SSC and a salt bridge using blotting paper (15 x 20 cm) was placed on top of the dish with the upper and lower ends of the blotting paper submerged in 20x SSC. Two pieces of blotting paper (15 x 15 cm), pre-soaked in 20x SSC, were placed on top of the salt bridge. Air bubbles were rolled out and the gel placed face down on top of the blotting papers. Air bubbles were rolled out and the Hybond-N+ membrane was placed on top of the gel, the top right corner was cut. Air bubbles were rolled out and another two pieces of wet blotting paper were placed on top of the membrane. Next, a stack of paper towels was placed on top, followed by 15 x 15 cm glass plate and a filled 1 L glass bottle. RNA was left to transfer overnight. After transfer, the transfer system was dismantled and membrane was washed with 2x SSC for 5 minutes, and dried at room temperature.

Membrane was UV cross-linked with a UVC500 crosslinker (GE Healthcare) for 3 minutes, followed by blocking in 20 ml of PerfectHyb Plus Hybridization buffer (Sigma, H7033) for 1 hour at 65°C prior to being hybridized with various probes. Mitochondrial probes used for visualization of mRNA and rRNA levels, Table 4, were restriction fragments labeled with α -³²P-dCTP and a Prime-It II Random Primer Labeling Kit (Agilent technologies, 300385). First, mRNA or rRNA probe (30 ng) was

mixed with random primers and primers denatured at 95°C for 5 minutes, followed by 2 minutes on ice, Table 5. Then, probes were mixed radioactive α -³²P-dCTP (Hartmann Analytic), non-radioactive dNTPs and DNA polymerase. Sample was incubated for 30 minutes at 37°C, Table 6.

The probe was purified with G-50 columns following manufactures instructions (Illustra™ Probe Quant™ G-50 Micro Columns, GE Healthcare, 28903408). Afterwards, 50 μ l of purified probe was added to the hybridization buffer used for blocking the membrane and incubated overnight at 65°C. Afterwards, membranes were first washed with 20 ml of 2x SSC/0.1 % SDS and then with 20 ml 0.2x SSC/0.1 % SDS for 20 minutes at 65°C. Membrane was sealed in a plastic bag and exposed to a phosphor screen and developed using a Typhoon FLA 7000 (GE healthcare) or exposed to autoradiography films for visualization of mRNA and rRNA.

Different tRNAs and 7S rRNA were detected using specific oligonucleotides end-labeled with γ -³²P-dATP following a similar protocol as for mRNA and rRNA with the following differences. Membranes were blocked with 10 ml of PerfectHyb Plus Hybridization buffer for 1 hour at 42°C. T₄ Polynucleotide Kinase end-labeling reaction for tRNA probes was prepared as shown in Table 7 and incubated for 30 minutes at 37°C.

tRNA probe was purified with a G-25 column (Illustra™ MicroSpin™ G-25 Columns, 27532501) following manufactures instructions. Afterwards, 50 μ l of purified probe was added to the hybridization buffer used for blocking membrane and incubated overnight at 42°C. Lastly, membranes were washed and membranes exposed as described above.

Table 4: Mitochondrial probes for Northern and Southern blot

Target	Probe	Oligonucleotide Sequence
mRNA	<i>Ndl</i>	ACGCAAAATCTTAGGGTACATACTACGAAAAGGCCCTAACATTGTTGGTCCATACG GCATTTTACAACCATTGCGAGACGCCATAAAATTATTTATAAAAAGAACCAATACGCCCT TTAACAACCTCTATATCCTTATTTATTATTGCACCTACCCTATCACTCACACTAGCATTAA GTCTATGAGTCCCTACCAATACCACACCCATTAATTAATTTAAACCTAGGGATTTTAT TTATTTTAGCAACATCTAGCCTATCAGTTTACTCCATTCTATGATCAGGATGAGCCTCAA ACTCAAATACTCACTATTCGGAGCTTACGAGCCGTAGCCCAAACAATTTTCATATGAA GTAACCATAGCTATTATCCTTTTATCAGTTCTATTAATAAATGGATCCTACTCTCTACAA ACACTTATTACAACCCAAGAACACATATGATTACTTCTGCCAGCCTGACCCATAGCCAT AATATGATTTATCTCAACCCTAGCAGAAACAAAC
mRNA	<i>CoxI</i>	GTTCAATATTTTTGGTTGGTTGCTTGGGTTAGCATTAAAGCCTTACCTATTTATGGAG GTTTAGGTTAATTGTTAGTGGGTTTGTGGTTGTTAATGGTTTTAGGGTTTGGTGA TCGTTTTAGGTTAATAGTTTTTTAATTTATTTAGGGGGGATGTTGGTTGTGTTGGA TATACGACTGCTATAGCTACTGAGGAATATCCAGAGACTTGGGGATCTAACTGATTAAT TTTGGGTTTTTAGTATTGGGGGTGATTATAGAGGTTTTTTAATTTGTGTGCTAATTA TTATGATGAAGTTGGAGTAATTAATCTTGATGGTTTGGGAGATTGGTTGATGTATGAGG TTGATGATGTTGGAGTTATGTTGGAAGGAGGGATTGGGGTAGCGGCAATATATAGTTG TGCTACTTGAATGATGGTAGTGTGGGTGATCTTTGTTTGGGGTATTTTTATT
mRNA	<i>CoxII</i>	GGTCTACAAGACGCCACATCCCCTATTATAGAAGAGCTAATAAATTTCCATGATCACAC ACAATAATTGTTTTCTAATTAGCTCCTTAGTCTCTATATCATCTCGTAATATTAACA ACAAAATAACACATACAAGCACAATAGATGCACAAGAAGTTGAAACCATTTGAACATAT TCTACCAGCTGTAATCCTTATCATAATTGCTCTCCCCTCTACGCATTCTATATATAATA GACGAAATCACAACCCCGTATTAACCGTTAAAACCATAGGGCACCAATGATACTGAAGC TACGAATATACTGACTATGAAGACCTATGCTTTGATTCATATATAATCCCAACAAACGA CCTAAAACCTGGTGAACACTGACTGCTAGAAGTTGATAACCGAGTCGTTCTGCCAA
mRNA	<i>Nd5</i>	ACAAGACATCCGAAAAATAGGAAACATCACAAAAATCATACCATTACATCATCATGCC TAGTAATCGGAAGCCTCGCCCTCACAGGAATACCATTCTAACAGGGTTCTACTCAAAA GACCTAATTATTGAAGCAATTAATACCTGCAACACCAACGCCTGAGCCCTACTAATTAC ACTAATCGCCACTTCTATAACAGCTATGTACAGCATAACGAATCATTACTTCTGTAACAAT AACAAAACCGGTTTTCCCCCCTAATCTCCATTAACGAAAATGACCCAGACCTCATAA ACCCAATCAAACGCCTAGCATTGGAAGCATCTTTCAGGATTTGTCTCATATAAT ATTCCACCAACCAGCATTCCAGTCTCACAATACCATGATTTTTAAAAACACAGCCCTA ATTATTTAGTATTAGGATTCCTAATCGCACTAGAATAAACAACCTAACCCATAAAACT ATCAATAAATAAAGCAAATCCATATTCATCCTTCTCAACTTACTGGGGTTTTTCCCATC TAT TATTCACCGCATTACACC
mRNA	<i>Cytb</i>	AGTAGACAAAGCCACCTTGACCCGATTCTTCGTTTCCACTTCATCTTACCATTTATTAT CGCGGCCCTAGCAATCGTTCACCTCCTCTTCTCCACGAAACAGGATCAAACAACCCAA CAGGATTAACCTCAGATGCAGATAAAATTCATTTACCCCTACTATACAATCAAAGAT ATCCTAGGTATCCTAATCATATTCTTAATTCTCATAACCCTAGTATTATTTTTCCAGACA TACTAGGAGACCCAGACAACCTACATACCAGCTAATCCACTAAACACCCCAACCCATATT AAACCCGAATGATATTTCTATTTGCATACGCCATTCTACGCTCAATCCCCAATAAACTA GGAGGTGTCCTAGCCTTAATCTTATCTATCCTAATTTTAGCCCTAATACCTTTCTTCAT ACCTCAAAGCAACGAAGCCTAATATTCGGCCCAATCACACAAATTTTGTACTGAATCCT AGTAGCCAACCTACTTATCTTAACCTGAATTGGGGGCCAACCAGTAGAACACCCATTT
mRNA	<i>12S</i>	TACACATGCAAACCTCCATAGACCGGTGTAATAATCCCTTAAACATTTACTTAAAATTTAA GGAGAGGGTATCAAGCACATTAATAATAGCTTAAGACACCTTGCTAGCCACACCCCAAC GGGACTCAGCAGTGATAAATATTAAGCAATAAACGAAAGTTTGAAGTTATACCTCT TAGGGTTGGTAAATTTCTGTCAGCCACCGCGGTCATACGATTAACCCAACTAATTAT CTTCGGCGTAAAACGTGTCAACTATAAATAAATAAATAAATAAATAAATAAATAAATAA GTGAAAATTCATTGTTAGGACCTAAACTCAATAACGAAAGTAATTCTAGTCATTTATAA TACACGACAGCTAAGACCCAAACTGGGATTAAGATACCCACTATGCTTAGCCATAAACC TAAATAATTAATTTAACAAAACCTATTTGCCAGAGAACTACTAGCCATAGCTTAAAAC CAAAGGACTTGGCGTACTTTATATCCATCTAGAGGAGCCTGTTCTATAATCGATAAAC CCCGCTCTACCTACCATCTCTTGCTAA

<i>mRNA</i>	<i>18S</i>	GGTCTACAAGACGCCACATCCCCTATTATAGAAGAGCTAATAAATTTCCATGATCACAC ACTAATAATTGTTTTCTAATTAGCTCCTTAGTCCTCTATATCATCTCGCTAATATTAACA ACAAAATAACACATACAAGCACAATAGATGCACAAGAAGTTGAAACCATTTGAACTAT TCTACCAGCTGTAATCCTTATCATAATTGCTCTCCCCTCTCTACGCATTCTATATAATA GACGAAATCAACAACCCCGTATTAACCGTAAAACCATAGGGCACCAATGATACTGAA GCTACGAATATACTGACTATGAAGACCTATGCTTTGATTATATAATCCCAACAAAC GACCTAAAACCTGGTGAAGTACGACTGCTAGAAGTTGATAACCGAGTCGTTCTGCCAA
tRNA	tRNA ^{<i>Phe</i>}	CATTTTCAGTGCTTTGCTTTGTTATTA
tRNA	tRNA ^{<i>Leu1</i>}	AAGTCTTACGCAATTTCTGGCTCTG
tRNA	tRNA ^{<i>Pro</i>}	TCAAGAAGAAGGAGCTACT
tRNA	tRNA ^{<i>Glu</i>}	AACTGCGACCAATGACATGAAAAATC
<i>rRNA</i>	<i>7S rRNA</i>	GACATATAATATTAACCTATCAAACCCCTATGTCCTGATCAATTCTA
DNA	<i>7S DNA</i>	AGTACATAAATTTACATAGTACAACAGTACATTTATGTATATCGTACATTAACCTATTTT CCCCAAGCATATAAGCTAGTACATTAATCAATGGTTCAGGTCATAAAATATCATCAA CATAAATCAATATATATACCATGAATATTATCTTAAACACATTAACCTAATGTTATAAGG ACATATCTGTGTTATCTGACATACACCATACAGTCATAAACTCTTCTTCCATATGACT ATCCCCTTCCCATTGGTCTATTAATCTACCATCCTCCGTGAAACCAACAACCCGCCCA CCAATGCCCTCTTCTCGCTCCGGGCCATTAACCTGGGGGTAGCTAAACTGAACTT TATCAGACATCTGGTCTTACTTCAGGGCCATCAAATGCGTTATCGCCCATACGTTCCCC TTAAATAAGACATCTCGATGGTATCGGGTCTAATCAGCCCATGACCAACATAACTGTGG TGTCATGCATTTGGTATCTTTTTATTTGGCCTACTTTCATCAACATAGCCGTCAAGGCA TGAAAGGACAGCACACAGTCTAGACGCACCTACGGTGAAGAATCATTAGTCCGCAAAA CCCAATCACCTAAGGCTAATTATTCATGCTTGTAGACATAAATGCTACTCAATACCAA TTTTAACTCTCAAACCCCCACCCCTCCTTAATGCCAAACCCCAAAACACTAAGA ACTTGAAAGACATATAATATTAACCTATCAAACCCCTATGTCCTGATCAATTCTAGTAGTTC CCAAAATATGACTTATATTTAGTACTTGTAATAATTTTACAAAATCATGTTCCGTGAAC CAAACTCTAATCATACTCTATTACGCAATAAACATTAACAA
DNA	pAM1	Whole mitochondrial genome sequence

Table 5: Random primers preparation

Chemical	Volume
Random 9-mer primers	10 µl
30 ng mRNA or rRNA probe	1 µl
DEPC water	23 µl

Table 6: Probe synthesis reaction

Chemical	Volume
Probe with random primers mix	34 µl
5x dCTP buffer (with all dNTPs except dCTPs)	10 µl
Exo (-) Klenow polymerase 5 U/µl	1 µl
50 µCi α-32P-CTP	5 µl

Table 7: tRNA end-labeling reaction

Chemical	Volume
10x Polynucleotide buffer (NEB)	2 µl
T ₄ Polynucleotide Kinase (NEB)	1 µl
10 µM primers	2 µl
30 µCi γ-32P-ATP	3 µl
DEPC water	12 µl

5.5.2 Phenol Chloroform Extraction

Total DNA from ear clippings was isolated by phenol chloroform extraction. Ear clippings were digested in 200 μ l of TNES buffer (100 mM Tris pH 8, 200 mM NaCl, 5 mM EDTA pH 8, and 0.2 % SDS) in the presence of 1 mg/ml Proteinase K for 1 hour at 56°C with vigorous shaking. After complete digestion of tissue, 200 μ l of phenol-chloroform (Carl Roth, A156.1) was added, samples vortexed, centrifuged at 5,000xg for 3 minutes, and upper layer aspirated into a new 1.5 ml microcentrifuge tube. To precipitate DNA, 20 μ l of 8M potassium-acetate was added to each sample, vortexed, and followed by addition of 1 ml of pure ethanol. Samples were mixed by inversion and overnight storage at -20°C for overnight. DNA was pelleted by centrifugation at max speed for 20 minutes at 4°C. Supernatant was discarded, DNA pellet air-dried, and DNA resuspended in 250 μ l TE (10 mM Tris-HCl pH 8.0, 1 mM EDTA pH 8.0) buffer.

5.5.3 Southern Blot

Total DNA was extracted from pulverized heart tissue using phenol/chloroform; see *DNA isolation from mouse tissue* for detail on this step. DNA (5 μ g) was digested with *SacI* (20U, New England Biolabs, R3156) overnight at 37°C to digest nuclear DNA and linearize mitochondria DNA, Table 8. DNA was precipitated and resuspend in 24 μ l of TE buffer. Afterwards, 6 μ l of 6x DNA loading dye was added (New England Biolabs, B7024S) and DNA separated on a 0.8 % agarose gel containing ethidium bromide, running at 40 volts for about 16 hours. Agarose gel was then subjected to treatment with 0.2 M HCl for 20 minutes, two washes with water for 5 minutes each, 20 minutes incubation with denaturing solution (1.5 M NaCl and 0.5 M NaOH), two washes with water for 5 minutes each, 20 minutes incubation with neutralization solution (1.5 M NaCl and 0.5 M Tris-HCl pH 7.4), then both Hybond-N+ membrane (15 x15 cm) and gel were incubated in water for 10 minutes, followed by 20 minutes incubation in 20x SSC prior to gel transfer assembly. DNA was transferred on a Hybond-N+ membrane; see *Northern blot* for details on transfer. Membranes were then UV cross-linked, blocked in PerfectHyb Plus Hybridization buffer as described for *Northern blot*. Radioactivity-labeled probes recognizing mtDNA (pAM1) and nuclear DNA (18S) were prepared as described for probes for mRNA and rRNA, see

Northern blot and tables 5 and 6. Membrane was sealed in a plastic bag and exposed to a phosphor screen and developed using a Typhoon FLA 7000 (GE healthcare) or exposed to autoradiography films for visualization of DNA.

Table 8: Restriction digest of DNA

<i>Chemical</i>	<i>Volume</i>
Total DNA (200 ng - 5 µg)	X µl
10x CutSmart buffer	2 µl
SacI-HF 20U	1 µl
DEPC water	Up to 20 µl

5.5.4 D-loop Southern Blot

Southern blotting on isolated mtDNA allows for comparison of 7S DNA levels. Mitochondria were isolated as described in *Isolation of heart mitochondria* for biochemistry. Isolated heart mitochondria (from an entire heart sample) were digested and DNA extracted by phenol/chloroform, see *DNA isolation from mouse tissue* for details. Isolated mtDNA was then RNase A (Qiagen, 19101) treated for 1 hour at 37°C. Concentration of DNA was determined using a NanoDrop 2000 (Thermo Fisher Scientific). mtDNA (3 µg) was then linearized by overnight *SacI* digestion at 37°C. See *Southern blot* and Tables 8 for details on restriction digestion, gel electrophoresis, transfer to membrane, and labeling DNA with radioactive probe. To detect mitochondrial 7S DNA, a specific probe was designed which recognizes full-length mtDNA and 7S DNA. Of special note, during the α -³²P-dCTP labeling of the 7S DNA probe, the hybridization temperature was set to 42°C, instead of 65°C. Membrane was sealed in a plastic bag and exposed to a phosphor screen and developed using a Typhoon FLA 7000 (GE healthcare) or exposed to autoradiography films for visualization of DNA.

5.5.5 mtDNA Topology Analysis

Mitochondrial DNA is organized as a circular dsDNA structure and can be found in various topological conformations under physiological conditions. These native conformations of mtDNA can be separated by gel electrophoresis and visualized by Southern blot. The following method was modified from Kolesar et al., 2013. Heart tissue (20 mg) was minced and lysed in 600 µl of lysis buffer (100 mM Tris-HCl pH

7.5, 100 mM EDTA, 100 mM NaCl, 0.5 % SDS, 0.5 mg/ml Proteinase K) at 55°C for 3 hours followed by 2 hours incubation on ice with premixed 820 mM lithium chloride and 270 mM potassium-acetate to precipitate contaminants. Precipitate was removed from sample by centrifugation for 10 minutes at 10,000 rpm at room temperature. Next, DNA was precipitated with isopropanol overnight. The pelleted DNA was washed with 75 % ethanol and resuspended in 10 mM Tris-HCl, 1 mM EDTA pH 8.0 followed by quantification with Qubit dsDNA BR assay kit (Thermo Fisher Scientific, Q32850). As controls, different topological isomers of the mtDNA were identified by treatment with different restriction and topological enzymes. To this end, total DNA (200 ng) from control was incubated at 37°C for 30 minutes with the following enzymes: SacI (New England Biolabs, R0156S; 20 U), Nt.BbvCI (New England Biolabs, R0632S; 10 U), Topoisomerase I (New England Biolabs, M0301S; 5 U), Topoisomerase II (USB Affymetrix, 78303; 20 U), DNA gyrase (New England Biolabs, M0306; 5 U). Total DNA (200 ng) from experimental samples was then resolved in a 0.4 % agarose gel (15 x 15 cm) without ethidium bromide at 35 volts for 20 hours, and DNA transferred overnight onto Hybond-N+ membrane. For details on DNA transfer, radioactive labeling of pAM₁ probe, and visualization of DNA see *Southern blot*.

5.5.6 Quantitative PCR

The relative abundance of mRNA expression level and mtDNA molecules was determined by quantitative polymerase chain reaction (qPCR). For mtRNA expression analysis the following steps were taken. Total RNA was extracted from pulverized heart tissue using RNeasy Mini kit (Qiagen, 74104) according to manufactures instructions. Isolated RNA was DNase treated following instructions from TURBO DNA-free Kit (Thermo Fisher Scientific, AM2238). RNA concentration was determined using a NanoDrop 2000 (Thermo Fisher Scientific) and 2 µg of RNA subjected to reverse transcription PCR (RT-PCR) for cDNA synthesis according to the High Capacity cDNA reverse transcription kit (Thermo Fisher Scientific, 4368814). A standard curve was created using cDNA from samples and serial dilutions at 1:2. cDNA from samples were diluted 1:5 with DNase-free water and 1 µl used for PCR. A single 9 µl PCR reaction mix consisted of 1x Taqman mix (4.8 ul from

2x stock), 0.5 μ l from 20x Taqman probe, 1 μ l of cDNA, and water (3.2 μ l), kept on ice. Triplicates of samples were loaded on a 364-well plate (Thermo Fisher Scientific, 4309849) and sealed with adhesive film (Thermo Fisher Scientific, 4311971). Plates were centrifuged for 1 minute at 1,200 rpm. A QuantStudio 6 Flex Real-Time PCR system (Thermo Fisher Scientific) was used to perform real-time quantitative reverse transcription PCR (qRT-PCR) under Absolute Quantification mode. Taqman probes used for qPCR analysis of mRNA expression are listed in Table 9. The quantity of transcripts was normalized to β -2-microglobulin (*B2M*) as a reference gene transcript.

Table 9: Taqman probes

Probe	Species	Target	Assay ID	Reporter	Source
Mfn1	Mouse	cDNA	Mm01289372_m1	FAM	Thermo Fisher Scientific
Mfn2	Mouse	cDNA	Mm00500120_m1	FAM	Thermo Fisher Scientific
B2M	Mouse	cDNA	Mm00437762_m1	FAM	Thermo Fisher Scientific
ATP6	Mouse	mtDNA	Mm03649417-g1	FAM	Thermo Fisher Scientific
16S	Mouse	mtDNA	Mm04260181_s1	FAM	Thermo Fisher Scientific
7S DNA	Mouse	7S DNA & mtDNA	Custom-order	FAM	Thermo Fisher Scientific
β -actin	Mouse	nDNA	Mm01205647_g1	FAM	Thermo Fisher Scientific
18S	Human	nDNA	Hs9999901_s1	FAM	Thermo Fisher Scientific

The relative abundance of mtDNA and 7S DNA was determined by quantitative PCR analysis. Total DNA from pulverized heart tissue and immortalized MEFs was extracted using the DNeasy Tissue and Blood Kit (QIAGEN, 69504) based on manufacturer's instructions. DNA concentration was determined using a NanoDrop 2000 (Thermo Fisher Scientific). A standard curve was created using total DNA from samples and serial diluting down to 1:1,000. The a single PCR reaction consisted of 1x Taqman mix (4.8 μ l from 2x stock), 0.5 μ l from 20x Taqman probe, 5 ng of DNA, and water for final volume of 9 μ l. Reactions were kept on ice. Samples were prepared for qPCR as describes above. Taqman probes used for qPCR analysis of mtDNA copy number are listed in Table 9. The quantity of mtDNA was normalized to nuclear DNA. To quantify mitochondrial 7S DNA, a custom Taqman probe recognizing mouse 7S DNA was constructed through Thermo Fisher Scientific's custom primer and probe service. The mouse 7S DNA probe sequences are the following: forward primer, CTAATGTTATAAGGACATATCTGTGTTATCTGACATAC; reverse primer, GGTTTCACGGAGGATGGTAGATTAA; FAM reporter

primer, ACCATACAGTCATAAACTCTT. The specificity of 7S DNA probe was validated using models known to have changes in 7S DNA levels. The abundance of 7S DNA was determined by normalizing the values of 7S DNA to ATP6, since the probe will recognize both 7S DNA and the displaced mtDNA complementary strand (Figure 5.1).

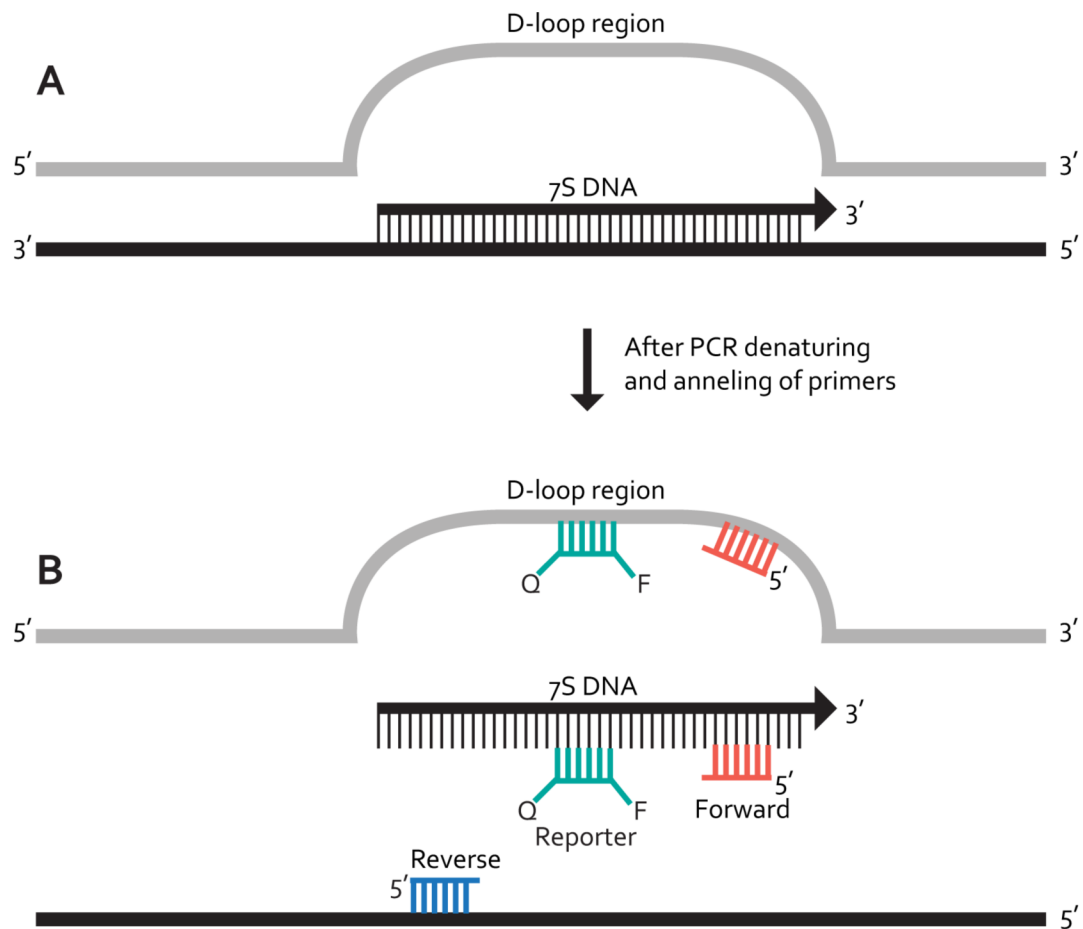


Figure 5.1 Scheme of custom-designed 7S DNA Taqman probe binding

(A) The non-coding region of mtDNA is depicted. 7S DNA binds to mtDNA to create a displacement loop (D-loop) in the non-coding region. (B) During PCR, DNA is denatured followed by annealing of custom-designed Taqman primers to mtDNA and 7S DNA. The FAM reporter containing quencher (Q) and FAM dye (F) anneals at two locations, at an internal site of 7S DNA and D-loop region.

5.5.7 Mutation Load Analysis

Total DNA was extracted from hearts tissue. The somatic mtDNA mutation load was determined by post-PCR, cloning, and sequencing as described previously (Wanrooij et al., 2012). Primers that amplified a region of the mtDNA spanning the 3' end of *mtNAD2* through approximately a third of *mtCO1* (nucleotide pair 4950-5923 of the mouse reference mtDNA sequence GenBank NC_005089). The resulting clones were filtered to remove sequences derived from the known mitochondrial Numts sequences within the nuclear genome of the mice.

5.5.8 DNA Sequencing

DNA from isolated heart mitochondria was used to generate libraries for sequencing to detect mtDNA deletions. Total genomic DNA from the Deletor mouse was provided by Anu Suomalainen-Wartiovaara and used as a positive control for the detection of mtDNA deletions (Tynismaa et al., 2005). A standard Illumina TrueSeq paired-end library was prepared with ~500 base pair fragment inserts. Paired-end 100 base pair sequencing was conducted using an Illumina HiSeq 2500. The reads were mapped to the genomic sequence without the mitochondria using bowtie (VN: 2.1.0) to remove nuclear-genomic sequences (Langmead et al., 2009). The unmapped reads were then mapped to the mitochondrial sequence (GenBank JF286601.1) using bwa (n=0.04, VN: 0.6.2-r126) (Li and Durbin, 2010) with unmapped reads undergoing an additional mapping round after trimming fastx_trimmer, VN: 0.0.13.2) to ensure higher mapping results. Using samtools (Li et al., 2009) (VN: 1.0: samtools -f1 -F14) reads where the two paired sequences were observed to be greater than 600 base pair apart were identified as those containing deletion breakpoints. These reads were extracted for additional analysis.

5.6 IN ORGANELLO ASSAYS

5.6.1 *de novo* mtDNA Transcription

Heart mitochondria were isolated by differential centrifugation, see *Isolation of heart mitochondria* for procedure details. For each biological sample, three aliquots of mitochondria were taken. 1) 300 µg of mitochondria was used to determine the levels of mtDNA and 7S DNA by Southern blot using [α - 32 P]-dCTP-labeled DNA probes specific for 7S DNA, see *Southern blot* for details. 2) 30 µg of mitochondria were used as a loading control using mouse anti-VDAC antibody, see *Western blot* for details. 3) 300 µg of mitochondria were used to radioactively label newly synthesized mt-RNA. First, mitochondria storage buffer was removed by centrifugation at 9,000 rpm for 4 minutes at 4°C. Mitochondria were washed twice with 500 µl *in organello* buffer (25 mM sucrose, 75 mM sorbitol, 100 mM KCl, 10 mM K₂HPO₄, 50 µM EDTA, 5 mM MgCl₂, 10 mM glutamate, 2.5 mM malate, 10 mM Tris-HCl pH 7.4, freshly added 1 mM ADP and 1 mg/ml BSA essential fatty acid free). Mitochondria were then pelleted again and resuspend in 1 ml of *in organello* buffer and 50 µCi of [α - 32 P]-UTP (Perkin-Elmer) was added. Samples were incubated at 37°C for 1 hour with constant rotation. Afterwards, radioactive-UTP buffer was removed by pelleting mitochondria at 9,000 rpm for 4 minutes at 4°C and discarding the supernatant. A short for 10-minute chase, to remove background signal, was performed at 37°C with mitochondria resuspended in 500 µl of *in organello* buffer supplemented with 2 mM UTP. After chase samples were centrifuged at 9,000 rpm for 4 minutes at 4°C and washed twice with 500 µl of washing buffer (10 mM Tris-HCl pH 6.8, 0.15 mM MgCl₂, 10% glycerol). Mitochondrial RNA was isolated by resuspending mitochondria in 250 µl washing buffer and 750 µl Trizol LS reagent (Invitrogen, cat #10296010) and incubated for 5 minutes at room temperature. Next 200 µl of chloroform was added, vortex, and incubated for 3 minutes. Samples were then centrifuged at 12,000x *g* for 15 minutes at 4°C. The upper aqueous phase containing RNA was collected and transferred to a new 1.5 ml microcentrifuge tube. RNA was precipitated with 500 µl of isopropanol and incubated for 10 minutes. Samples were centrifuged for 10 minutes at 12,000x *g* at 4°C. Supernatant was discarded. RNA can be seen as a colorless gel-like pellet after centrifugation. RNA

was washed with 1 ml of 75 % ethanol, vortexed, and centrifuged at 7,500x *g* for 5 minutes at 4°C. Supernatant was discarded and RNA pellet was air-dried for 10 minutes, and resuspended in 10 µl RNase/DNase-free water. RNA sample loading buffer (Sigma, R1386) was added and samples were incubated at 65°C for 10 minutes. A 15x15 cm 1 % low-melting agarose (Biozym, 840001) gel prepared with 18 % formaldehyde, 1x MOPs Northern running buffer (in DEPC water) was casted and thin-well combed used. 2-5 µl of RNA were loaded onto the gel and ran at 90 volts until RNA loading dye reached 2/3 of the gel. 1x MOPs northern running buffer was used for electrophoresis. Afterwards, the gel was washed twice with water for 15 minutes, followed by 20 minutes incubation with 20x SSC. In parallel, a 15x15 cm Hybond-N+ membrane was also subjected to the same incubation periods as the gel. RNA from the agarose gel was transferred overnight onto a Hybond-N+ membrane; see *Northern blot* for details on transfer set up and detection of radioactive signals.

5.6.2 *de novo* mtDNA Replication

Heart mitochondria were isolated by differential centrifugation, see *Isolation of heart mitochondria* for procedure details. 300 µg of mitochondria were washed with 500 µl of ice-cold *in organello* buffer. Mitochondria were pelleted by centrifugation at 9,000 rpm for 4 minutes at 4°C and resuspended in *in organello* buffer containing 50 µM of dCTP, dGTP, dTTP and 20 µCi of radioactive α -³²P-dATP. Samples were incubated for 2 hours at 37°C with constant rotation. After incubation with radioactive dNTP, mitochondria were centrifuged at 9,000 rpm for 4 minutes at 4°C and washed 3x with 500 µl of ice-cold washing buffer. Mitochondria were resuspended in 50 µl of washing buffer and 4 µl of sample (about 24 µg of protein) was taken as a VDAC loading control, see *Western blot* for details. Next, mitochondria were centrifuged again at 9,000 rpm for 4 minutes at 4°C and resuspended in 25 µl of TNES buffer containing 1.2 mg/ml of Proteinase K. DNA extracted with phenol/chloroform, see *DNA isolation from mouse tissue* for details. DNA was resuspended in 30 µl TE buffer and 5 µl from 6x DNA loading dye was added. DNA was split in half: one sample was boiled at 95°C for 5 minutes to release 7S DNA from mtDNA, the other half was not boiled. DNA was separated by gel electrophoresis on a 15x15 cm 0.8 % agarose gel containing no ethidium bromine for 15 hours at 20 volts or at 90 volts for 220 minutes. After gel electrophoresis DNA was transferred onto a Hybond-N+ membrane. See *Northern blotting* for details from transfer to visualization of radioactive signal. When radioactive signal reached about 50 net counts per second using a Geiger counter, steady-state mtDNA and 7S DNA were detected using α -³²P-dATP-labeled DNA probes specific for 7S DNA. *de novo* mtDNA replication images were quantified by densitometry analysis using ImageJ. The cumulative abortive mtDNA products were defined as the signal directly above and below the 7S DNA band.

5.7 IN CELLULO ASSAYS

5.7.1 Growth Curve

The growth rate of log-phase cells was assessed for consecutive 5 days. The growth rate was determined in either glucose or galactose containing media, Table 10. For galactose growth curve only, cells were equilibrated to galactose medium 3 days prior to seeding for experiment. For both type of growth curves, cells were seeded on six-well plates, each well containing 27,000 cells in 3 ml of medium. Cells were collected every 24 hours by trypsinization with 1 ml of 0.05 % Trypsin-EDTA (Thermo Fisher Scientific, 25300-054) and viable cells counted using a Vi-Cell XR analyzer (Beckman Coulter).

Table 10: Growth Curve media composition

Media	Ingredient	Source
Galactose	DMEM 1x (+) L-Glutamine, (-) D-Glucose, (-) Sodium Pyruvate	Thermo Fisher Scientific, 11966025
	15 mM Galactose – sterile filtered	Sigma G5388-100G
	1mM sodium pyruvate	Thermo Fisher Scientific, 11360-039
	10 % FBS	
	1 % Penicillin/Streptomycin, 1 % non-essential amino acids	Thermo Fisher Scientific, 15070-063 Thermo Fisher Scientific, 11140-050
	50 µg/ml uridine –sterile filtered	Sigma-Aldrich, U3750
Glucose	DMEM GlutaMax, 25 mM glucose	Thermo Fisher Scientific, 31966-021
	10 % FBS	Thermo Fisher Scientific, 10270-106
	1 % Penicillin/Streptomycin, 1 % non-essential amino acids	Thermo Fisher Scientific, 15070-063 Thermo Fisher Scientific, 11140-050
	50 µg/ml uridine)	Sigma-Aldrich, U3750

5.7.2 mtDNA Depletion and Repopulation

MEFs (0.5 million for control, *Mfn1* KO, and *Mfn2* KO; 1.5 million for *dMfn* and *Opa1* KO) were cultivated in 18 ml of DMEM GlutaMax containing 25 mM glucose and supplemented with 10 % FBS, 100 U/ml penicillin and streptomycin, 1x non-essential amino acids, and fresh 100 ng/ml ethidium bromine (Sigma-Aldrich, E8751). After 6 days of cultivation in the presence of ethidium bromine, cells were switched to medium containing no ethidium bromine for 6 days. Cells were passaged every 2-3 days during both conditions. Cell pellets were stored at -20°C until further processing. Total DNA was extracted using the DNeasy Tissue and Blood Kit (QIAGEN) and mtDNA levels determined by qPCR, see *Quantitative PCR* for details.

5.8 MASS SPECTROMETRY

5.8.1 UPLC-MS/MS: Coenzyme Q Analysis

MEFs were grown in 175 cm² flasks for one week in DMEM GlutaMax containing 25 mM glucose and supplemented with 1 % dialyzed FBS (Sigma-Aldrich, A3382001), 100 U/ml penicillin and streptomycin, 1 % non-essential amino acids, and 50 µg/ml uridine. Quinones were extracted from cell pellets or pulverized heart tissue by suspending in 200 µl of 1 mM cupric sulfate followed by addition of 200 µl ethanol. Samples were sonicated and vortexed in the presence of 400 µl of hexane. The upper phase was collected and placed in a new tube: both lower and upper phases were dried using a SpeedVac apparatus at 60°C for 1-2 hours. The lower phase pellet was used to determine the protein concentration. The upper phase pellet was further processed for CoQ determination by dissolving the pellet in 200 µl ethanol/methanol (9:1), vortexed, sonicated for 2 minutes, filtrated through a 0.2 µm modified nylon centrifugal filter (VWR, 82031-358) with an eppendorf centrifuge 5424R set to 6°C and 15,000 rpm, and lastly diluted 1/25.

For absolute quantification of Q₉ and Q₁₀ in positive ESI MRM (multi reaction monitoring) mode an Acquity UPLC (Waters) was connected to a XevoTM TQ (Waters). An Acquity UPLC BEH C₁₈ 1.7 µm, 2.1 x 50 mm column was used at 40°C. Solvent A was 90 % methanol + 10 % propanol + 0.1 % formic acid and B was 45 % acetonitril/acetone + 10 % propanol + 0.1 % formic acid. A linear gradient from 100 % A to 0 % in 3 minutes at a flow rate of 0.5 ml/minute was applied. 2 µL were injected three times. The sample manager was set to 8°C for the standards and the samples were defrosted and directly injected. The source temperature was set to 150°C, desolvation temperature was 550°C and desolvation gas was set to 800 L/h, cone gas to 50 L/h. The capillary voltage was set to 1.5 kv. The following MRM transitions were used for Q₉ m/z 795.58 to 196.95 (quantifier) collision 30 V, 795.58 to 95.02 (qualifier) collision 50 V, 795.58 to 106.46 (qualifier) collision 64V, cone was in all cases 31 V for Q₁₀ m/z 863.67 to 196.94 (quantifier) collision energy 36 V, m/z 863.67 to 95.02 (qualifier) collision 54 V, m/z 863.67 to 80.97 (qualifier) collision 66 V, cone was in all cases 35 V. MassLynx (Waters) software was used for data management and TargetLynx (Waters) software for data evaluation and absolute

quantification. All compounds were prepared fresh and dissolved in ethanol/methanol (9:1). For Q₉ and Q₁₀ an external standard calibration curve was calculated using following concentrations: For Q₉ from 100 to 20,000 ng/mL and Q₁₀ from 4 to 3,500 ng/ml (all of them were prepared from stock solutions of 100 µg/ml). Correlation coefficient: $r < 0.990$; response type: internal standard, area; curve type linear; weighting 1/x. The peak integrations were corrected manually, if necessary. Quality control standards of each standard were used during sample analysis and showed between 0.5 % and 40 % deviation respectively. Blanks after the standards, quality control and sample batch proved to be sufficient. No carryover was detected. Q values were normalized to the total amount of protein extracted from cells (lower phase during extraction). Protein samples were resuspend in 20 µl of reagent A of DC protein assay and protein concentration determined as described in *DC protein assay*.

5.8.2 UPLC-MS/MS: Cellular dNTP Analysis

Method was adapted from Olafsson et al., 2017. Cells were grown on 100 mm dishes in DMEM GlutaMax containing 25 mM glucose and supplemented with 10 % FBS, 100 U/ml penicillin and streptomycin, 1x non-essential amino acids, and 50 µg/ml uridine. As a negative dNTP control, a group of control cells were treated with hydroxyurea (Sigma-Aldrich, H8627) at 2 mM for 30 hours to mildly depleted purines. Extraction of dNTP from cells was performed as follows. Adherent cells were quickly washed with ice-cold PBS, detached by trypsinization with 0.05 % trypsin, resuspended in medium, and the total number of cells was determined using a Vi-cell XR cell analyzer (Beckman Coulter). Approximately 2 million cells were centrifuged at 800x *g* for 5 minutes, washed with ice-cold PBS, and resuspended in 1 ml of ice-cold 60 % methanol. Samples were then vortexed rigorously, frozen for 30 minutes at -20°C, and sonicated for 15 minutes on ice. After sonication, samples were centrifuged at 1000x *g* for 5 minutes at 4°C and supernatants collected. Extraction solution was evaporated using an Eppendorf Concentrator plus at room temperature.

Dried pellets were solved in 100 µl of Milli-Q water, vortexed and sonicated for 2 minutes. After sonication, samples were vortexed again and filtrated through a

0.2 μm modified nylon centrifugal filter (VWR) with an Eppendorf centrifuge 5424R set to 8°C and 12000 rpm. The external standard calibration curve was prepared in concentrations from 5 to 600 ng/ml of the dNTPs. All solutions were daily fresh prepared from stock solutions of 100 $\mu\text{g/ml}$ and dissolved in Milli-Q water. dNTP analysis was conducted using a Dionex ICS-5000 (Thermo Fisher Scientific) Anion exchange chromatography using an Dionex Ionpac AS11-HC column (2 mm x 250 mm, 4 μm particle size, Thermo Fisher Scientific, 082313) at 30°C. A guard column, Dionex Ionpac AG11-HC b (2 mm x 50 mm, 4 μm particle size, Thermo Fisher Scientific), was placed before the separation column. The eluent (KOH) was generated in-situ by a KOH cartridge and deionized water. At a flow rate of 0.380 mL/min a gradient was used for the separation: 0-3 min 10 mM KOH, 3-12 min 10-50 mM, 12-19 min 50-100 mM, 19-21 min 100 mM, 21-25 min 10 mM. A 2 mm Dionex suppressor AERS 500 was used for the exchange of the KOH and operated with 95 mA at 15°C. The suppressor pump flow was set at 0.6 mL/min. 10 μL of sample in a full loop mode (overflow factor 3) was injected. Autosampler was set to 6°C. The Dionex ICS-5000 was connected to a XevoTM TQ (Waters) and operated in negative ESI MRM (multi reaction monitoring) mode. The source temperature was set to 150°C, desolvation temperature was 350°C and desolvation gas was set to 50 L/h, cone gas to 50 L/h. The following MRM transitions were used for quantification: dGTP, transition 505.98 \rightarrow 408.00, cone 30, collision 20; dATP, transition 490.02 \rightarrow 158.89, cone 30, collision 26; dTTP, transition 480.83 \rightarrow 158.88, cone 28, collision 46; dCTP, transition 465.98 \rightarrow 158.81, cone 28, collision 30. The software MassLynx and TargetLynx (Waters) were used for data management and data evaluation & quantification. The calibration curve presented a correlation coefficient: $r_2 > 0.990$ for all the compounds (response type: area; curve type linear). Quality control standards were tested during the sample analysis. The deviation along the run was between 0.5% and 40 % respectively. Blanks after the standards, quality control and samples did not present significant peaks. dNTP values were normalized to the total number of cells used for extraction.

5.8.3 LC-MS/MS: Proteomic Analysis

Cells were subjected to stable isotope labeling by amino acids (SILAC) as previously described Ong and Mann, 2006. One set of cells were grown in 75 cm² flasks for seven days with SILAC DMEM medium (Thermo Fischer Scientific, 89985) supplemented with 10 % dialyzed FBS, 100 U/ml penicillin and streptomycin, 1x non-essential amino acids, and 50 µg/ml uridine in the presence of either light or heavy arginine and lysine (¹³C₆ ¹⁵N₄-L-arginine-, ¹³C₆ ¹⁵N₄-L-lysine, Thermo Fisher Scientific, 88434 and 88429). Seven days were sufficient for near full incorporation of the amino acids into proteins (> 98 %). The other set of cells was grown in the same medium containing non-isotopic amino acids for seven days. Cells were passaged during labeling phase when cell confluency reached 80-90 %. After seven days, cells were pelleted at 800xg for 5 minutes at 4°C and pellets storage at -20°C.

Pellets of labeled and non-labeled control or *dMfn* KO MEFs were lysed with with 100 – 200 µl of MS-lysis buffer (6 M guanidinium chloride, 10 mM Tris(2-carboxyethyl)phosphine hydrochloride, 40 mM chloroacetamide and 100 mM Tris-HCl) and mixed 1:1 (three pairs of SILAC labeled control mixed with non-labeled *dMfn* KO MEFs; three pairs non-labeled control mixed with SILAC-labeled *dMfn* KO MEFs). Samples were sonicated with a needle sonicator (1 minute/100 % amplitude) and heated twice for 5 to 10 minutes at 95°C. Following centrifugation at 20,000x g for 20 minutes and room temperature, supernatants were diluted 1:10 with 20 mM Tris pH 8.3 and centrifuged again for 5 minutes. Supernatants were collected and digested overnight in a water-bath with 3 µg Trypsin Gold at 37°C. The next day, peptides were desalted and cleaned using 150 µg-Empore C18-SD 4 mm/1 ml Extraction disc cartridges. Washing was performed with 1 ml of 0.1 % formic acid and peptides were eluted with 200 µl 60 % acetonitrile/0.1 % formic acid and dried at 45°C for 45 minutes with a vacuum concentrator plus (Eppendorf). The cleaned peptides were resuspended with 30 µl 0.1 % formic acid.

Isolated crude heart mitochondria were prepared for mass spectrometry by pelleting 100 µg of mitochondria at 10,000x g for 5 minutes at 4°C and lysis with MS-lysis buffer. Next, 50 µg of lysed mitochondria were diluted 1:10 with 20 mM Tris pH 8.3 and digested overnight in a water-bath at 37°C with 1 µg Trypsin Gold (Promega, V5280). The digest was stopped using formic acid to a final

concentration of 1 %. Peptides were cleaned using home-made 45 µg-StageTips (Empore Octadecyl C18, 3M) and eluted with 80 µl 60 % acetonitrile/0.1 % formic acid and subsequently dried at 45°C for 45 minutes with a vacuum concentrator plus (Eppendorf). Peptides were resuspended in 10 µl of 0.1 % formic acid.

A high pH reversed phase separation was applied to SILAC-labeled samples. SILAC-labeled peptides derived from each biological replicate were separated on a 4.6 x 250 mm ZORBAX 300 Extend-C18, 5 µm, column (Agilent Technologies) at a 1 ml flow rate using a NGC Quest 10 chromatography system (Bio-Rad). Buffer A was 5 % acetonitrile 0.01 M ammonium bicarbonate, buffer B was 80 % acetonitrile 0.01M ammonium bicarbonate. All buffers were prepared with liquid chromatography–mass spectrometry grade water. Peptide separation was performed using a segmented gradient from 5 % to 27 % buffer B for 65 minutes and from 27 % to 45 % buffer B for 30 minutes. Eluting peptides were collected for 72 minutes using a BioFrac fraction collector (Bio-Rad). Fraction collection pattern was set to row and fraction collection size was set to 0.75 ml. In total, 96 fractions were collected in a 1.2 ml V-shaped 96 well plate (Biotix). Upon sample collection, plates were dried overnight and peptides were resuspended in 20 µL 0.1 % formic acid. All 96 fractions were concatenated into 12 final fractions by combining every 12th, following the row based collection. Each peptide pool was dried and resuspended in 10 µL 0.1 % formic acid from which 5 µL were used for analysis by liquid chromatography – mass spectrometry (LC-MS/MS analysis).

LC-MS/MS analysis of SILAC-labeled peptides were separated on a 25 cm, 75 µm internal diameter PicoFrit analytical column (New Objective) packed with 1.9 µm ReproSil-Pur media (Dr. Maisch) using an EASY-nLC 1200 (Thermo Fisher Scientific). The column was maintained at 50°C. Buffer A and B were 0.1 % formic acid in water and 80 % acetonitrile, 0.1 % formic acid, respectively. Peptides were separated on a segmented gradient from 5 % to 31 % buffer B for 80 minutes, and from 31 % to 44 % buffer B for 10 minutes at 200 nl/min. Eluting peptides were analyzed on a QExactive HF mass spectrometer (Thermo Fisher Scientific). Peptide precursor mass to charge ratio (m/z) measurements (MS_1) were carried out at 120,000 resolution in the 350 to 1,500 m/z range. The top ten most intense precursors, with charge state from 2 to 6 only, were selected for higher-energy

collisional dissociation (HCD) fragmentation using 27 % normalized collision energy. The m/z of the peptide fragments (MS₂) were measured at 30,000 resolution using an AGC target of 2e5 and 80 ms maximum injection time. Upon fragmentation precursors were put on an exclusion list for 45 seconds.

For shot-gun LC-MS/MS of non-labelled peptides, the same column and EASY-nLC 1200 were used. The LC runs lasted 180 minutes with a concentration of 6 % solvent B (0.1 % formic acid in 80 % acetonitrile) increasing to 31 % over 155 minutes and further to 50 % over 20 minutes. The column was subsequently washed and re-equilibrated. The flowing rate was 200 nl/min. Spectra were acquired on a QExactive HF mass spectrometer (Thermo Fisher Scientific). For MS₁, the mass range was set to 300–1500 m/z and resolution to 60K at 200 m/z . The automatic gain control (AGC) target of MS was set to 3e6, and the maximum injection time was 80 ms. Peptides were fragmented with HCD with collision energy of 25. For MS₂, the resolution was set to 30K. The AGC target of MSMS was 5e5 and the maximum injection time was 100 ms.

Raw data were analyzed using MaxQuant version 1.5.2.8. Peptide fragmentation spectra were searched against the canonical and isoform sequences of the mouse reference proteome (proteome ID UP000000589, August 2015 from UniProt). MaxQuant complemented the database with 245 sequences of contaminating proteins. For the analysis methionine oxidation and protein N-terminal acetylation were set as variable modifications. The digestion parameters were set to "specific" and "Trypsin/P," allowing for cleavage after lysine and arginine also when followed by proline. The minimum number of peptides and razor peptides for protein identification was 1; the minimum number of unique peptides was 0. Protein identification was performed at a peptide spectrum matches and protein false discovery rate of 0.01. The "second peptide" option was on to identify co-fragmented peptides. For SILAC quantification, multiplicity was set to two and heavy labels were set to Arg10 and Lys8. A minimum ratio count of one was required for protein quantification. For label-free quantification, the minimum ratio count was set to two. Also, "match between runs" was selected for advanced identification. Protein quantification was based on razor plus unique peptides.

Analysis of the quantitative proteomic of SILAC data was performed using R

(R Development Core Team, 2010). Proteins assigned as “Reverse”, “Only identified by site”, and “Potential contaminant” were removed. Normalized ratio H/L values were log₂ transformed and the ratio H/L values for selected experiments were reversed in order to contain higher ratio H/L values for proteins with higher protein expression in the *dMfn* KO compared to the control MEFs. Differential expression analysis was performed using limma. Proteins with an adjusted p-value (Benjamini-Hochberg correction) of less than 0.05 were designated as differentially expressed.

Protein quantification significant analysis of label-free data was performed with the Perseus statistical framework (<http://www.perseus-framework.org/>) version 1.5.2.4. After removing the contaminants and reverse identifications, the intensities were transformed to log₂ and followed by Z Score normalization. Two-sample test was performed to identify the significantly different proteins between knockout and control groups. Proteins with an adjusted p-value (Benjamini-Hochberg correction) of less than 0.05 were designated as differentially expressed.

The database for annotation, visualization and integrated discovery (DAVID) bioinformatics resources 6.8 was used to determine the enrichment of functional annotation terms (Huang et al., 2008). Protein IDs of down-regulated proteins based on the LC-MS/MS data analysis were used for functional annotation. Protein IDs were converted to a gene list using DAVID gene accession conversion tool. *Mus musculus* was selected as species and background. Functional annotation clustering of the gene list was performed using the Kyoto encyclopedia of genes and genomes pathway (KEGG; (Kanehisa and Goto, 2000) and gene ontology (GO; (Ashburner et al., 2000). The GO domain for functional annotation of biological process (GOTERM_BP_FAT) was used. Categories showing a Benjamini adjusted p-value for enrichment of 0.05 or lower were considered significant. Benjamini adjusted p-values were expressed as the -log₁₀.

5.9 MICROSCOPY

5.9.1 Immunocytochemistry

MEFs (approximately 80,000 cells per well) were plated into 12-well plates containing 15 mm autoclaved glass coverslips and standard culture media. The following day, cells were washed with PBS, fixed with 4% paraformaldehyde (Thermo Fisher Scientific, 28908) for 10 minutes at room temperature, cells hydrated with two washes of PBS, and stored at 4°C until further processing.

Immunocytochemistry was performed as follows for fixed cells; cells were permeabilized with 0.1 % Triton X-100 (Sigma-Aldrich, X100) in PBS for 5 minutes, coverslips transferred to a humid chamber, blocked in 3 % protease-free BSA (Sigma-Aldrich, A3059) in PBS for 30 minutes, and incubated overnight at 4°C with primary antibodies prepared in 3 % BSA/PBS, Table 11. The following day, coverslips were washed 3x with 3 % BSA/PBS for 10 minutes and secondary antibodies were applied for 2 hours at room temperature at dilution of 1:500 prepared in 3 % BSA/PBS. Coverslips were extensively washed with PBS, nuclei counterstained with DAPI in PBS (1:1000, Invitrogen, 62248) before mounting with Aqua/Poly-mount (Polyscience Inc., 18606-20).

Freshly isolated hearts were fixed by immersion in 4 % paraformaldehyde, cryopreserved in 30 % sucrose and frozen in optimal cutting temperature compound (Sakura, SA62550). 10 µm-thick cryosections were cut and air dried prior to fluorescent immunohistochemistry. Sections were permeabilized in 0.5 % Triton X-100 in PBS and binding of antibodies to unspecific sites was prevented by incubation in 3 % BSA/PBS for 30 minutes. Primary antibody incubation in 3 % BSA/PBS was performed overnight at 4°C, see Table 11. The following day, coverslips were washed 3x with 3 % BSA/PBS for 10 minutes and secondary antibodies were applied for 2 hours at room temperature at dilution of 1:500 prepared in 3 % BSA/PBS. Coverslips were extensively washed with PBS, nuclei counterstained with DAPI in PBS (1:1000) before mounting a coverslip with Aqua/Poly-mount.

Table 11: Primary and secondary antibodies immunocytochemistry

Target	Host	Source	Catalogue #	Dilution
Fixed- MEFs				
Anti-DNA	Mouse IgM	Progen	61014	1:250
Anti-TOM20	Rabbit	Santa Cruz	sc-11415	1:1000
Anti-HSP60	Goat	Santa Cruz	sc-1052	1:500
Anti-LRPPRC	Rabbit	Santa Cruz	sc-66844	1:500
Anti-BrdU	Rat	Abcam	ab6326	1:250
Anti-TFAM	Rabbit	Abcam	ab131607	1:1000
Anti-TFAM	Rabbit	Agrisera	custom-order	1:3000
Anti-SSBP1	Rabbit	Sigma	HPA002866	1:500
Anti-GFP (heart sections)	Chicken	Aves	GFP-1020	1:500
Anti-ATP5A	Mouse	Abcam	ab14748	1:1000
Anti-mouse IgM Alexa 488	Donkey	Jackson Immuno	715-546-020	1:500
Anti-goat Alexa 633	Donkey	Thermo Fisher Scientific	A21082	1:500
Anti-rat DyLight 488	Donkey	Thermo Fisher Scientific	SA5-10026	1:500
Anti-rabbit Cy3	Donkey	Jackson Immuno	711-165-152	1:500
Frozen Heart sections				
Anti-DNA	Mouse IgM	Progen	61014	1:100
Anti-chicken Alexa 488	Donkey	Jackson Immuno	703-546-155	1:500
Anti-mouse IgM Alexa 594	Goat	Thermo Fisher Scientific	A21044	1:500

5.9.2 Fluorescence *in situ* Hybridization (FISH)

MEFs were prepared on coverslips and fixed with 4 % paraformaldehyde as described in the *Immunocytochemistry* section. FISH was performed first to visualize mRNA using the ViewRNA ISH Cell Assay (Thermo Fisher Scientific, QVC0001), following the manufacturer's instructions. This assay entailed hybridizing cells for 3 hours at 40°C with *Cox1*mRNA probe at a dilution of 1:500 in hybridization buffer provided in the kit (Thermo Fisher Scientific, VB4-3116013-VC). Probe specificity towards RNA was confirmed with RNase T1 (New England Biolabs, EN0542) and DNase1 (New England Biolabs, M03035) treatments (both at 250U/mL, 37°C, 40 minutes). After FISH, samples were processed for standard immunocytochemistry.

5.9.3 Bromouridine Labeling

MEFs were prepared on coverslips and fixed with 4 % paraformaldehyde as described in the *Immunocytochemistry* section. Except for this experiment cells were cultured on coverslips with DMEM medium, containing no uridine supplementation for 24 hours. BrU (Sigma-Aldrich, 850187) was prepared fresh for each experiment. Newly synthesized RNA was labeled with 5 mM BrU for 1 hour at 37°C. A short chase to remove background was performed using DMEM medium containing 50 µg/ml uridine, followed by a PBS wash prior to fixation. Standard immunocytochemistry procedures were carried out to visualize the mitochondrial network, mtDNA, the mt-RNA binding protein LRPPRC, and nascent BrU-labeled RNA.

5.9.4 Confocal Microscopy

Fluorescence images were acquired using a laser-scanning Leica TCS SP8-X inverted confocal microscope, equipped with a white light laser, a 405-nm diode UV laser, Leica HyD photodetectors, and a 100x oil immersion objective (HCX PL APO 100x, 1.46 N.A). Stack images were acquired in sequential mode using a scanning speed of 400 Hz, an image size of 1,024 x 1,024 pixels, and z-step of 0.2-0.3 µm or 0.15 µm when 300x zoom was applied.

5.9.5 Confocal Microscopy Image Analysis

The amount mtDNA foci per cell was determined using stacked images acquired by confocal microscopy and analyzed with ImageJ. Prior to analysis, the DAPI channel was used to manually trace nuclear DNA with the polygon section tool, a region of interest (ROI) selected, and this same area omitted from the anti-DNA channel to quantify only mtDNA foci for each cell. The find maxima tool was used to count mtDNA foci with noise tolerance manually determined between 50-60. To determine the levels of mtDNA relative to TOM20 surface area, binary images were generated from stacked images. An ROI encompassing the mitochondrial network, as visualized by immunostaining for TOM20, was selected for each cell and the analyze particles tool was used to determine the total surface area. The same ROI was then applied to the anti-DNA image with an omitted nuclear DNA area to determine the total number of mtDNA particles.

Analysis of *Cox1* mRNA and BrU-labeled RNA in MEFs was performed in ImageJ. For quantification of *Cox1* mRNA and BrU-labeled RNA amount per cell, a ROI corresponding to the cell boundaries was drawn, and the DAPI channel was used to exclude the nuclear region prior to analysis. Integrated density of the signal coming from the *COX1* mRNA channel or the BrU channel was then quantified based on surface area per cell. For quantification of nucleoids positive for *Cox1* mRNA or BrU-labeled RNA, dual color pictures of DNA, *Cox1* mRNA, and BrU channels were generated in ImageJ. Nucleoids were then classified based on the presence or absence of *Cox1* mRNA foci or BrU foci in their proximity and quantified using the Cell Counter plug-in from ImageJ.

5.9.6 Cytochemistry for STED Microscopy

Cells were grown on coverslips overnight, fixed with methanol at -20°C for 5 minutes, blocked with 5 % BSA in PBS for 5 minutes, incubated with 20 µg/ml RNase A (Sigma Aldrich, R6513) in 0.5 % Tween 20 (Sigma Aldrich, P1379) in PBS for 2 hours at 37°C. Cells were incubated with Quant-iT PicoGreen dsDNA Reagent (Thermo Fisher Scientific, P11496) in PBS for 30 minutes or incubated for 1 hour with anti-dsDNA antibodies (Abcam, ab27156). After several washing steps, the samples were mounted in Mowiol. Samples were imaged within three hours after the sample preparation.

5.9.7 STED Microscopy

STED images were acquired with a two-color Abberior STED 775 QUAD scanning nanoscope (Abberior Instruments, Goettingen Germany) using a 485 nm excitation laser and a pulsed 595 nm STED laser (PicoGreen labeling) or a 640 nm excitation laser together with a 775 nm STED laser (Antibody labeling) and a 100x oil immersion objective lens and N.A of 1.4.

5.9.8 STED Microscopy Image Analysis

Image analysis was performed manually using Inspector Software, by measuring the diameter of nucleoids at full width at half maximum (Abberior Instruments, Goettingen Germany).

5.9.9 Transmission Electron Microscopy

Electron micrographs of heart mitochondria were obtained from small pieces of the left myocardium. Tissues were fixed in a mix of 2 % glutaraldehyde and 1 % paraformaldehyde in 0.1 M phosphate buffer pH 7.4, at room temperature for 30 minutes, followed by 24 hours at 4°C. Specimens were rinsed in 0.1 M phosphate buffer and post-fixed in 2 % osmium tetroxide for 2 hours, dehydrated and embedded in LX-112 resin. Ultra-thin sections (approximately 50–60 nm) from longitudinal parts were cut and sections were examined in a transmission electron microscope (Tecnai 12, FEI Company, Netherlands) at 80 kV. Digital images at a final magnification of 8,200x were randomly taken on myofibrils from sections of the myocardium. The volume density of mitochondria was calculated on printed digital images by point counting using a 2 cm square lattice (Weibel, 1979). To determine the number of images needed for an appropriate sampling, a cumulative mean plot was used (Weibel, 1979). 15 randomly taken images were used from each animal.

5.9.10 Image Processing

Image panels were assembled with Photoshop (Adobe); no digital manipulation was applied except for adjustment of brightness and contrast.

5.10 QUANTIFICATION AND STATISTICAL ANALYSIS

Data are presented as mean \pm SEM unless otherwise indicated in figure legends. Sample number (n) indicates the number of independent biological samples (individual mice, number of cells, or wells of cells) in each experiment. Sample numbers and experimental repeats are indicated in the figures. Data were analyzed using the unpaired Student's t-test, one-way ANOVA using Turkey's multiple comparison test, two-way ANOVA using Bonferroni multiple comparison test between group comparison, as indicated in figure legends. A p-value \leq 0.05 was considered statistically significant.

6.0 ABBREVIATIONS

<i>Abbreviation</i>	<i>Full name</i>
$^{13}\text{C}_6$	Carbon-13
$^{15}\text{N}_4$	Nitrogen-15
ADP	Adenosine diphosphate
AfP	Affinity purified
AGC	Automatic gain control
ANOVA	Analysis of variance
Arg10	$^{13}\text{C}_6$, $^{15}\text{N}_4$ -labeled arginine
ATAD3A	ATPase family AAA domain containing 3A protein
ATP	Adenosine triphosphate
ATP5A	ATP synthase F1 subunit alpha
ATP6	Mitochondrially Encoded ATP Synthase Membrane Subunit 6
ATP8	Mitochondrially Encoded ATP Synthase Membrane Subunit 8
BN-PAGE	Blue native polyacrylamide gel electrophoresis
BrU	Bromouridine
BSA	Bovine serum albumin
Ckmm	Muscle creatinine kinase
CO	Complex
CO ₂	Carbon dioxide
CoQ	Coenzyme Q
Cox1	Cytochrome C oxidase I
Cre	Cre-recombinase protein
CTRL	Control
Cyt.c	Cytochrome c
D-loop	Displacement loop
DC	Detergent compatible
DCPIP	dichlorophenolindophenol
DDM	n-Dodecyl β -D-maltoside
Dguok	deoxyguanosine kinase
DMEM	Dulbecco's modified eagle medium
<i>dMfn</i>	Double mitofusin1-2
DNA	Deoxyribonucleic acid
DNM2	Dynamin 2
dNTP	Deoxynucleotide
DRP1	Dynamin-related protein 1
DTNB	5,5'-dithiobis-2-nitrobenzoic acid
DTT	Dithiothreitol
EDTA	Ethylenediaminetetraacetic acid
EGTA	Ethylene glycol-bis(β -aminoethyl ether)-N,N,N',N'-tetraacetic acid
ER	Endoplasmic reticulum
et al	Latin phrase meaning 'and others'
EtBr	Ethidium bromide
ETC	Electron transport chain
FAD ₂ H	Flavin adenine dinucleotide
FELASA	Federation of European Laboratory Animal Science Associations

FISH	Fluorescence <i>in situ</i> hybridization
Flp	Flippase
For	Forward
Frt	Flippase recognition target
Fzo1p	FuZzy Onions 1 protein
GFP	Green fluorescence protein
GSH	Oxidized glutathione
GSH/GSSH	Glutathione
GSSH	Reduced glutathione
GTPase	Guanosine triphosphate hydrolase
H-strand	Heavy-strand
H ₂ O ₂	Hydrogen peroxide
HCD	Higher-energy collisional dissociation
HCl	Hydrochloric acid
HClO ₄	Perchloric acid
HEPES	4-(2-hydroxyethyl)-1-piperazineethanesulfonic acid
HR2	Heptad repeat 2
HSP	H-strand promoter
HSP60	Heat shock protein 60
IMM	Inner mitochondrial membrane
IMS	Intermembrane space
IMS	Intermembrane space
KCl	Potassium chloride
KCN	Potassium cyanide
KH ₂ PO ₄	Monopotassium phosphate
KO	Knockout
KOH	Potassium hydroxide
L-isoform	Large isoform
L-strand	Light-strand
LC-MS/MS	Liquid chromatography-tandem mass spectrometry
LETM1	Leucine zipper and EF-hand containing transmembrane protein 1
loxP	Locus of crossover x in P1
LRPPRC	Leucine rich pentatricopeptide repeat containing protein
LSP	L-strand promoter
Lys8	¹³ C ₆ , ¹⁵ N ₂ -labeled lysine
MEF	Mouse embryonic fibroblast
MFF	Mitochondrial fission factor
MFN	Mitofusin
MgCl ₂	Magnesium chloride
MGME1	Mitochondrial genome maintenance exonuclease 1
MIB	Mitochondria isolation buffer
MIC60	MICOS complex subunit 60
MiD49	Mitochondrial dynamics proteins 49
MiD51	Mitochondrial dynamics proteins 51
MLB	Mitochondrial lysis buffer
MOPS	3-(N-morpholino)propanesulfonic acid
mRNA	Messenger ribonucleic acid

mRNA	Messenger RNA
MS	Mass spectrometry
MSH	Mannitol, sucrose, HEPES
mt-	Mitochondrial
Mt-transcription	Mitochondrial transcription
mtDNA	Mitochondrial DNA
MTERF1	Mitochondrial transcription termination factor 1
MTERF3	Mitochondrial transcription termination factor 3
mtSSB	Mitochondrial single-stranded DNA binding protein
NADH	Nicotinamide adenine dinucleotide
NaOH	Sodium hydroxide
NCR	Non-coding region
ND4L	NADH:Ubiquinone Oxidoreductase Core Subunit 4L
NP-40	Nonyl phenoxypolyethoxylethanol -40
O _H	H-strand
O _L	L-strand
OMM	Outer mitochondrial membrane
OPA1	Optic atrophy protein 1
OXPPOS	Oxidative phosphorylation system
pAMI	Vector containing the entire mouse mtDNA genome cloned
PBS	Phosphate buffered saline
PCR	Polymerase chain reaction
PEO	Progressive external ophthalmoplegia
pH	Potential hydrogen
POLRMT	RNA polymerase mitochondrial
Polβ	DNA Polymerase Beta
Poly	Mitochondrial DNA polymerase γ
PolyA	Mitochondrial DNA polymerase γ subunit A
PolyB	Mitochondrial DNA polymerase γ subunit B
Polζ	DNA Polymerase Zeta
Polθ	DNA Polymerase Theta
PrimPol	Primase And DNA Directed Polymerase
PVDF	polyvinylidene difluoride
qPCR	Quantitative polymerase chain reaction
R-loops	RNA:DNA hybrids
Rev	Reverse
RNA	Ribonucleic acid
RNASEH1	Ribonuclease H1
ROI	Region of interest
ROS	Reactive oxygen species
RPKM	Reads per kilobase of transcript, per million mapped reads
rRNA	Ribosomal ribonucleic acid
S-isoform	Small isoform
SDS	Sodium dodecyl sulfate
SDS-PAGE	Sodium dodecyl sulfate polyacrylamide gel electrophoresis
SILAC	Stable isotope labeling by amino acids
SLIRP	SRA Stem-Loop Interacting RNA Binding Protein

SSBP ₁	The single-stranded DNA binding protein 1
SSC	Saline-sodium citrate
STED	Stimulated emission depletion
TBS	Tris Buffered Saline
TCA	Tricarboxylic acid
TE	Tris, EDTA
TEFM	Transcription elongation factor
TFAM	Mitochondrial transcription factor activator A
TFB ₂ M	Mitochondrial transcription factor B ₂
Tg	Transgenic
Tk ₂	Thymidine kinase
TMPD	Tetramethylphenylendiamin
TNES	Tris, NaCl, EDTA, SDS
TOM ₂₀	Translocase of outer mitochondrial membrane 20
TOP ₃ α	Mitochondrial topoisomerase ₃ α
Topo	Topoisomerase
tRNA	Transfer ribonucleic acid
TWINK	Twinkle
UPLC-MS/MS	Ultra-performance liquid chromatography-tandem mass spectrometry
UV	Ultraviolet
VDAC	Voltage-dependent anion channel
WBSCR ₁₆	Williams-Beuren syndrome critical region 16 protein
YFP	Yellow fluorescent protein

Units

%	Percentage
°C	Degree Celsius
bp	Base pair
cm	Centimeter
g	Gram
xg	Normal gravity acceleration (9,81 m x s ⁻¹)
Hz	Hertz
J	Joule
m/z	Mass to charge ratio
mg	Micrometer
ml	Millimeter
mM	Millimolar
N.A	Numerical aperture
nM	Nanomolar
nm	Nanometer
pmol	Picomolar
rpm	Revolution per minute
U	Unit
µg	Microgram
µl	Microliter
µm	Micromolar
V	Volt
W	Watt
ε	Extinction coefficient

Amino acid letter codes

1-letter	Amino Acid	3-letter	1-letter	Amino Acid	3-letter
A	Alanine	Ala	M	Methionine	Met
C	Cysteine	Cys	N	Asparagine	Asn
D	Aspartic Acid	Asp	P	Proline	Pro
E	Glutamic Acid	Glu	Q	Glutamine	Gln
F	Phenylalanine	Phe	R	Arginine	Arg
G	Glycine	Gly	S	Serine	Ser
H	Histidine	His	T	Threonine	Thr
I	Isoleucine	Ile	V	Valine	Val
K	Lysine	Lys	W	Tryptophan	Trp
L	Leucine	Leu	Y	Tyrosine	Tyr

7.0 ERKLÄRUNG

Ich versichere, dass ich die von mir vorgelegte Dissertation selbständig angefertigt, die benutzten Quellen und Hilfsmittel vollständig angegeben und die Stellen der Arbeit – einschließlich Tabellen, Karten und Abbildungen –, die anderen Werken im Wortlaut oder dem Sinn nach entnommen sind, in jedem Einzelfall als Entlehnung kenntlich gemacht habe; dass diese Dissertation noch keiner anderen Fakultät oder Universität zur Prüfung vorlegen hat, dass sie – abgesehen von unten angegebenen Teilpublikationen – noch nicht veröffentlicht worden ist sowie, dass ich eine solche Veröffentlichung vor Abschluß des Promotionsverfahrens nicht vornehmen werde. Die Bestimmungen dieser Promotionsordnung sind mir bekannt. Die von mir vorgelegte Dissertation ist von Prof. Dr. Nils-Göran Larsson betreut worden.

Köln, 25.08.2018

Eduardo Silva Ramos

8.0 ACKNOWLEDGEMENTS

First and foremost, I would like to thank Prof. Dr. Nils-Göran Larsson for giving me the opportunity to do my PhD in his lab. Thanks for trusting me on this project and for maintaining interest over the years. Your leadership was instrumental in bringing this research into its final form. Along the way, you connected me to a network of fantastic scientists.

I thank my thesis committee members Prof. Dr. Elena Rugarli and Prof. Dr. Jan Riemer for their time and support. I also thank Prof. Dr. Rudolf Wiesner for his encouragement and feedback over the years.

I had the good fortune to have two mentors during my studies. Together they taught me everything they knew about bioenergetics and high-resolution imaging, which today have become my strongest skill set. They also taught me to become an independent and critical scientist, which helped me face unforeseeable challenges during my studies. I thank Dr. Arnaud Mourier and Dr. Elisa Motori for their immeasurable support and mentorship.

I would also like to thank Dr. Dusanka Milenkovic and Jakob Busch for dedicating many hours in reviewing my manuscript and thesis, but also together with Dr. Ana Grönke for all the funny and scientific moments we shared in the office.

Thanks to all my collaborators that have helped bring this research to print. I also thank my fellow peers for placing trust on my expertise and involving me in their research; Dr. Marie Lagouge, Dr. Shan Jiang, Dr. Dusanka Milenkovic, Dr. Inge Köhl, Jakob Busch, Joana Gonclaves, and of course Dr. Arnaud Mourier.

I would like to thank all present and former members of the Larsson lab that I had the good fortune to meet. Thank you for all the sweets and cakes that made working long nights in the lab a little bit easier.

Lastly, I thank my family for their encouragement over the years. I also give special thanks to my dear friends Bridget, Stephanie, and Caro for your support and curiosity about mitochondria. I also thank Hervé for your tremendous support.